

DEC 22 1946

ARR No. L4J16

NATIONAL ADVISORY COMMITTEE FOR AERONAUTICS

# WARTIME REPORT

ORIGINALLY ISSUED

October 1944 as  
Advance Restricted Report L4J16

WIND-TUNNEL INVESTIGATION OF ROUNDED HORNS AND OF GUARDS

ON A HORIZONTAL TAIL SURFACE

By Robert B. Liddell and Vernard E. Lockwood

Langley Memorial Aeronautical Laboratory  
Langley Field, Va.

# NACA

WASHINGTON

NACA LIBRARY  
LANGLEY MEMORIAL AERONAUTICAL  
LABORATORY

Langley Field, Va.

NACA WARTIME REPORTS are reprints of papers originally issued to provide rapid distribution of advance research results to an authorized group requiring them for the war effort. They were previously held under a security status but are now unclassified. Some of these reports were not technically edited. All have been reproduced without change in order to expedite general distribution.

NACA ARR No. 14J16

## NATIONAL ADVISORY COMMITTEE FOR AERONAUTICS

## ADVANCE RESTRICTED REPORT

WIND-TUNNEL INVESTIGATION OF ROUNDED HORNS AND OF GUARDS  
ON A HORIZONTAL TAIL SURFACE

By Robert B. Liddell and Vernard E. Lockwood

## SUMMARY

An investigation was made to determine the aerodynamic effects of horn balances with various plan forms and of guards on a horizontal tail surface. The results indicate that rounding the adjacent horn and stabilizer edges caused negligible changes in the aerodynamic characteristics, except for the changes resulting from the decrease in the area moment of the horn. The use of guards mounted between the stabilizer and horn was found to increase the slope of the lift curves with angle of attack or with elevator deflection. The negative slopes of the curves of hinge moment against angle of attack and elevator deflection increased as the guard area was increased.

## INTRODUCTION

An investigation was made in the LMAL 7- by 10-foot tunnel of the 0.5-scale model of the left horizontal tail surface of the Grumman TBF-1 airplane with various horn and stabilizer modifications. The purpose of the investigation was to determine the aerodynamic effects of changing the plan forms of the horn balance and the adjacent fixed surface. Test results are included to show the aerodynamic effects of various guard arrangements that might be used on a horizontal tail having a horn balance. For convenience, the results presented in the various figures are listed in table I. Tuft tests of the outboard end of the model were made to determine the air-flow characteristics of four horn and stabilizer modifications.

Inasmuch as this investigation was general, the model was tested at higher angles of attack and with

elevator deflections much greater than would have been feasible for the actual TBF-1 airplane.

## SYMBOLS

$C_L$	lift coefficient ( $L/qS$ )
$C_D$	drag coefficient ( $D/qS$ )
$C_m$	pitching-moment coefficient about mounting axis ( $M/qSc$ )
$C_{h_e}$	elevator hinge-moment coefficient about hinge axis ( $H_e/qb_e\bar{c}_e^2$ )
$L$	twice the lift of the semispan model
$D$	twice the drag of the semispan model
$M$	twice the pitching moment of the semispan model
$H_e$	elevator moment about hinge axis, foot pounds; positive when it tends to depress elevator trailing edge
$q$	dynamic pressure
$S$	total horizontal-tail area
$b$	span of horizontal tail
$b_e$	span of left elevator
$c$	mean chord of the horizontal tail surface
$\bar{c}_e$	root-mean-square chord of the elevator
$S_g$	total guard area (two guards)
$\alpha$	angle of attack of the model
$\delta_e$	elevator deflection relative to the stabilizer, positive when trailing edge is deflected downward

$$C_{L\alpha} = \left( \frac{\partial C_L}{\partial \alpha} \right)_{\delta_e}$$

$$C_{L\delta_e} = \left( \frac{\partial C_L}{\partial \delta_e} \right)_{\alpha}$$

$$C_{h\alpha} = \left( \frac{\partial C_h}{\partial \alpha} \right)_{\delta_e}$$

$$C_{h\delta_e} = \left( \frac{\partial C_h}{\partial \delta_e} \right)_{\alpha}$$

$$a_{\delta_e} = \left( \frac{\partial \alpha}{\partial \delta_e} \right)_{C_L} = 0$$

All slope values quoted are for small values of angle of attack and flap deflection.

#### METHOD AND APPARATUS

A semispan model was mounted vertically in the LMAL 7- by 10-foot tunnel (reference 1) with the inboard end adjacent to the tunnel floor, which thereby acted as a reflection plane. The model was supported entirely by the balance frame with a small clearance at the tunnel floor in order that all the forces and moments acting on the model could be measured. The flow over the model simulated the flow over a complete horizontal tail consisting of the left semispan of the model joined to its reflection and mounted in a 10- by 14-foot tunnel. In order to present results for the full-span horizontal tail, the measured values taken for the tests were multiplied by 2. The test setup is shown schematically in figure 1.

Provisions were made for changing the angle of attack and the deflection of the elevator of the model while the tunnel was in operation. The elevator hinge moments were measured by means of an electrical strain gage mounted within the elevator.

The 0.5-scale model of the left horizontal tail surface for the TBF-1 airplane was furnished by the

Grumman Aircraft Corporation and conformed to the dimensions shown in figure 2. The model represented that part of the airplane shown crosshatched in figure 3. The geometric characteristics of the model are given in the following table:

Horizontal tail area, original configuration $H_1S_1$ , $S/2$ , square feet .....	13.69
Horizontal tail span, $b/2$ , feet .....	5.20
Elevator area aft of hinge line, square feet .....	5.93
Elevator root-mean-square chord, $\bar{c}_e$ , feet .....	1.268
Elevator movement, degrees .....	$\pm 36$
Guard area, $S_g/2$	
Guard 1, square feet .....	0.041
Guard 2 ( $\bar{c}_e = 0$ ), square feet .....	0.485
Guard 3, square feet .....	0.822
Guard 4, square feet .....	4.575

The modifications made on the model during the tests consisted primarily of a systematic change in the gap between the horn and stabilizer near the leading edge. This modification was made by providing the model with interchangeable horn- and stabilizer-tip blocks of various shapes. Figures 4 and 5 show these modifications to the model and indicate the method adopted for the designation of the various horn and stabilizer shapes. For comparative purposes, tests were also made of the model without a horn and with a full-span stabilizer ( $H_0S_0$ ).

Four different guards were also tested with the original horn configuration. The dimensions of each guard are given in figure 6 and photographs of the guard arrangements are presented as figure 7.

For most tests, the dynamic pressure was maintained at 16.37 pounds per square foot. At some high positive angles of attack and positive elevator deflections, values of drag and hinge moment too large for the indicating apparatus necessitated a reduction of the tunnel dynamic pressure to 12.53 pounds per square foot. These two dynamic pressures correspond to velocities, under standard sea-level conditions, of 80 and 70 miles per hour and to test Reynolds numbers of 1,970,000 and 1,720,000, respectively. The Reynolds numbers are based on a model chord of 2.63 feet. (Effective Reynolds number = Test Reynolds number  $\times$  Turbulence factor. The turbulence factor for the LMAL 7- by 10-foot tunnel is 1.6.)

## CORRECTIONS

The results have been corrected for the effects of the jet boundaries. The corrections which were applied to the angle of attack and the lift, drag, pitching-moment, and hinge-moment coefficients were:

$$\Delta\alpha = 1.48 \times C_L$$

$$\Delta C_L = -0.016 \times C_L$$

$$\Delta C_{D1} = 0.00235 \times C_L^2$$

$$\Delta C_m = 0.0069 \times C_L$$

$$\Delta C_{h_e} = 0.0046 \times C_L$$

No corrections have been made for the effects of the gap between the root section and the floor or for leakage around the support strut.

## RESULTS AND DISCUSSION

Horn and stabilizer modifications.- The aerodynamic characteristics of the horizontal tail are presented as a function of angle of attack for two elevator deflections in figure 8 and as a function of elevator deflection for two angles of attack in figure 9. Little if any significant change in the lift produced is noted for the various modifications, except for the tail surface without a horn ( $H_0S_0$ ).

The area of the horn decreased with the successive horn modifications and caused a proportionate decrease in balancing moment. Thus, rounding the horn increased slightly the negative slopes of the hinge-moment-coefficient curves, as is shown in figures 8 and 9. No improvement in the hinge-moment characteristics is apparent for a rounded horn.

Complete data are presented in figures 10, 11, and 12 for the model without a horn  $H_0S_0$ , for the original configuration  $H_1S_1$ , and for modification  $H_3S_2$ , respectively. The slope of the lift curve for the original

model  $H_1S_1$  equals 0.055. In general, little gain in lift may be obtained by deflecting the elevator more than  $20^\circ$  or by increasing the angle of attack above  $16^\circ$ , except for attitudes of the model in which the elevator deflection and angle of attack are of opposite sign.

The hinge-moment parameters are plotted in figure 13 against the ratio of the area moment of the horn to the area moment of the elevator. From this figure, the contribution of the horn to  $Ch_\alpha$  and  $Ch_{\delta_e}$  may be determined. The values of  $\Delta Ch_\alpha$  and  $\Delta Ch_{\delta_e}$  obtained are in good agreement with the values given in reference 2.

Effects of guards.— The aerodynamic effects of mounting various guards on the original model  $H_1S_1$  are shown in figures 14 and 15. The guards act as end plates on the airfoil and cause a small increase in  $CL_\alpha$  and  $CL_{\delta_e}$  as the guard area is increased (fig. 16).

The lift parameters increase in constant proportion to each other; the effectiveness  $a_{\delta_e}$  of the elevator is therefore shown to be constant with increasing guard area.

Inasmuch as  $Ch_\alpha$  and  $Ch_{\delta_e}$  increase negatively with an increase in guard area (fig. 16), the horn area would have to be increased proportionately with the increase in guard area if the hinge-moment parameters are to be kept constant. Since  $Ch_\alpha$  is positive, the hinge-moment parameters may be expected to become more positive, as did the lift parameters with increase in guard area. The opposite is apparently true if a horn is employed to obtain most of the control-surface balance. This result might be explained in the following manner: The airfoil may be considered as divided into two parts by the solid guard. The portion of the airfoil inboard of the guard has very little balance area and, therefore,  $Ch_\alpha$  and  $Ch_{\delta_e}$  are negative and would become increasingly negative with an increase of guard area. Values of  $CL_\alpha$  and  $CL_{\delta_e}$  also would become increasingly positive as the guard increased the aspect ratio. The portion of the airfoil outboard of the guard, however, decreases in aspect ratio with the addition of guard area. This decrease would cause the positive hinge-moment parameters for this portion of the airfoil to have little influence in the determination of the over-all parameter values.

By the use of figures 13 and 16 it would be possible to find the additional area moment of the horn required for any size of guard that would be used. These curves would be valid, however, only for guards mounted at the spanwise station tested. A solid guard at any other spanwise location would affect the lift and hinge-moment parameters differently.

Tuft studies.- The results of tuft studies made on the upper surface of the model for a series of angles of attack at various elevator deflections are presented in figures 17 to 20. These studies were made of the out-board end of the horizontal tail for four horn and stabilizer modifications and are believed to be the first detailed tuft studies made of flow conditions around an unshielded horn.

The photographs show that, at negative elevator deflections, little difference exists in air flow over the top surface of the model for the various horn and stabilizer modifications tested. At positive elevator deflections, however, the effect of the horn on the air-flow characteristics is not localized but affects the air-flow pattern over much of the surface shown. Separation occurs on all of the elevators surveyed when the elevator angle and angle of attack are  $3^\circ$ . (For example, see fig. 18(e).) On the other hand, for the model without a horn at the same attitude a smooth flow over the elevator is indicated (fig. 17(e)). The disturbing effect of the air flow through the horn-stabilizer gap and the hinge cut-out gap is evident from figures 18 to 20. Rounding off the stabilizer  $H_1S_2$  produces a slight improvement in flow conditions.

### CONCLUSIONS

The results of an investigation to determine the aerodynamic effects of varying the shape of horn balances on horizontal tail surfaces indicate that:

1. Rounding the adjacent horn and stabilizer edges had a negligible effect on the aerodynamic characteristics of the tail surface except for that caused by the decrease in horn area moment.

2. A solid horn guard mounted at the end of the stabilizer increased the rate of change of lift with angle of attack and with elevator deflection. The rate of change of hinge moment with angle of attack and with elevator deflection increased negatively as the guard area was increased.

Langley Memorial Aeronautical Laboratory  
National Advisory Committee for Aeronautics  
Langley Field, Va.

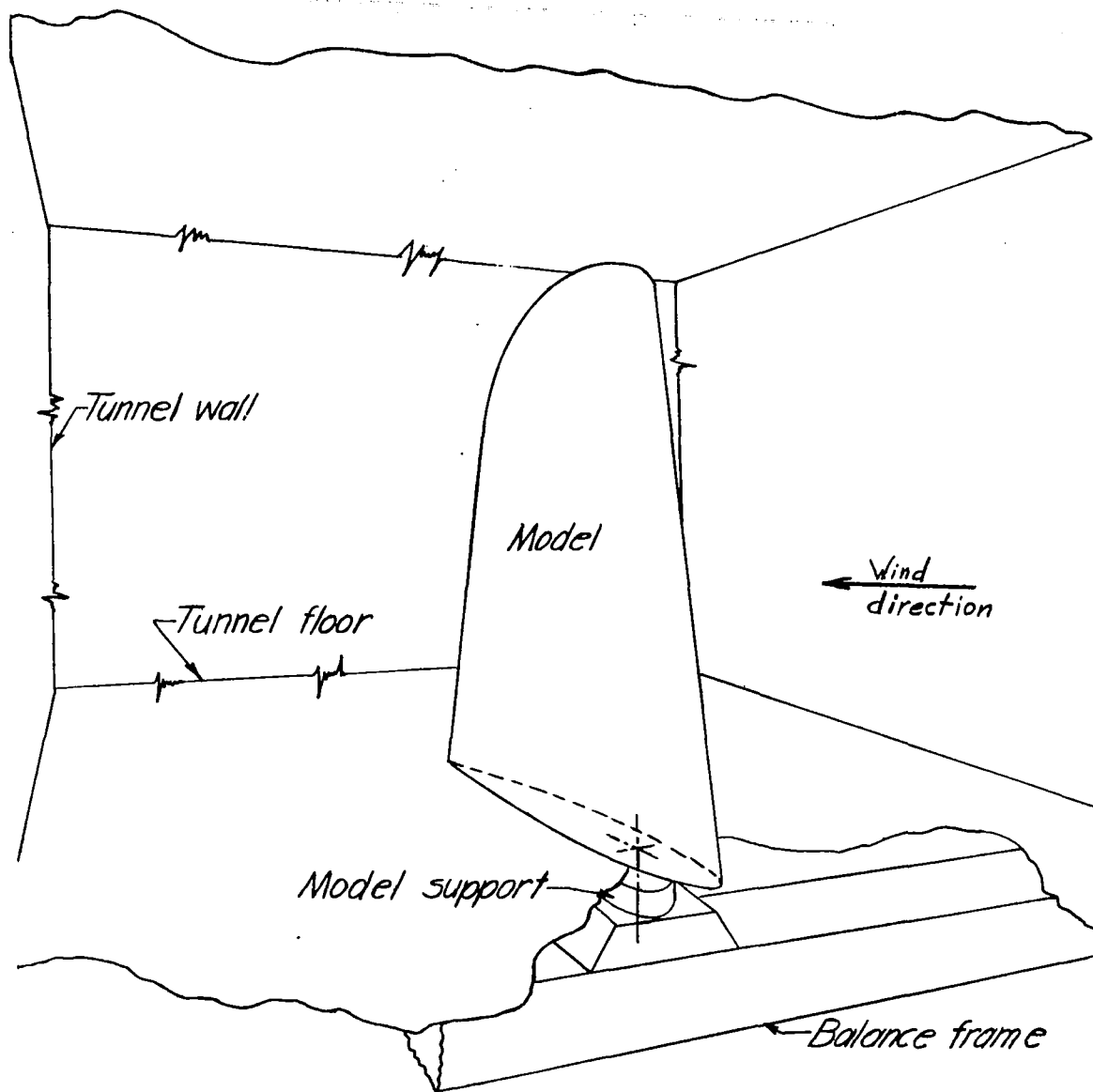
#### REFERENCES

1. Wenzinger, Carl J., and Harris, Thomas A.: Wind-Tunnel Investigation of an N.A.C.A. 23012 Airfoil with Various Arrangements of Slotted Flaps. NACA Rep. No. 664, 1939.
2. Lowry, John G.: Résumé of Hinge-Moment Data for Unshielded Horn-Balanced Control Surfaces. NACA RB No. 3F19, 1943.

## RESULTS IN VARIOUS FIGURES

Figure	$\alpha_T$ (deg)	$\delta_g$ (deg)	Horn	Stabilizer	Guard
8	-8 to 32	0 and -20	H <sub>0</sub>	S <sub>0</sub>	None
↓	↓	↓	H <sub>1</sub>	S <sub>1</sub>	↓
↓	↓	↓	H <sub>2</sub>	S <sub>1</sub>	↓
↓	↓	↓	H <sub>4</sub>	S <sub>1</sub>	↓
↓	↓	↓	H <sub>1</sub>	S <sub>2</sub>	↓
↓	↓	↓	H <sub>2</sub>	S <sub>2</sub>	↓
↓	↓	↓	H <sub>3</sub>	S <sub>2</sub>	↓
↓	↓	↓	H <sub>4</sub>	S <sub>2</sub>	↓
↓	↓	↓	H <sub>0</sub>	S <sub>0</sub>	↓
9	0 and 8	-36 to 36	H <sub>1</sub>	S <sub>1</sub>	↓
↓	↓	↓	H <sub>2</sub>	S <sub>1</sub>	↓
↓	↓	↓	H <sub>4</sub>	S <sub>1</sub>	↓
↓	↓	↓	H <sub>1</sub>	S <sub>2</sub>	↓
↓	↓	↓	H <sub>2</sub>	S <sub>2</sub>	↓
↓	↓	↓	H <sub>3</sub>	S <sub>2</sub>	↓
↓	↓	↓	H <sub>4</sub>	S <sub>2</sub>	↓
↓	↓	↓	H <sub>0</sub>	S <sub>0</sub>	↓
10	-8 to 32	-32 to 32	H <sub>1</sub>	S <sub>1</sub>	↓
11	↓	↓	H <sub>3</sub>	S <sub>2</sub>	↓
12	↓	↓	H <sub>1</sub>	S <sub>1</sub>	↓
14	↓	0 and -20	↓	↓	↓
↓	↓	↓	↓	↓	↓
↓	↓	↓	↓	↓	↓
15	0 and 8	-36 to 36	↓	↓	1
↓	↓	↓	↓	↓	2
↓	↓	↓	↓	↓	3
↓	↓	↓	↓	↓	4
↓	↓	↓	↓	↓	None
↓	↓	↓	↓	↓	1
↓	↓	↓	↓	↓	2
↓	↓	↓	↓	↓	3
↓	↓	↓	↓	↓	4

NATIONAL ADVISORY  
COMMITTEE FOR AERONAUTICS



NATIONAL ADVISORY  
COMMITTEE FOR AERONAUTICS

Figure 1 - Schematic diagram of test installation.

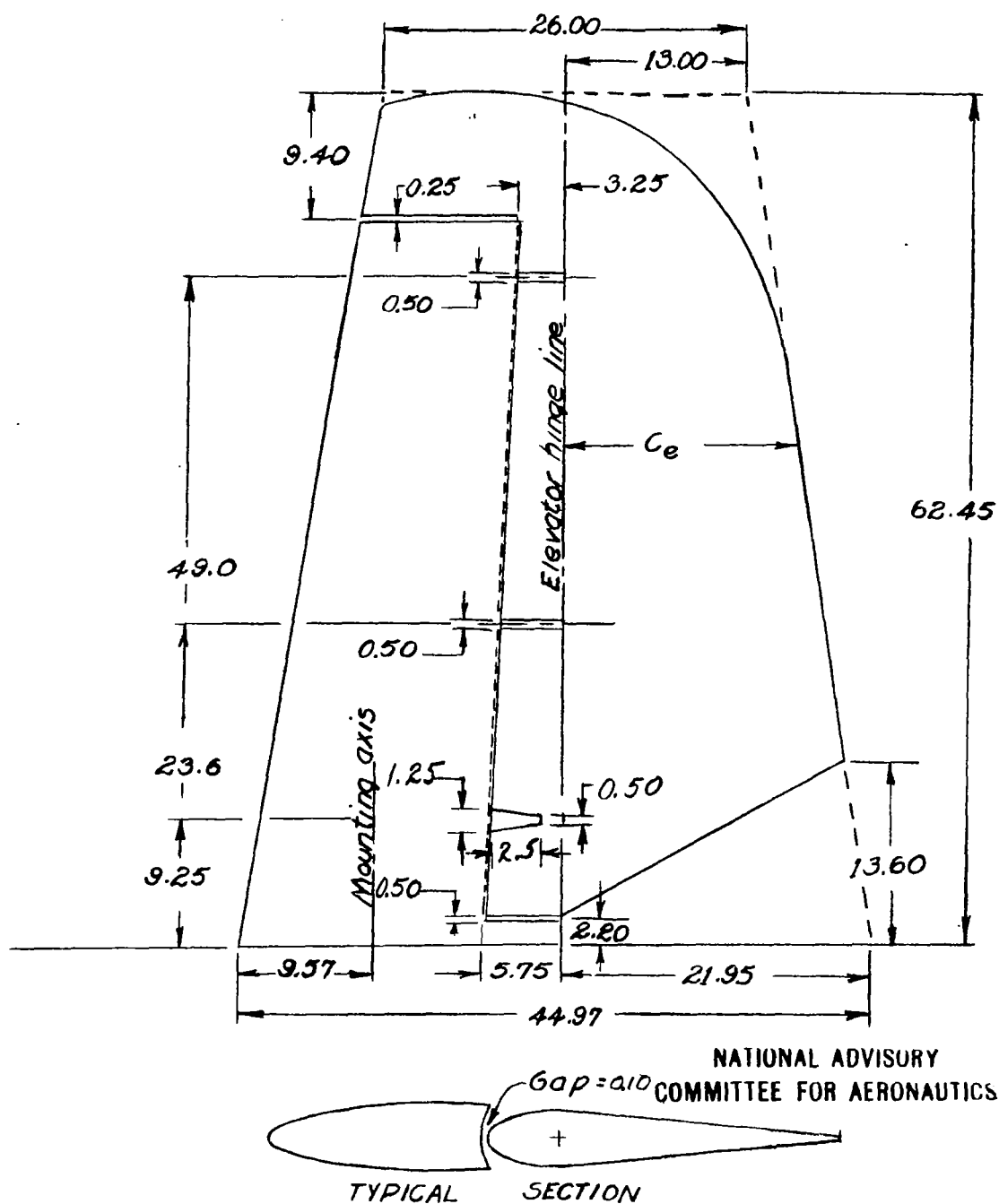
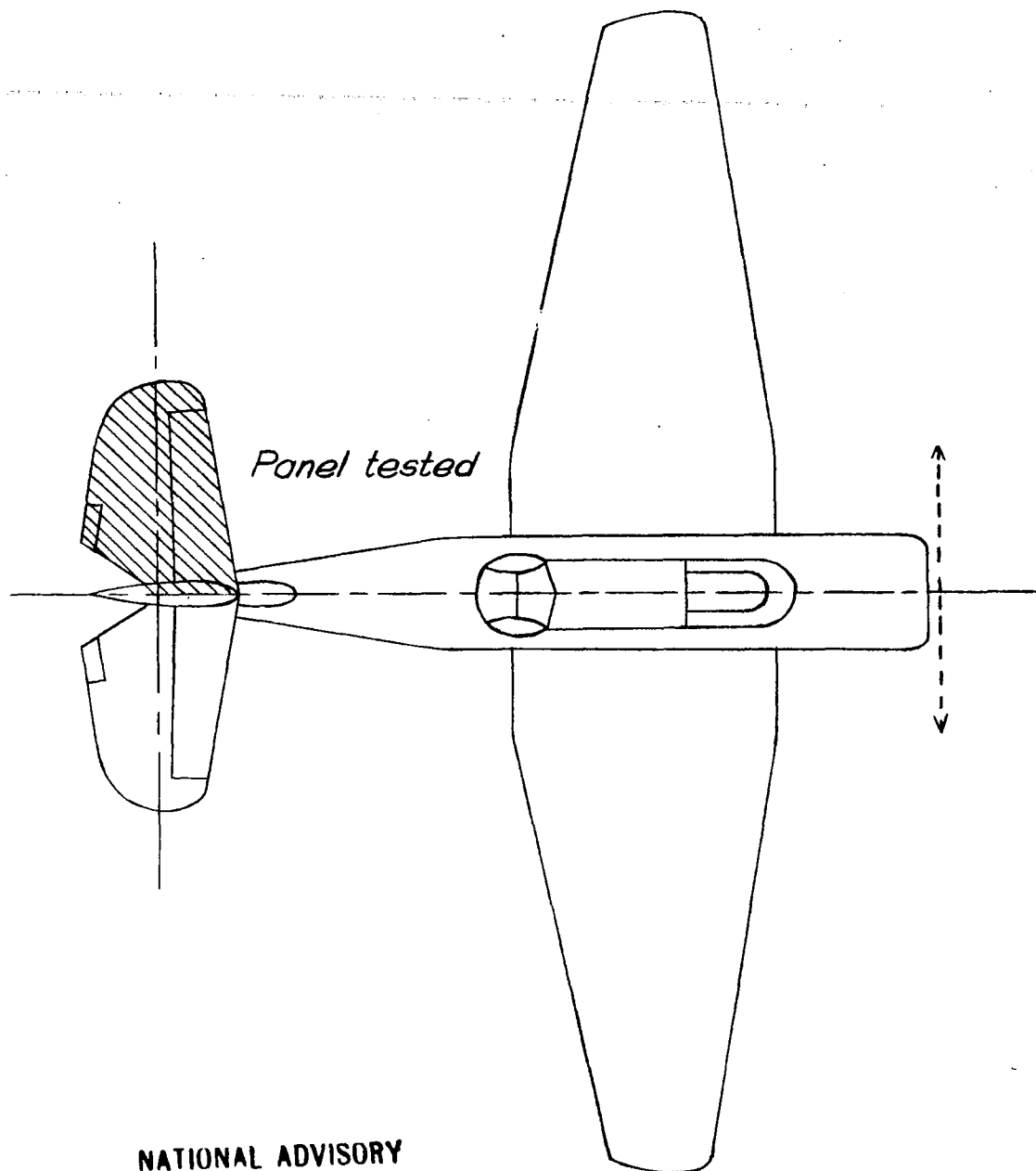
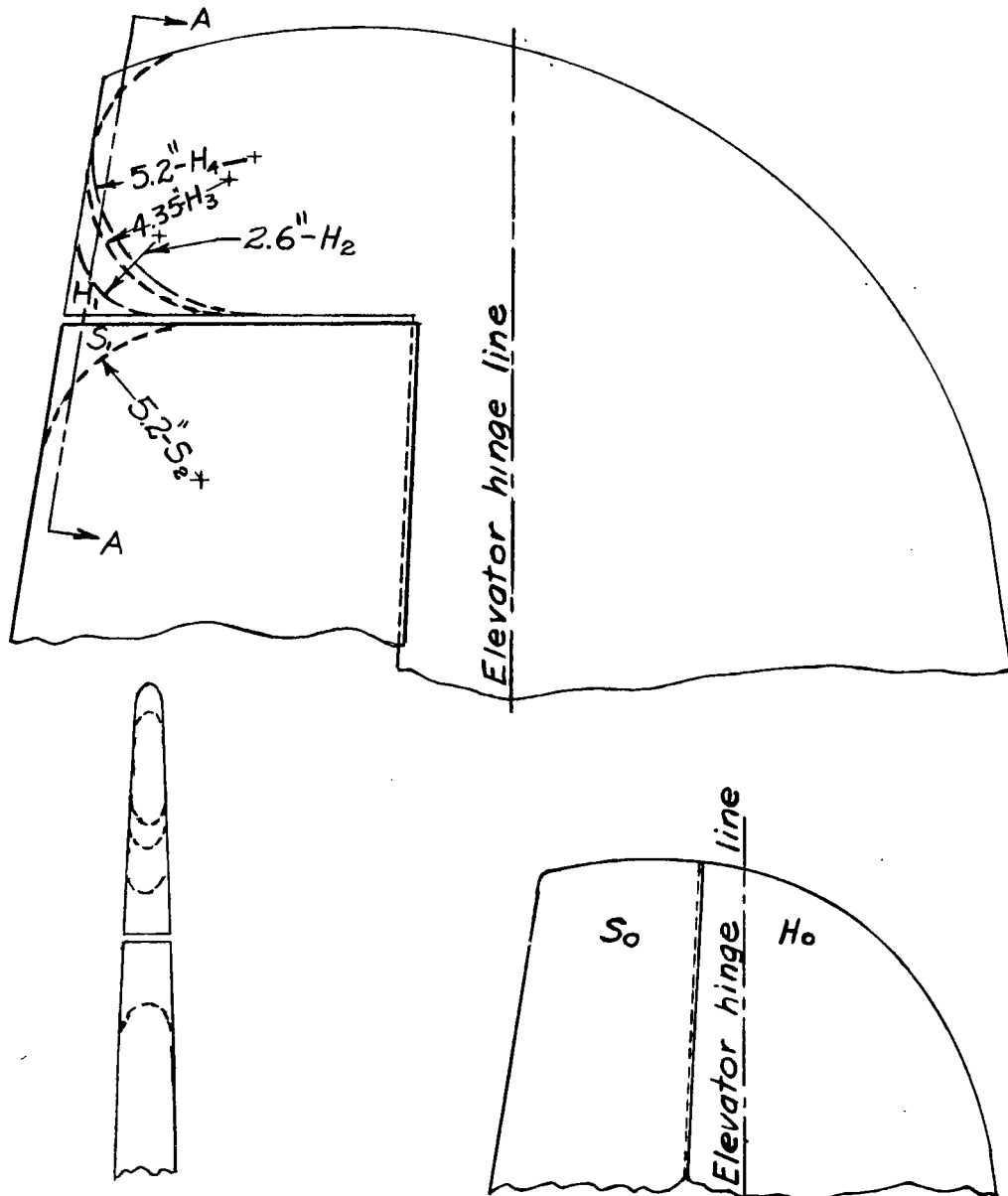


Figure 2.- The 0.5-scale model of TBF-1 left horizontal tail surface. All dimensions are in inches.



NATIONAL ADVISORY  
COMMITTEE FOR AERONAUTICS

Figure 3.- Plan form of the Grumman TBF-1  
airplane.

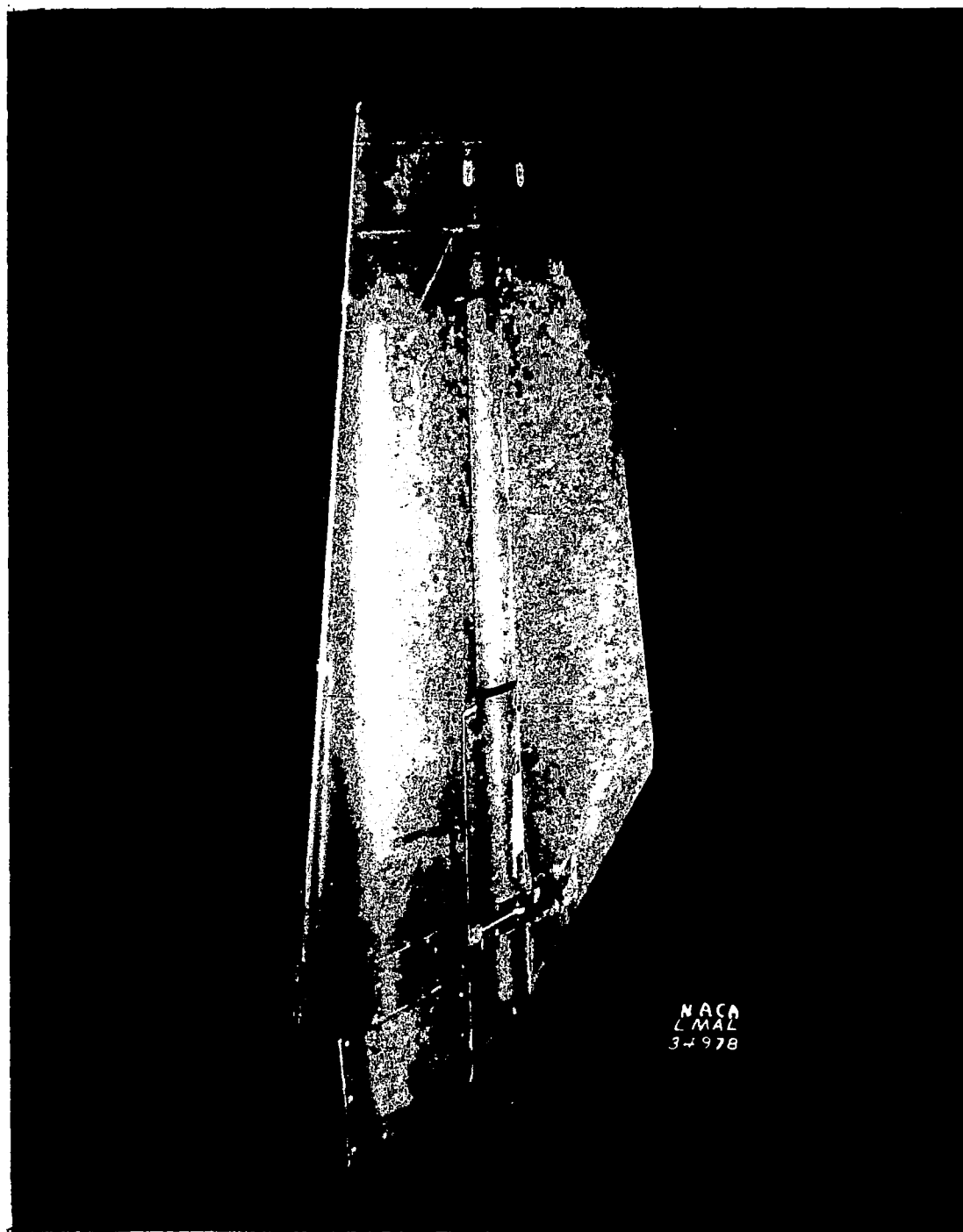


Section A-A

NATIONAL ADVISORY  
COMMITTEE FOR AERONAUTICS

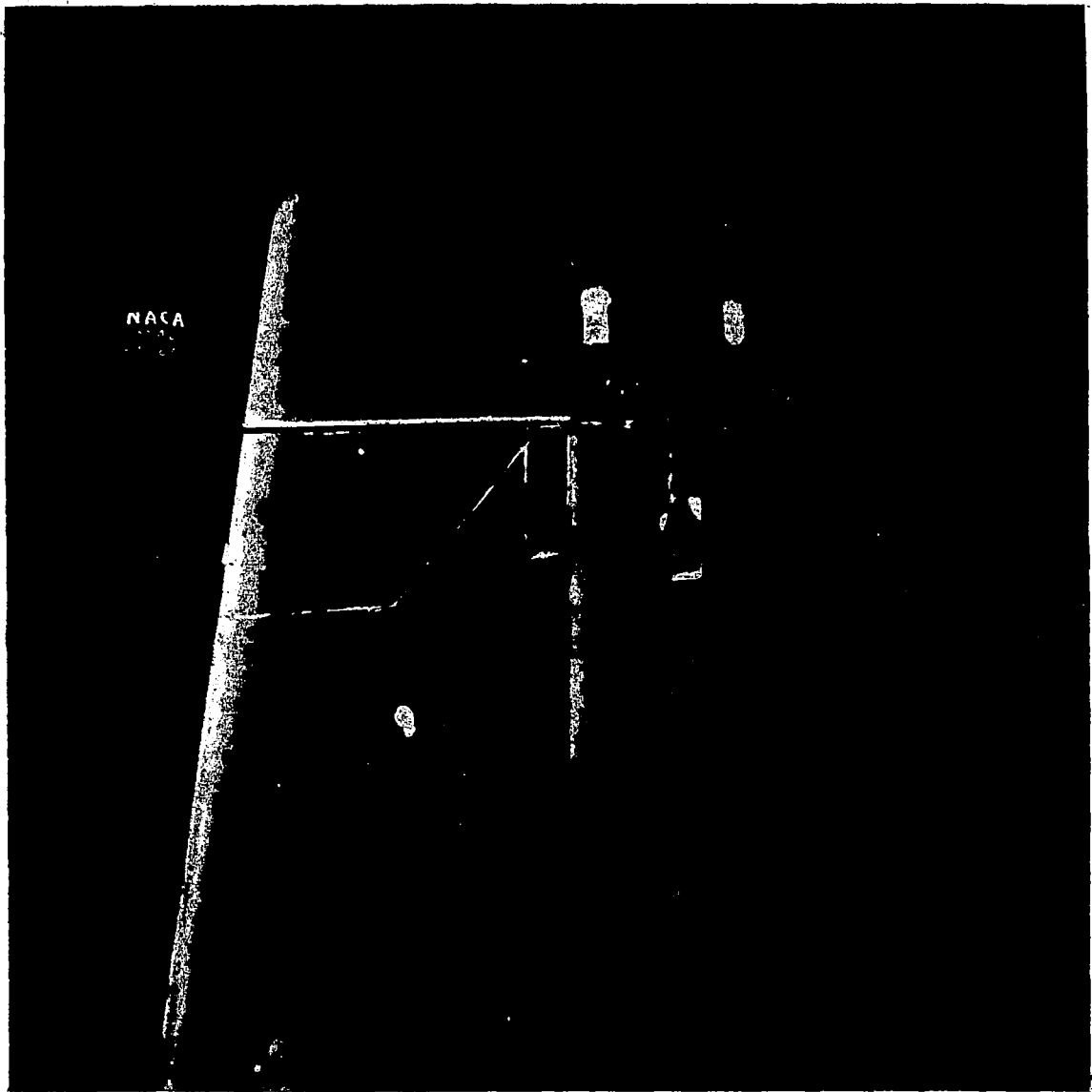
Full span stabilizer  
with no horn

Figure 4. - Details of horn and stabilizer modifications tested on the 0.5-scale model TBF-1 left horizontal tail surface. ( $H, S$ , Original horn and stabilizer).



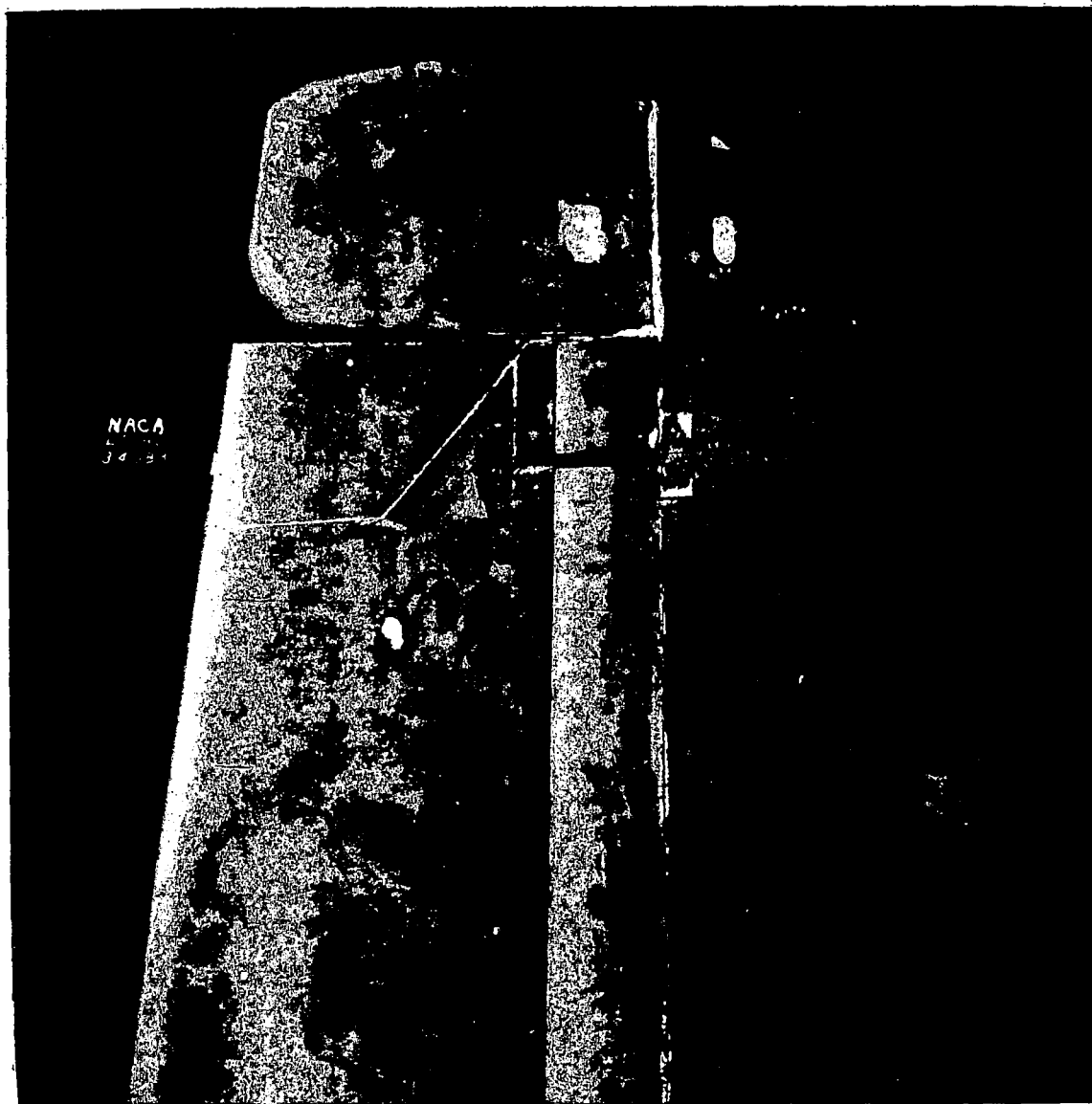
(a)  $\text{H}_2\text{SO}_4$ .

Figure 5.- Photographs of 0.5-scale semispan model of horizontal tail surface of TBF-1 airplane showing configurations tested.



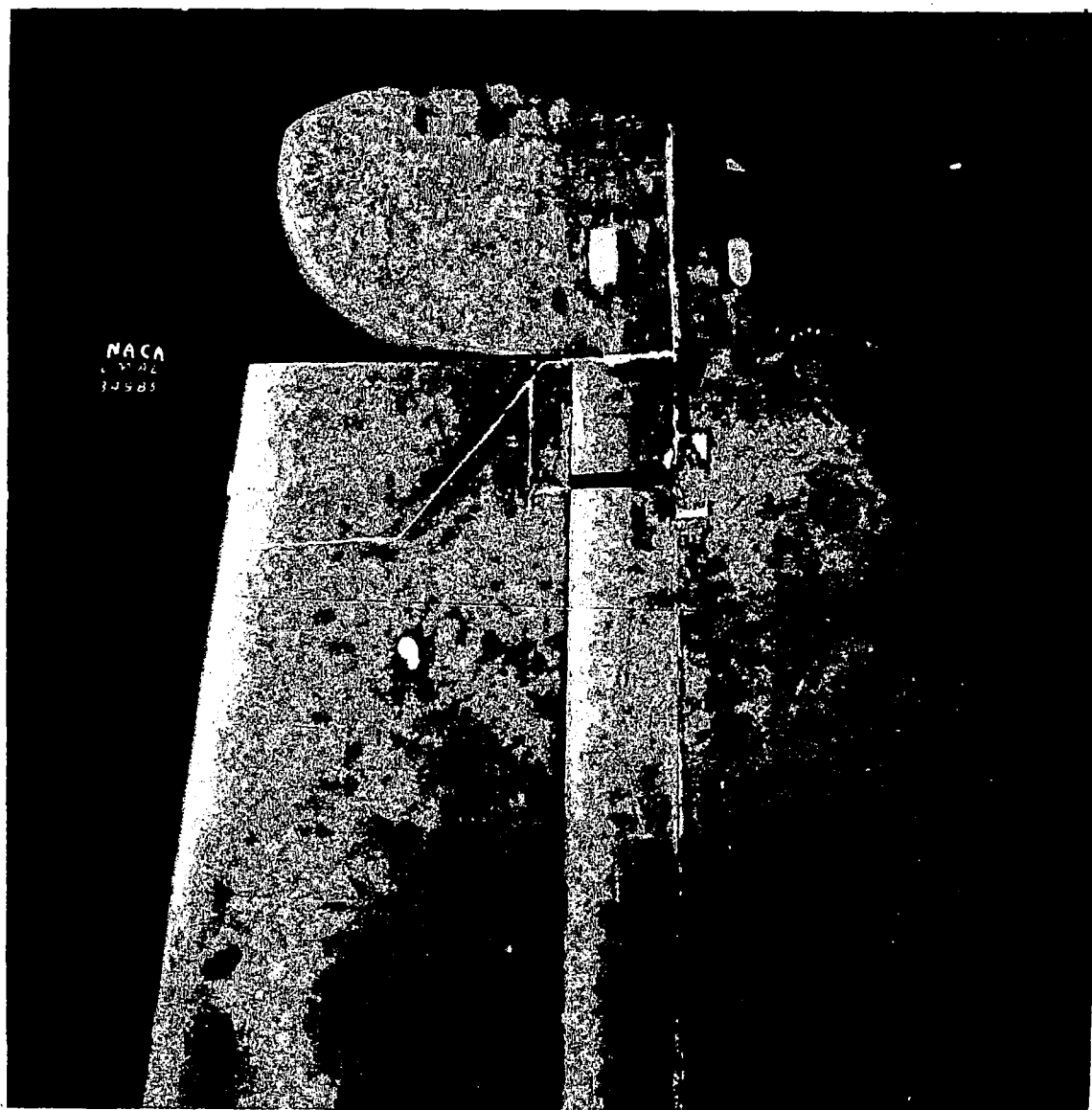
(b)  $H_1S_1$ .

Figure 5.- Continued.



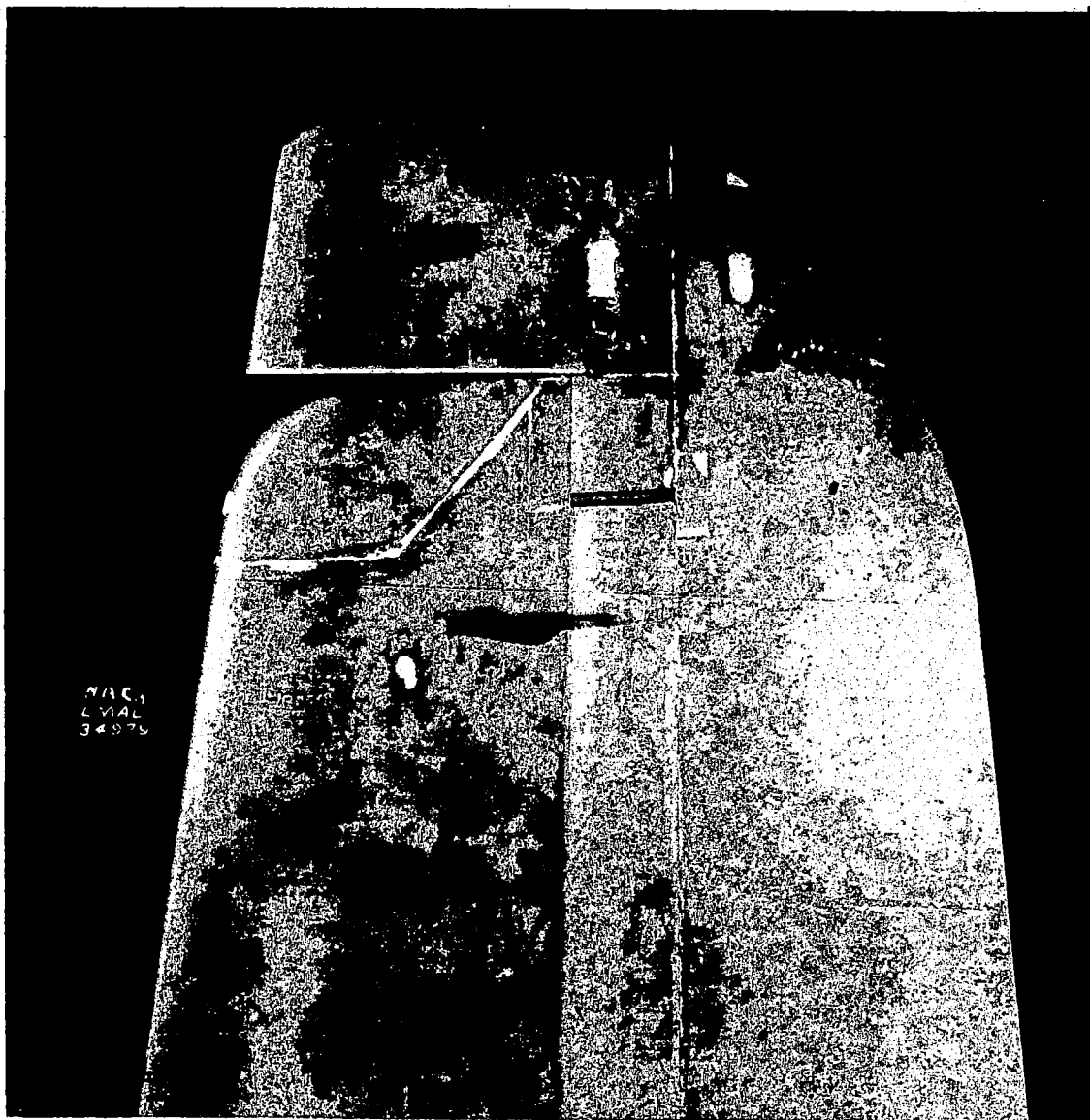
(c)  $H_2S_1$ .

Figure 5.- Continued.



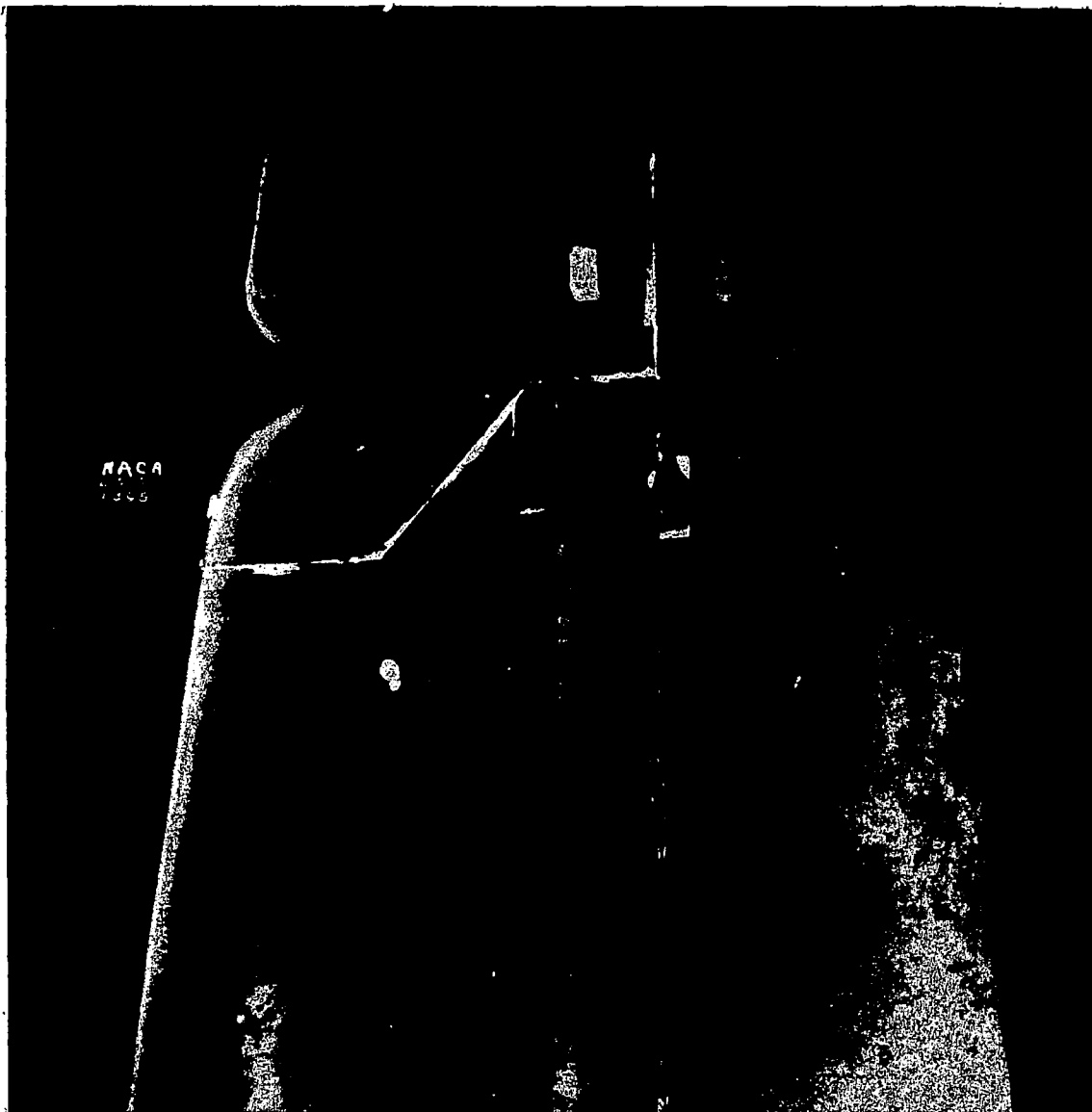
(d)  $H_4S_1$ .

Figure 5.- Continued.



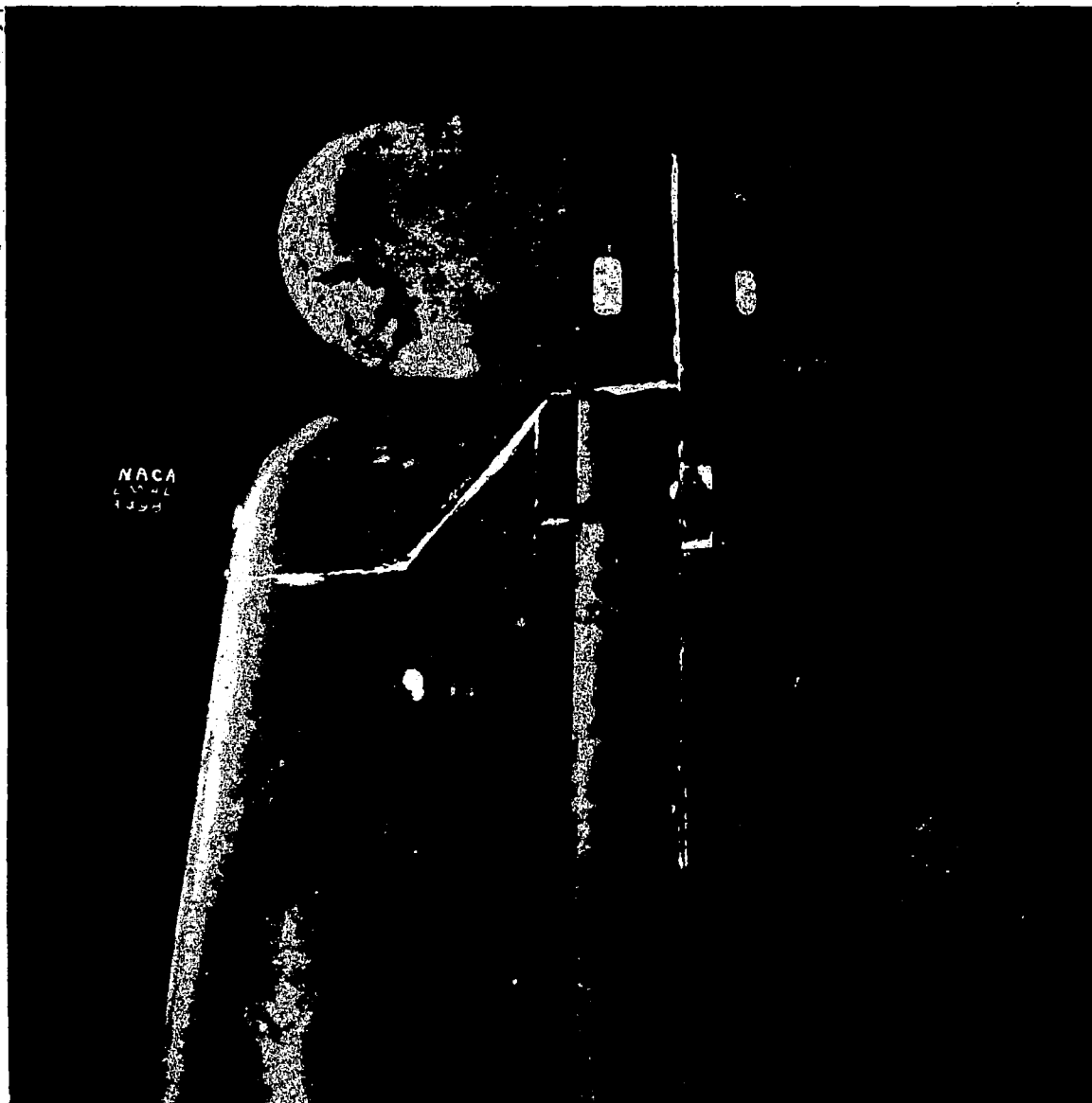
(e)  $H_1S_2$ .

Figure 5.- Continued.



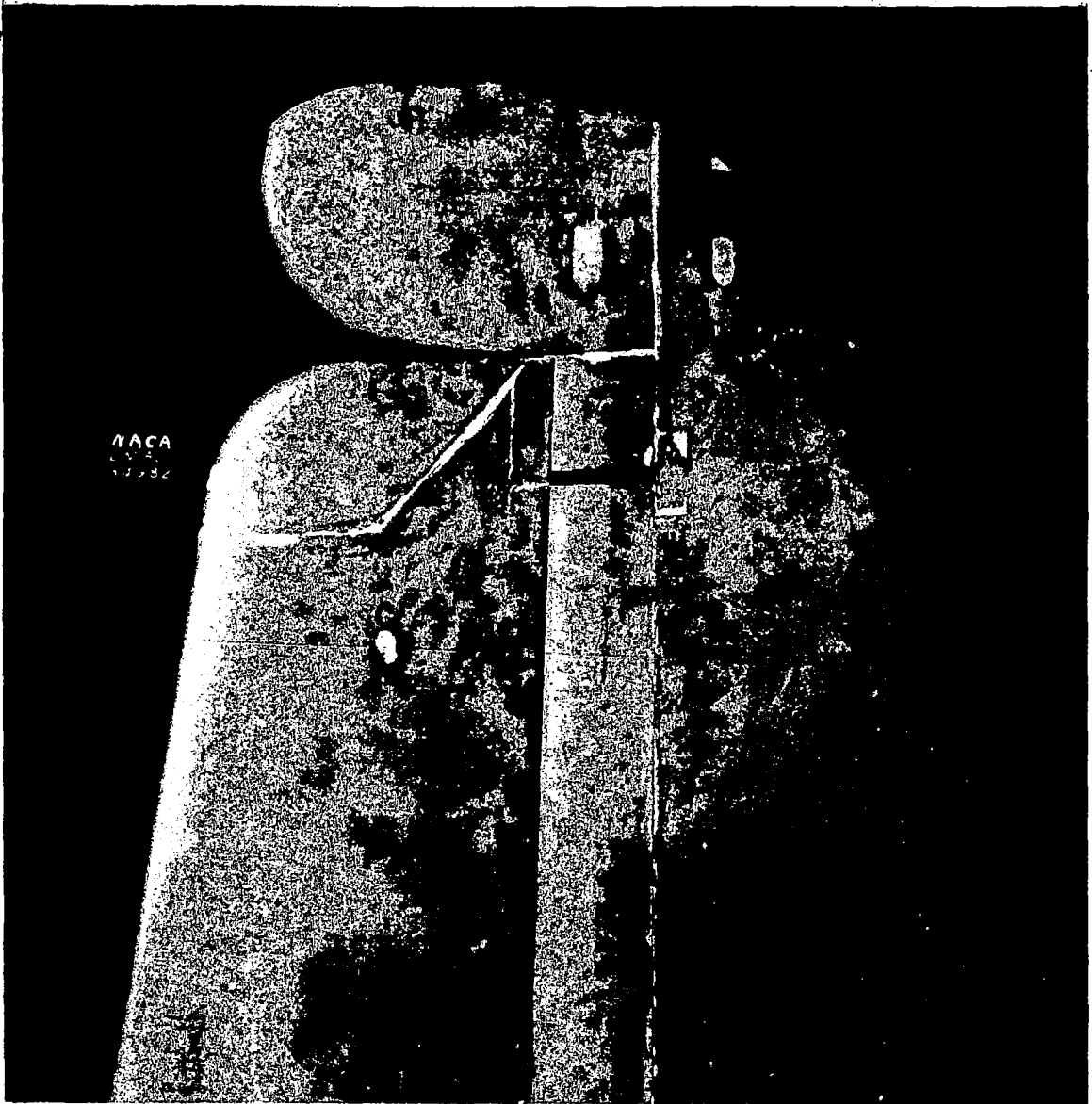
(f)  $\text{H}_2\text{S}_2$ .

Figure 5.- Continued.



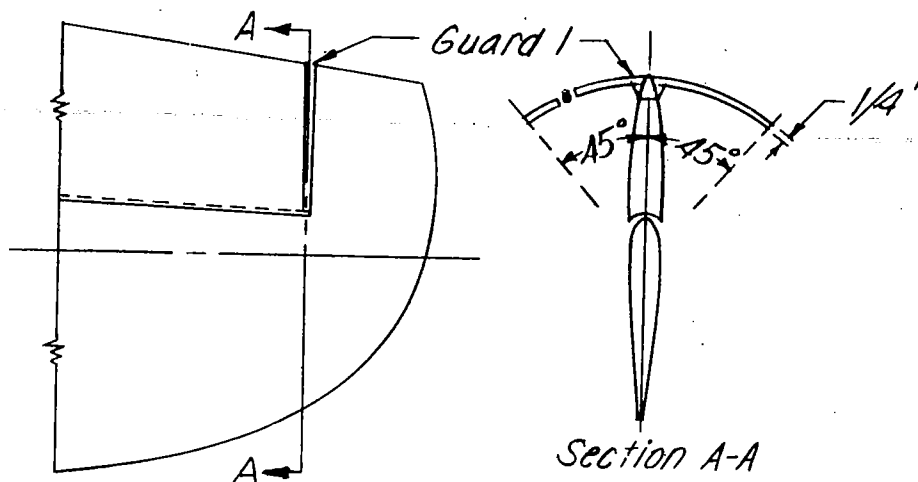
(g)  $H_3S_2$ .

Figure 5.- Continued.

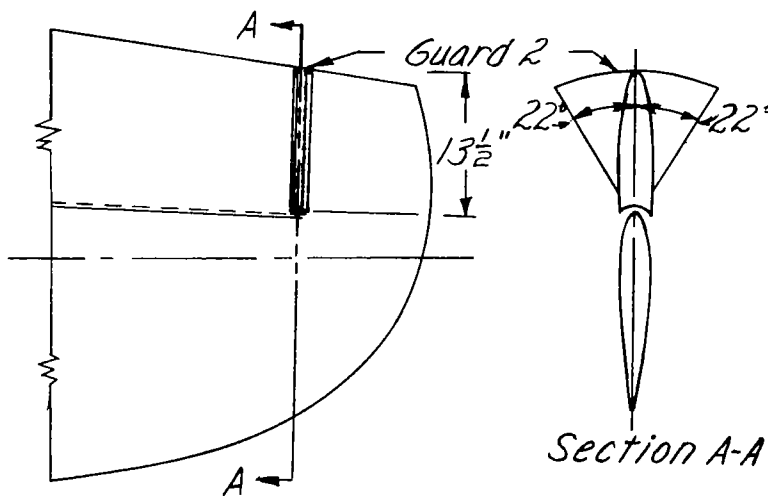


(h)  $H_4S_2$ .

Figure 5.- Concluded.



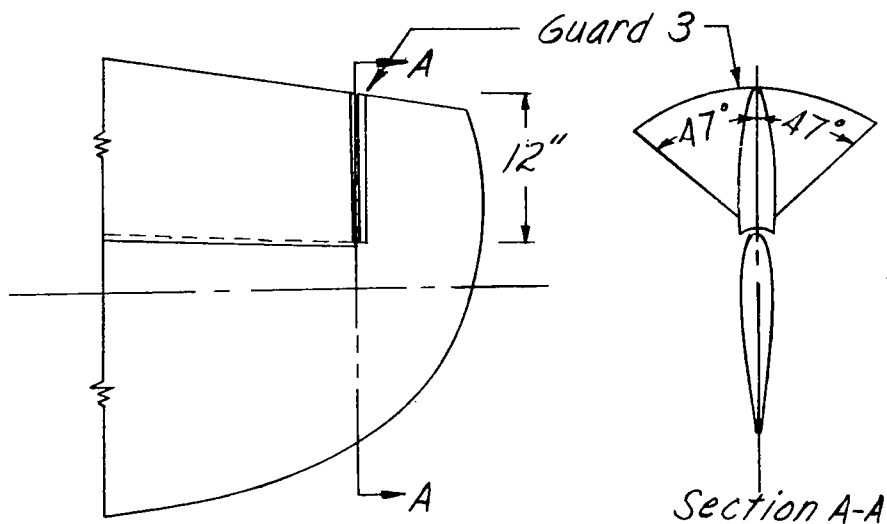
(a) Guard 1;  $\frac{1}{16}$ -inch steel; guard attached to stabilizer.



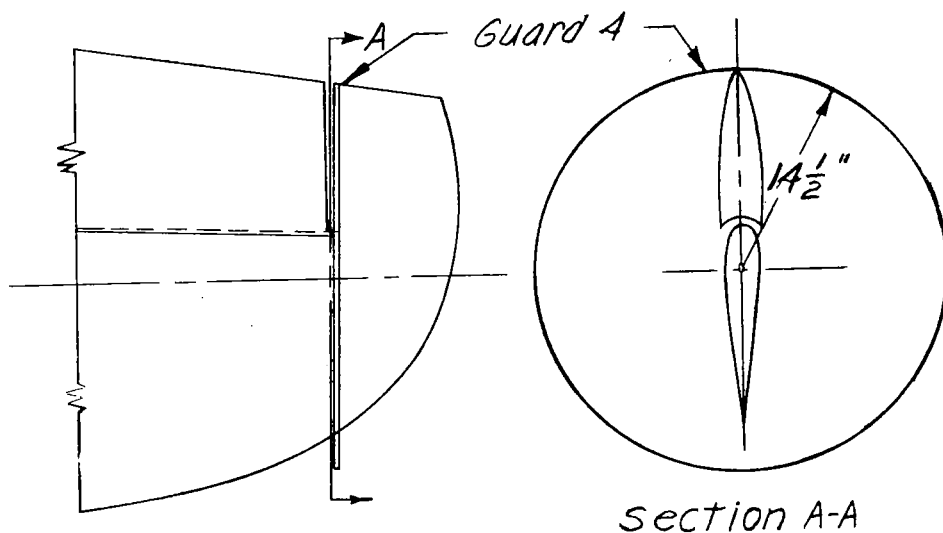
NATIONAL ADVISORY  
COMMITTEE FOR AERONAUTICS

(b) Guard 2;  $\frac{1}{16}$ -inch steel; one plate on horn and one on stabilizer.

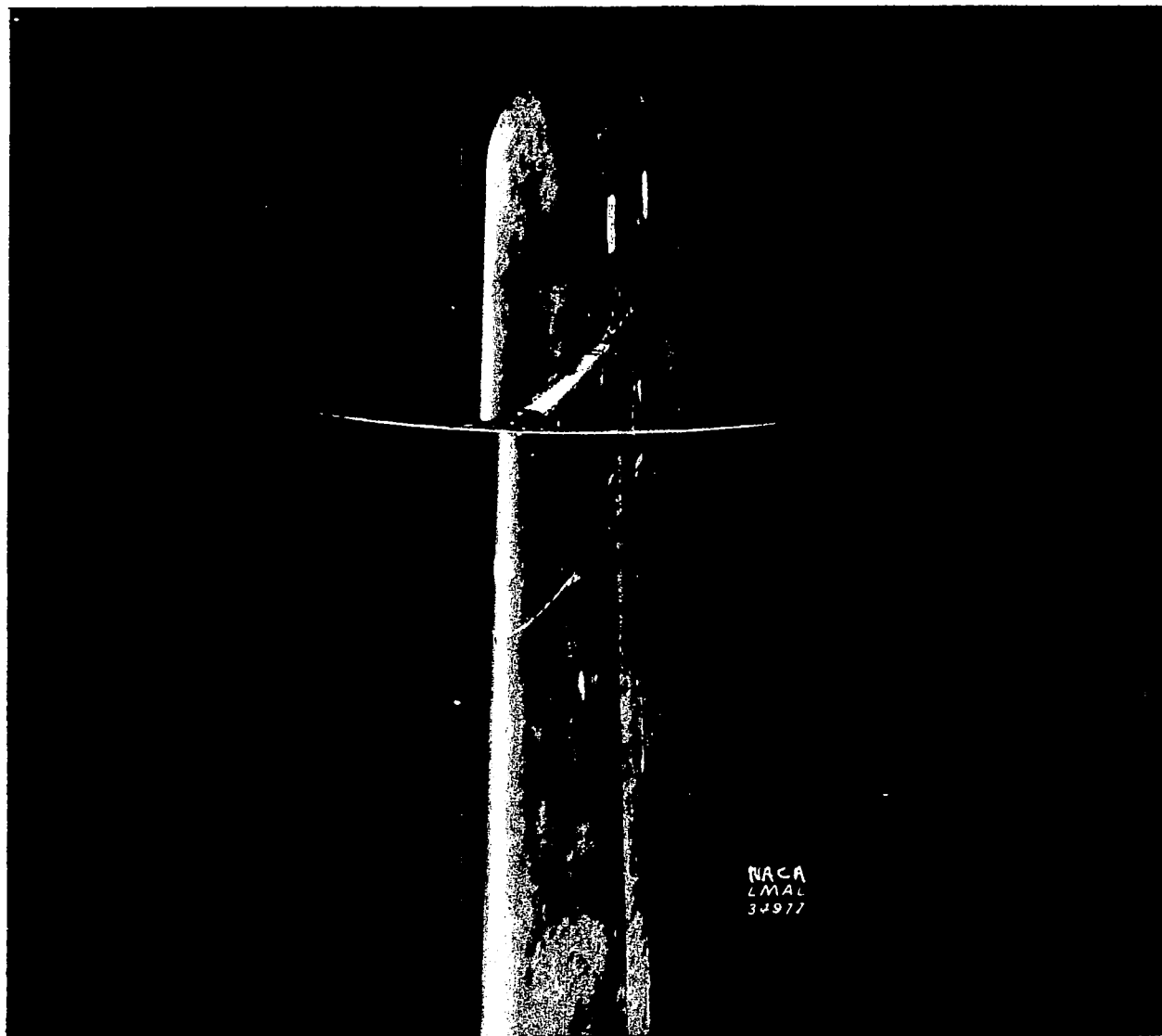
Figure 6.- Details of guards tested on 0.5-scale model TBF-1 left horizontal tail surface with original tail horn ( $H_1 S_1$ ).



(c) Guard 3 ; 1/4-inch masonite ; guard on horn.

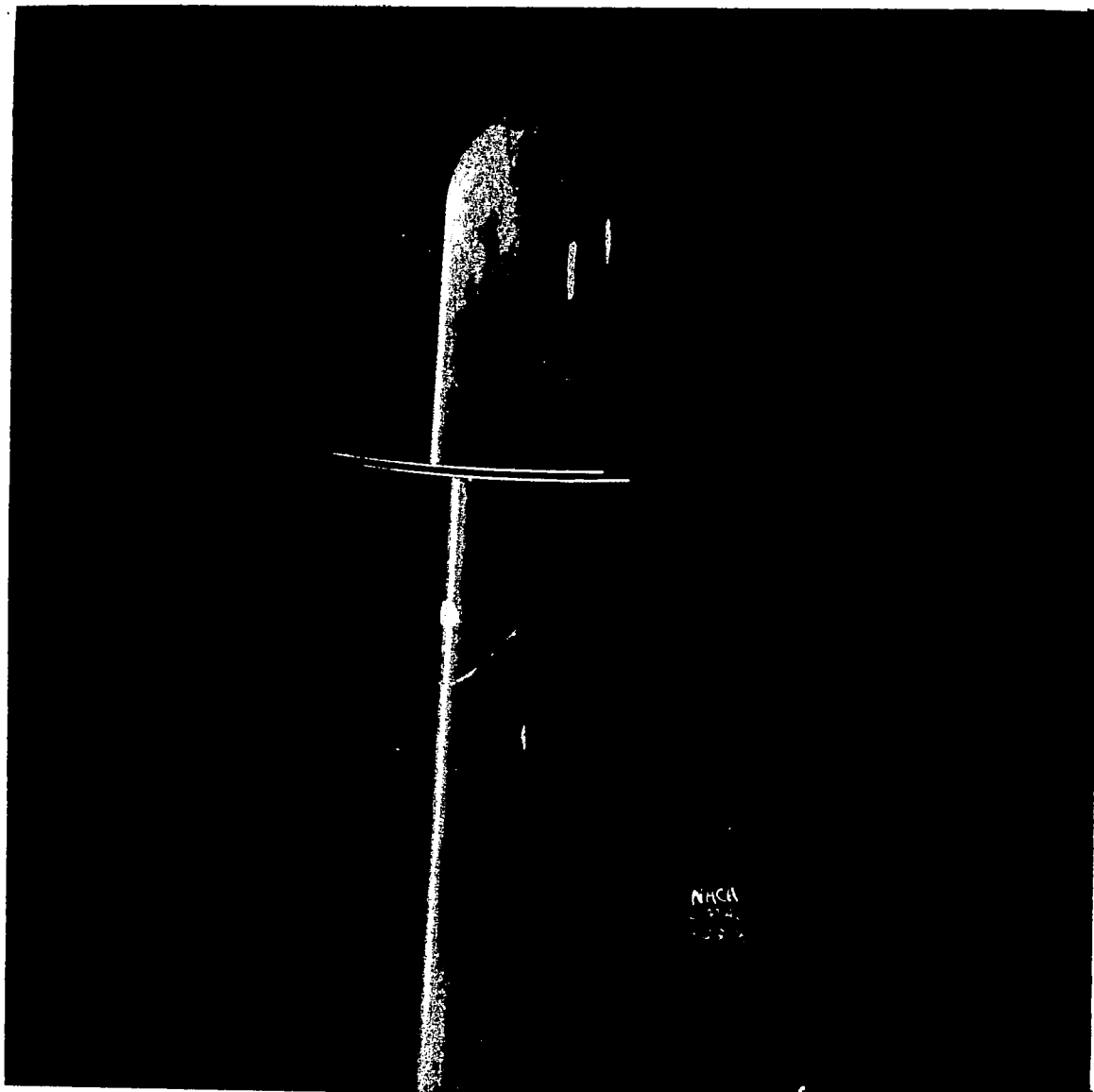


(d) Guard 4 ; 1/4 inch masonite ; guard attached to horn and elevator.

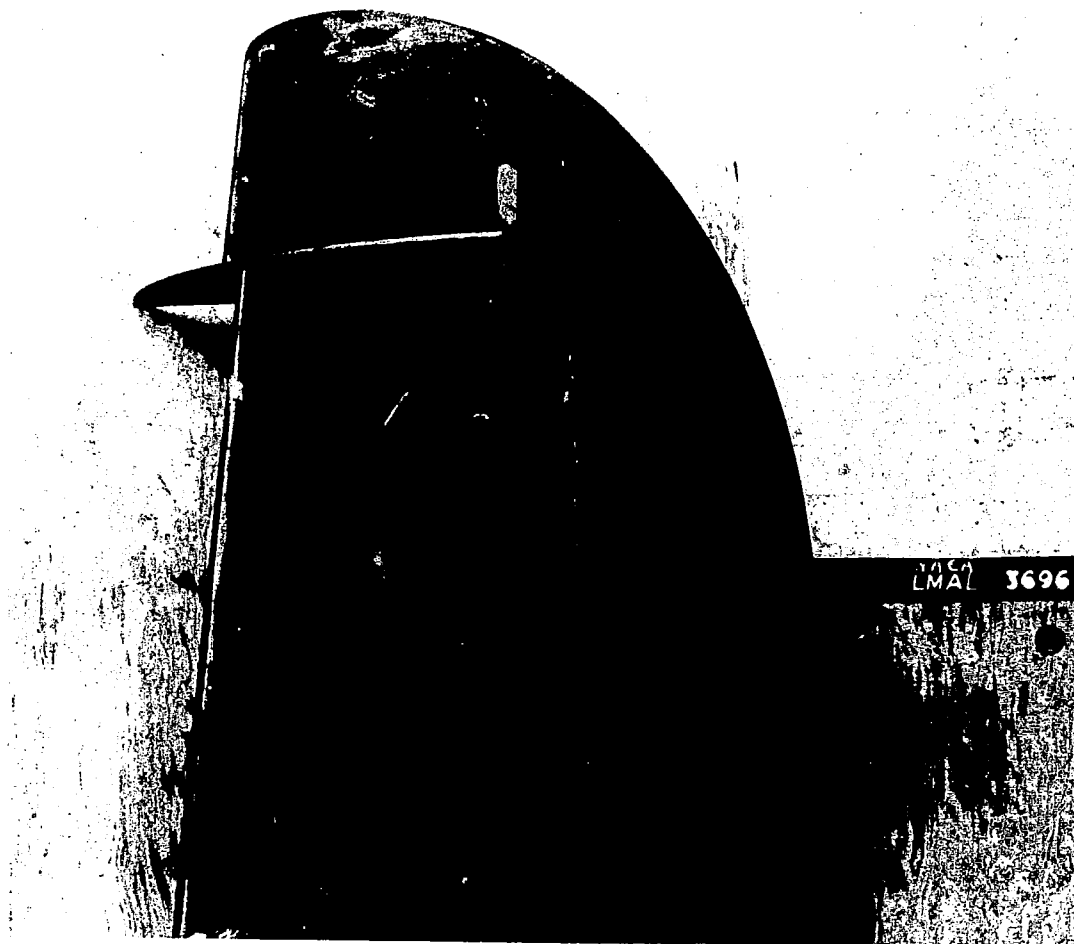


(a) Guard 1.

Figure 7.- Three-quarter front view of various guards on 0.5-scale semispan model of horizontal tail surface of TBF-1 airplane.



(b) Guard 2.

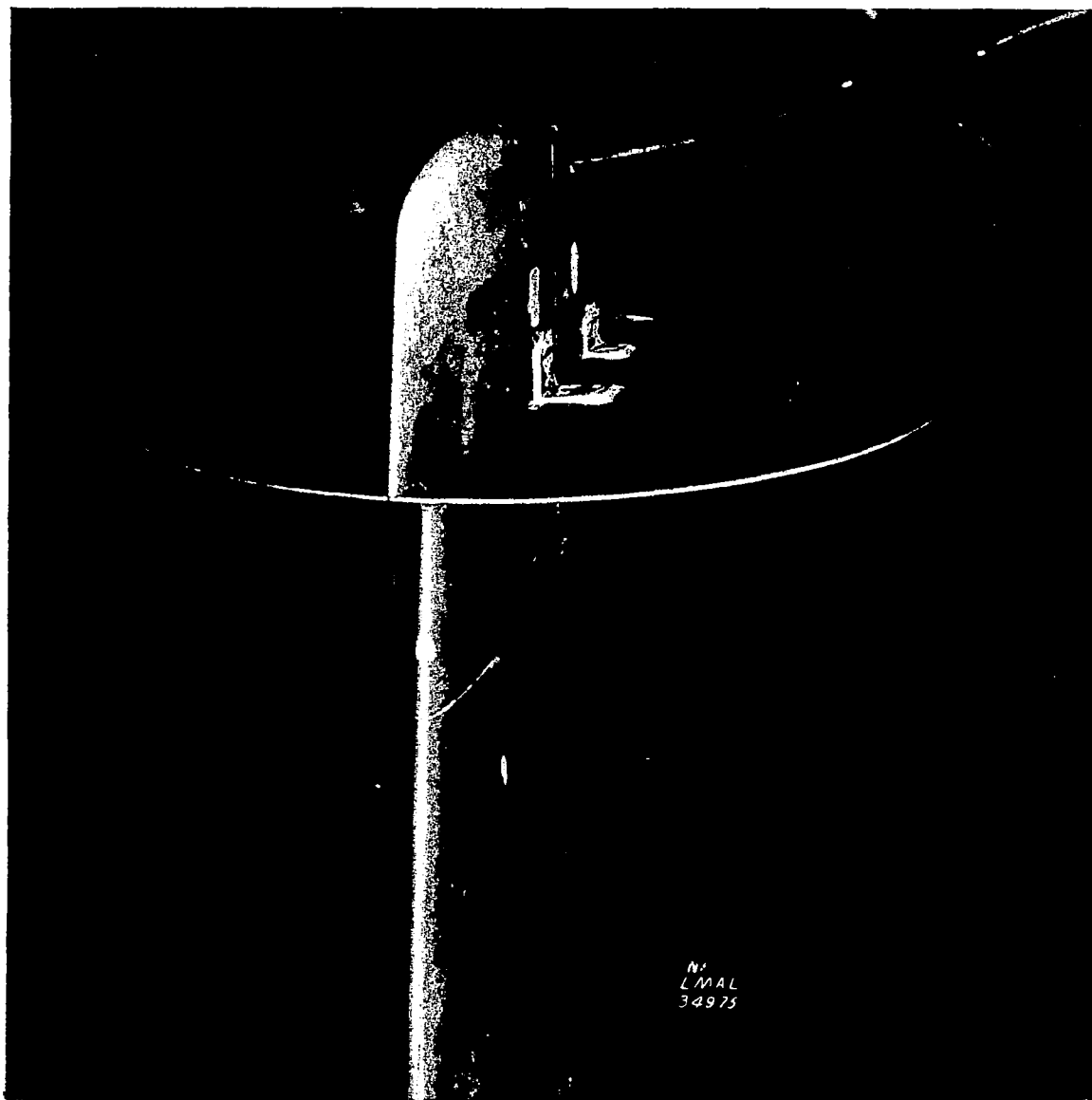


(c) Guard 3.

Figure 7.- Continued.

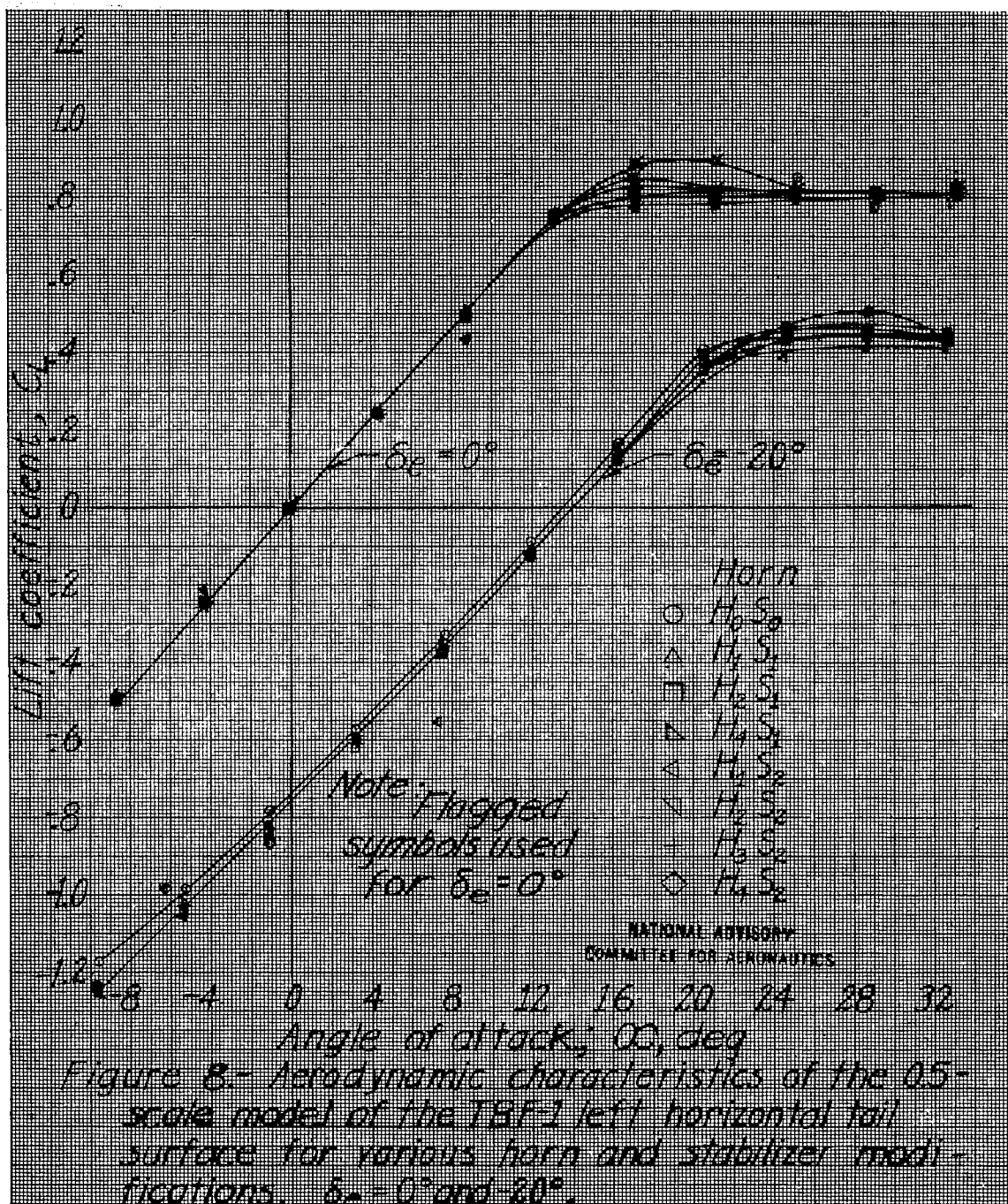
NACA ARR No. L4J16

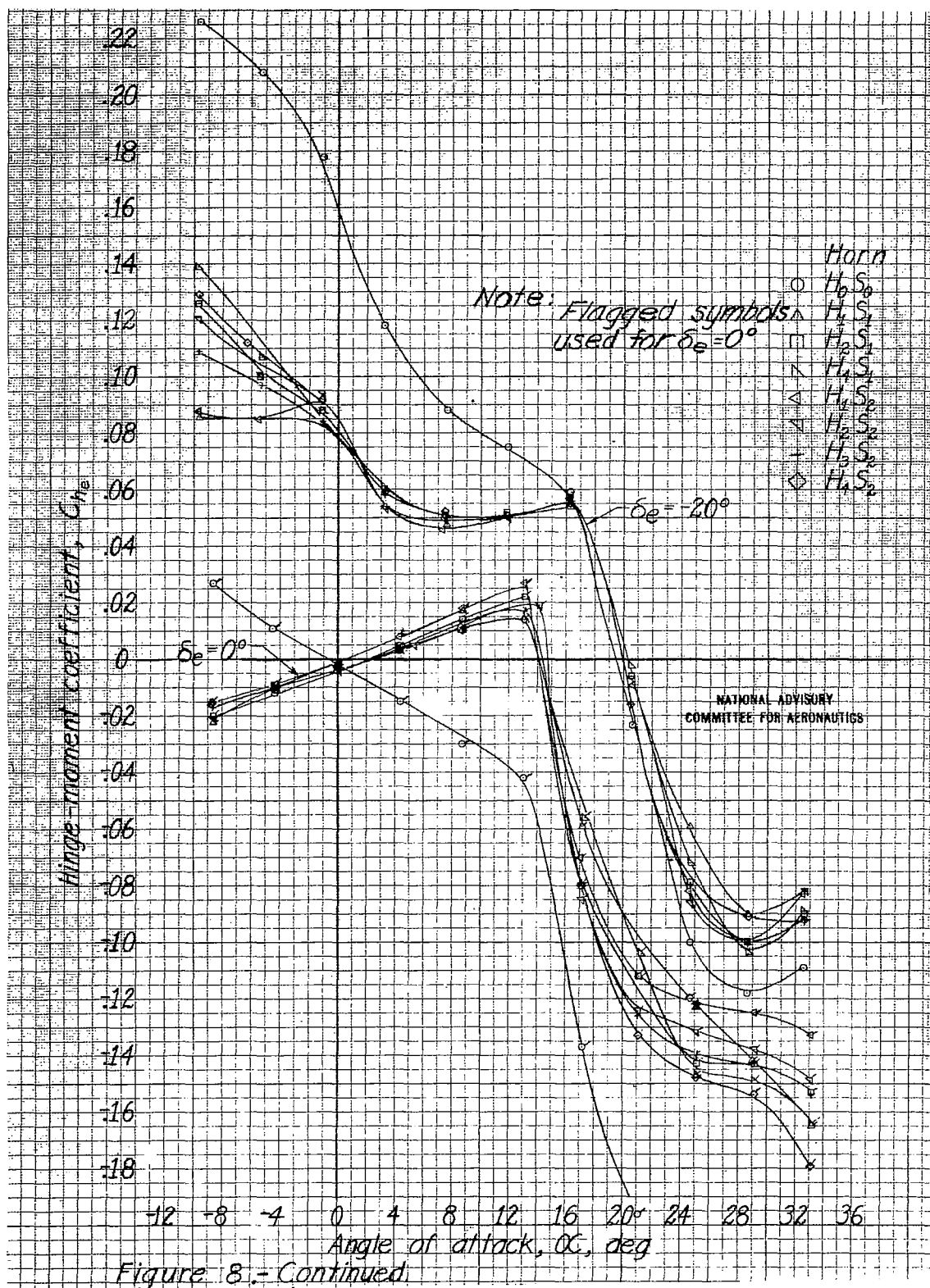
Fig. 7d

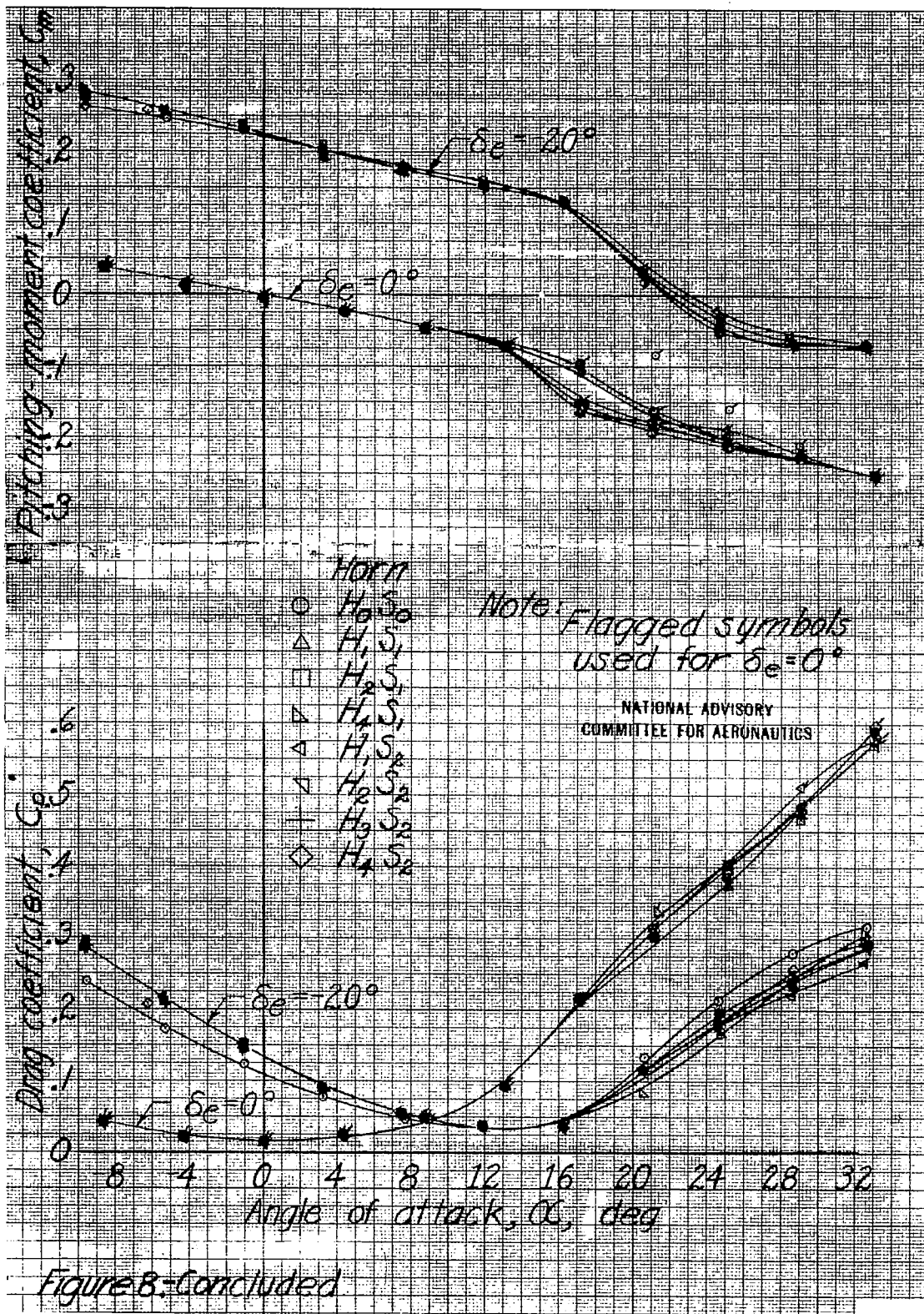


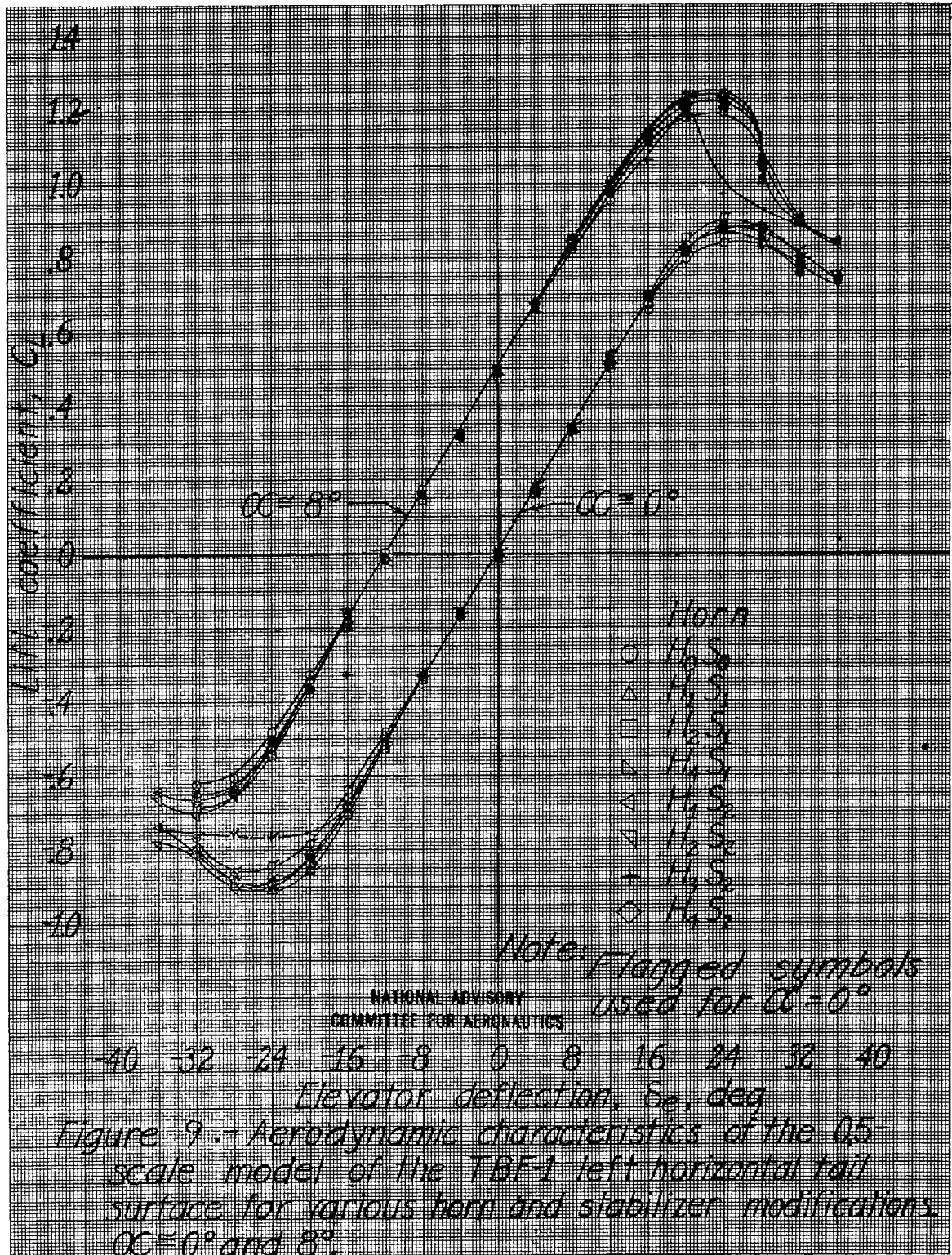
(d) Guard 4.

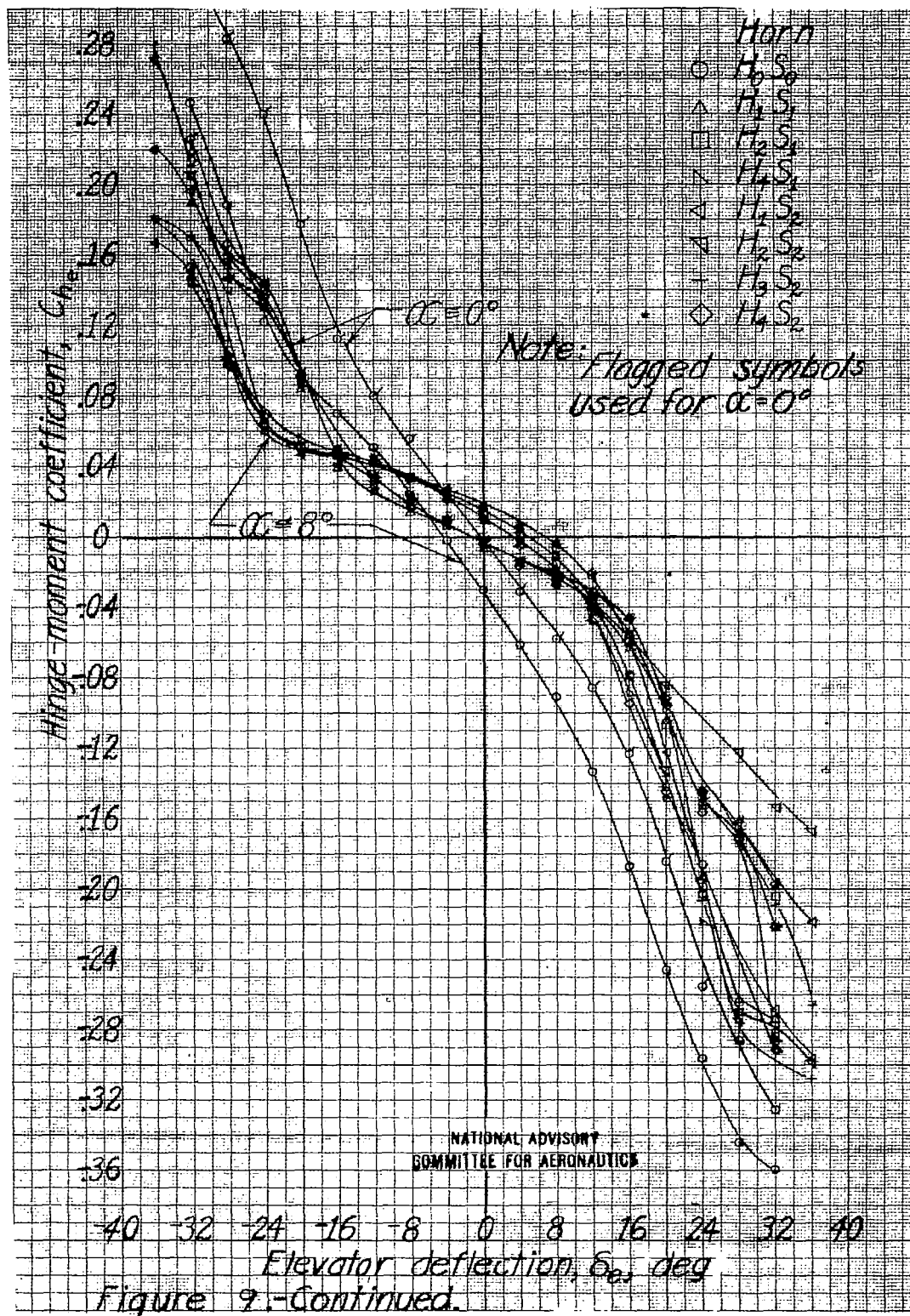
Figure 7.- Concluded.

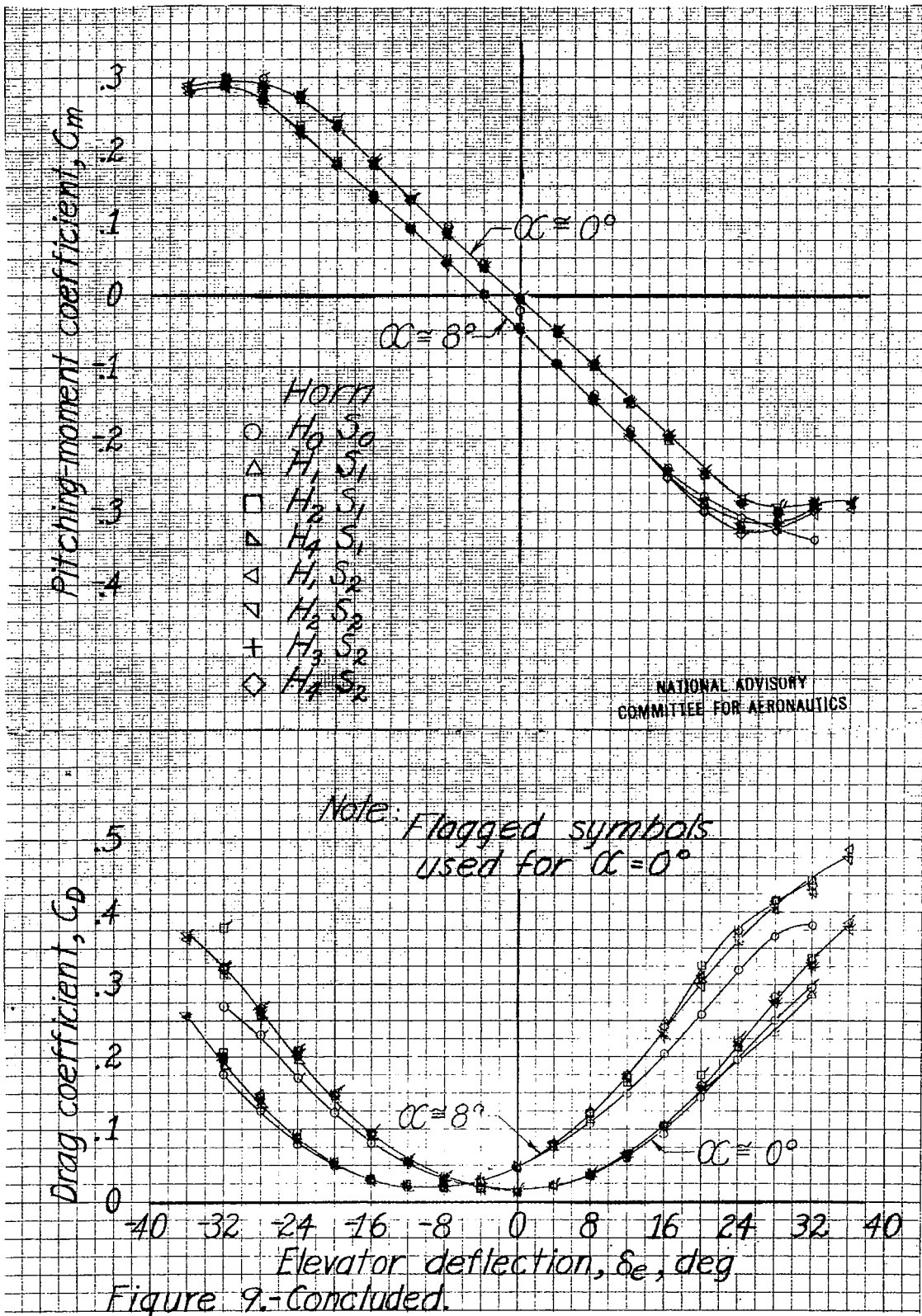












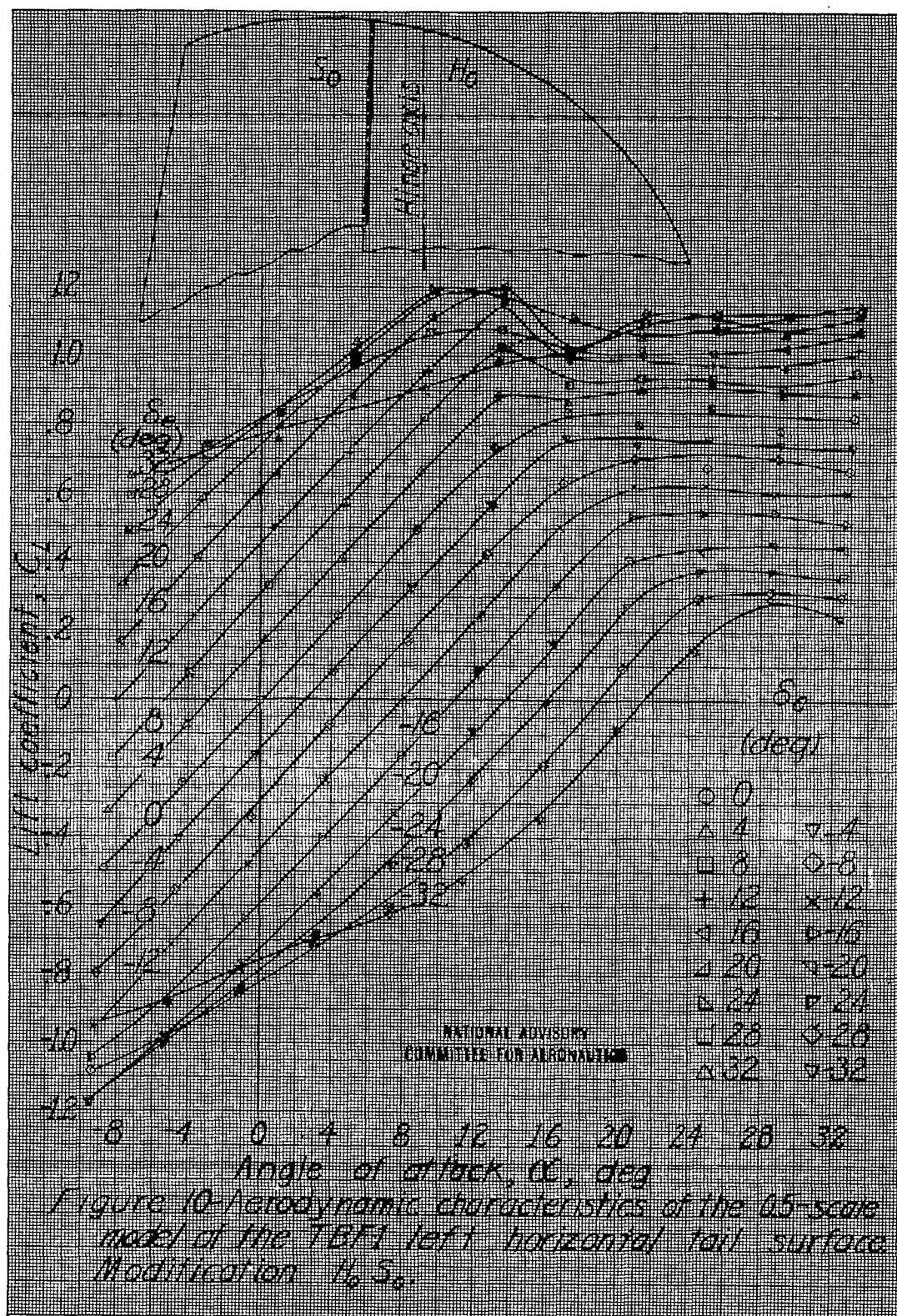
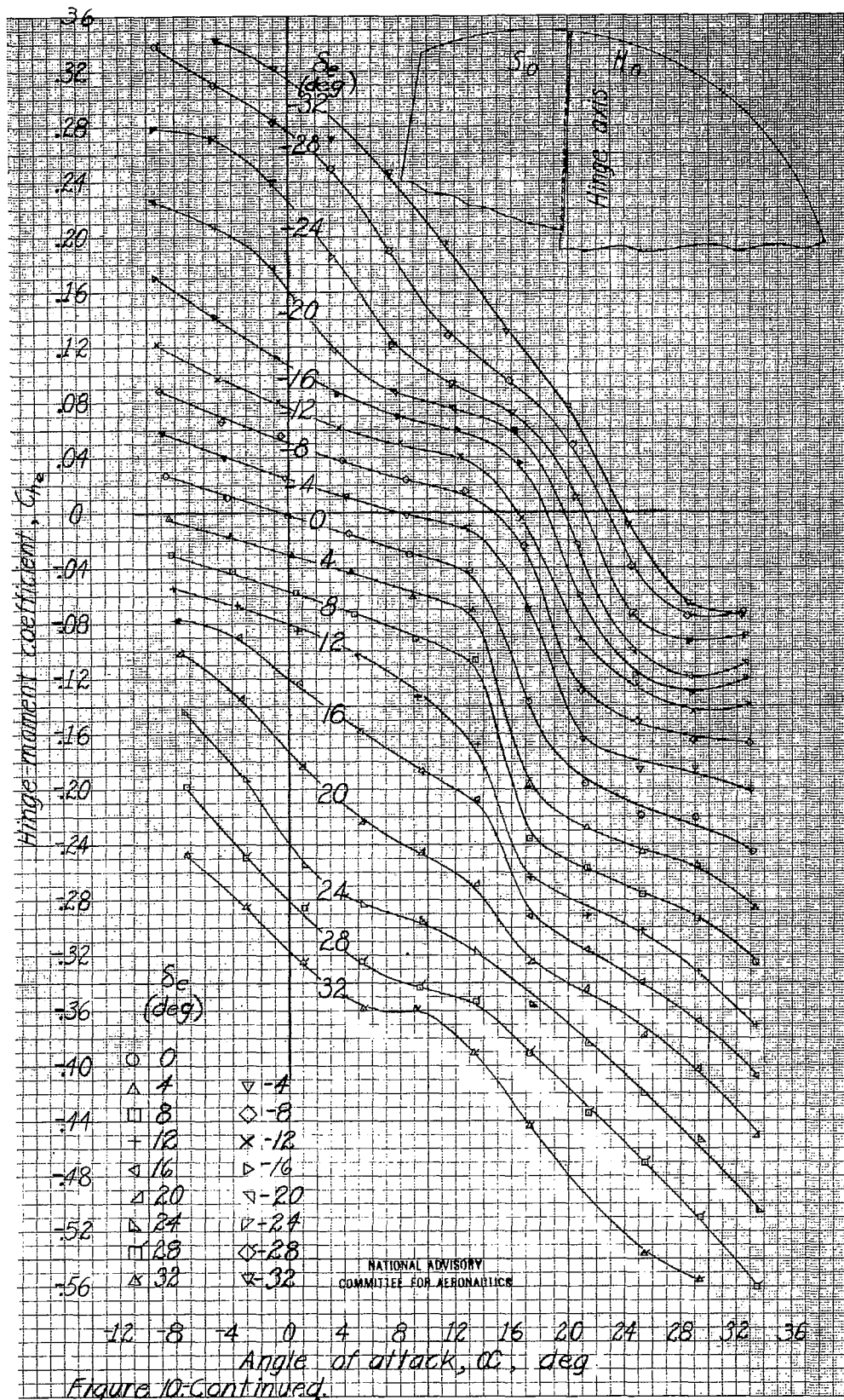
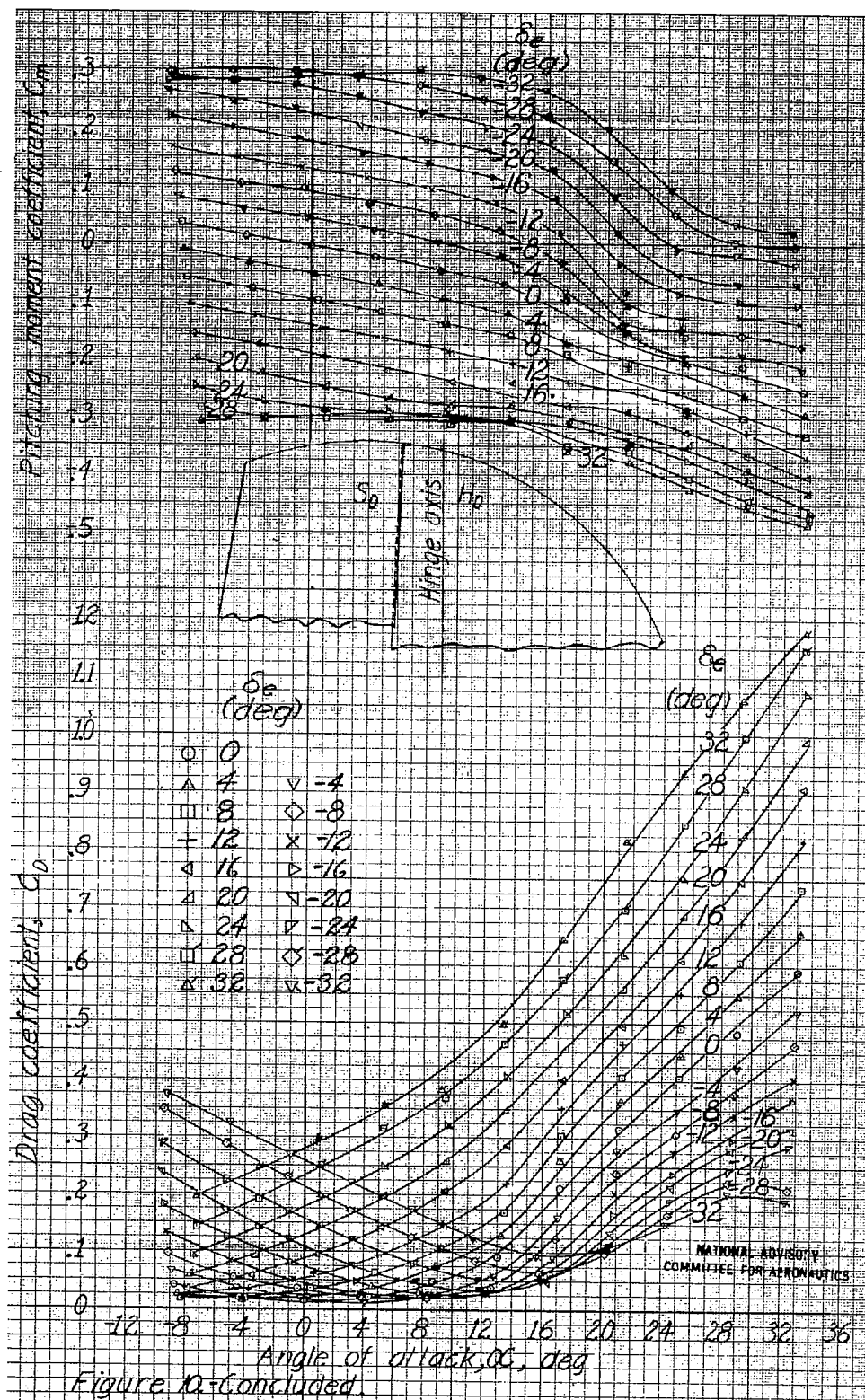
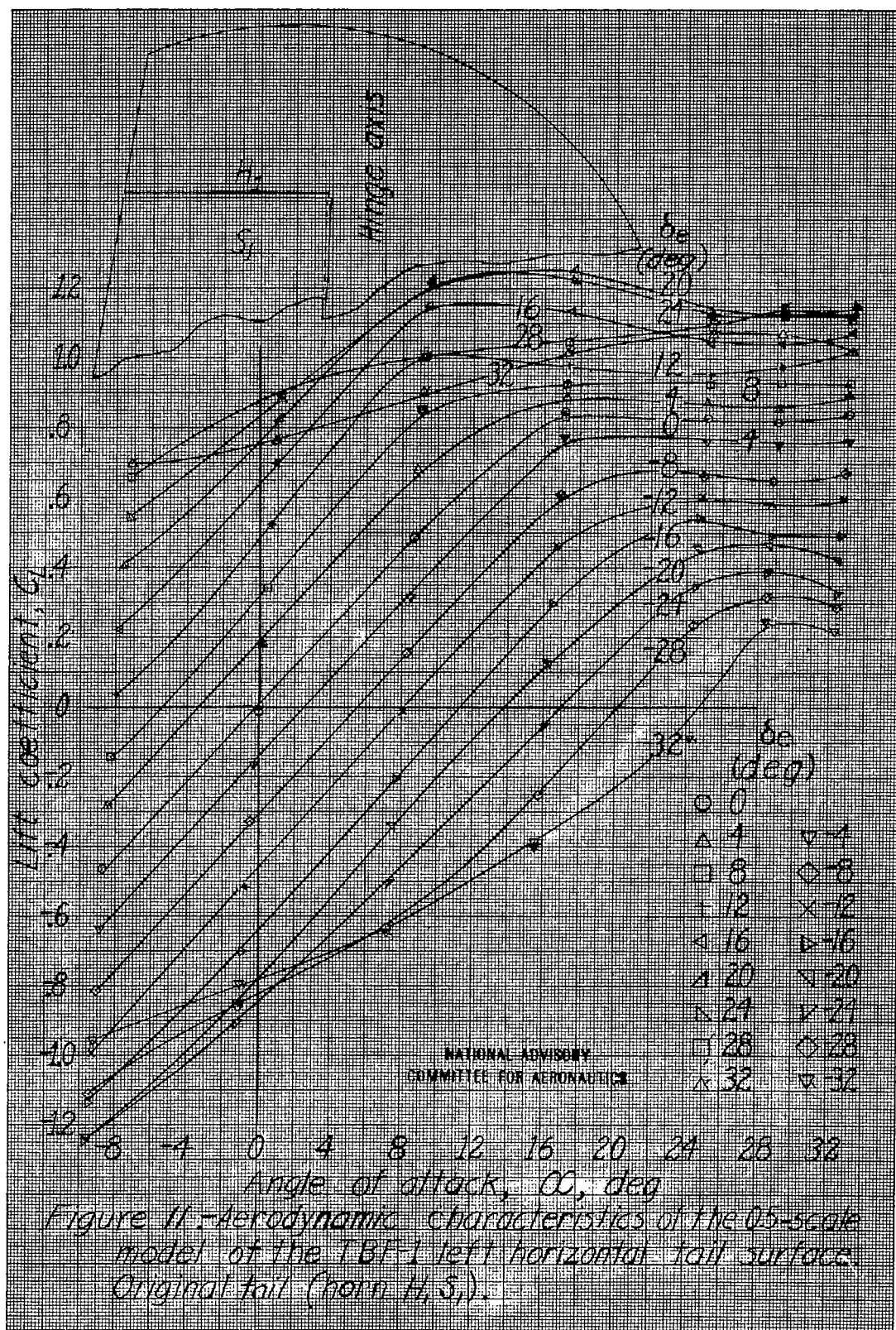


Fig. 10b

NACA ARR No. L4J16-







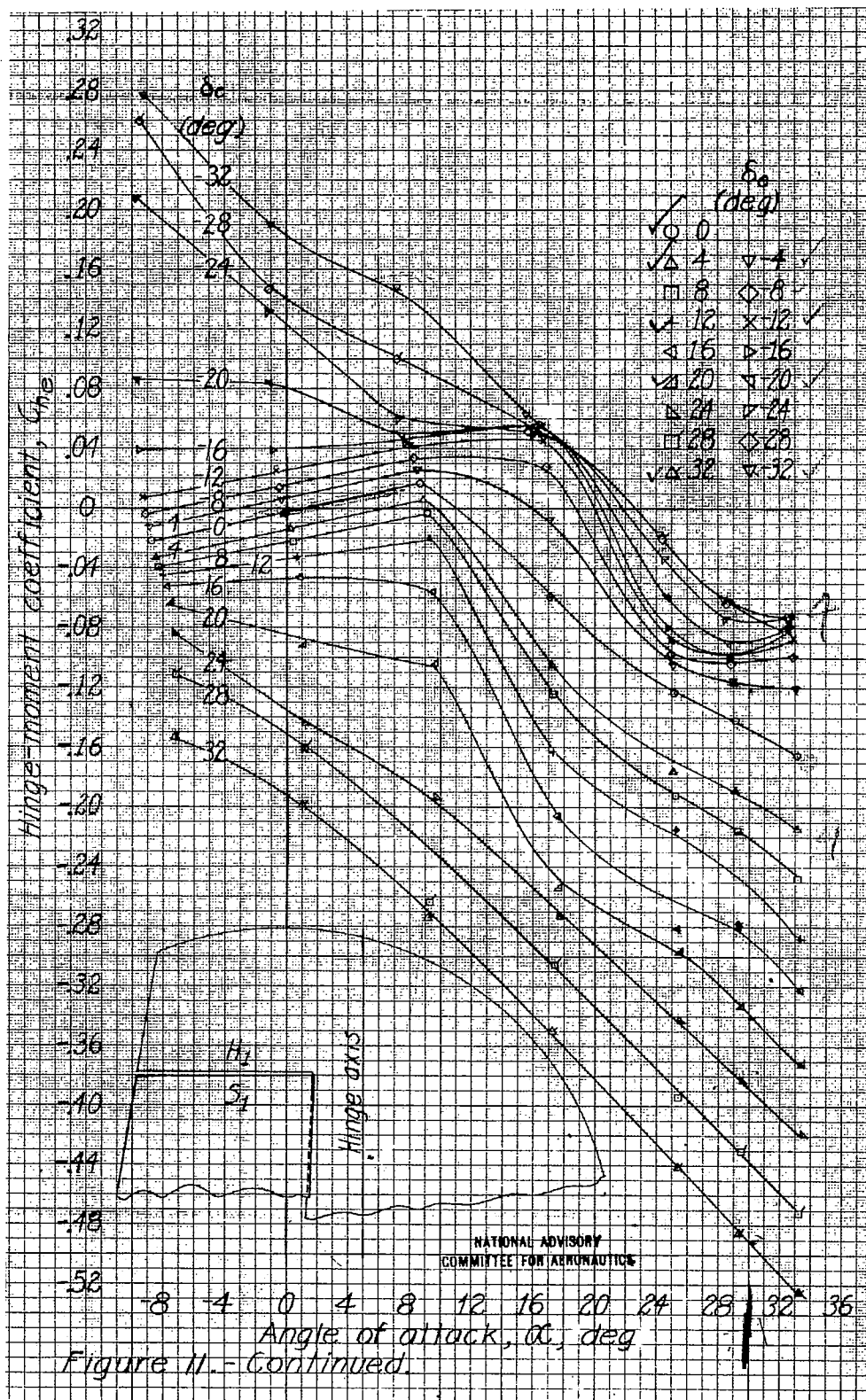
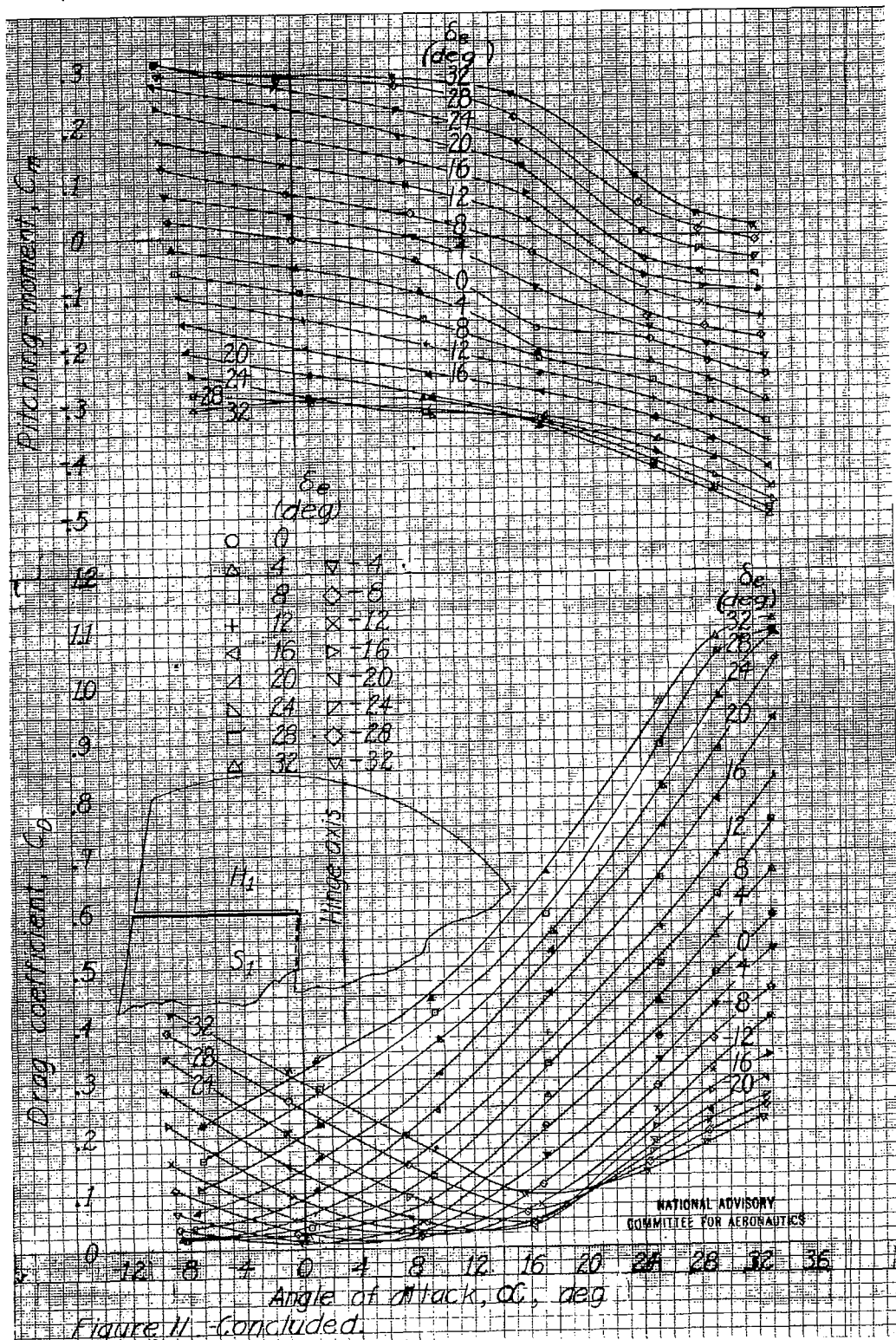


Fig. 11c

NACA ARR No. L4J16



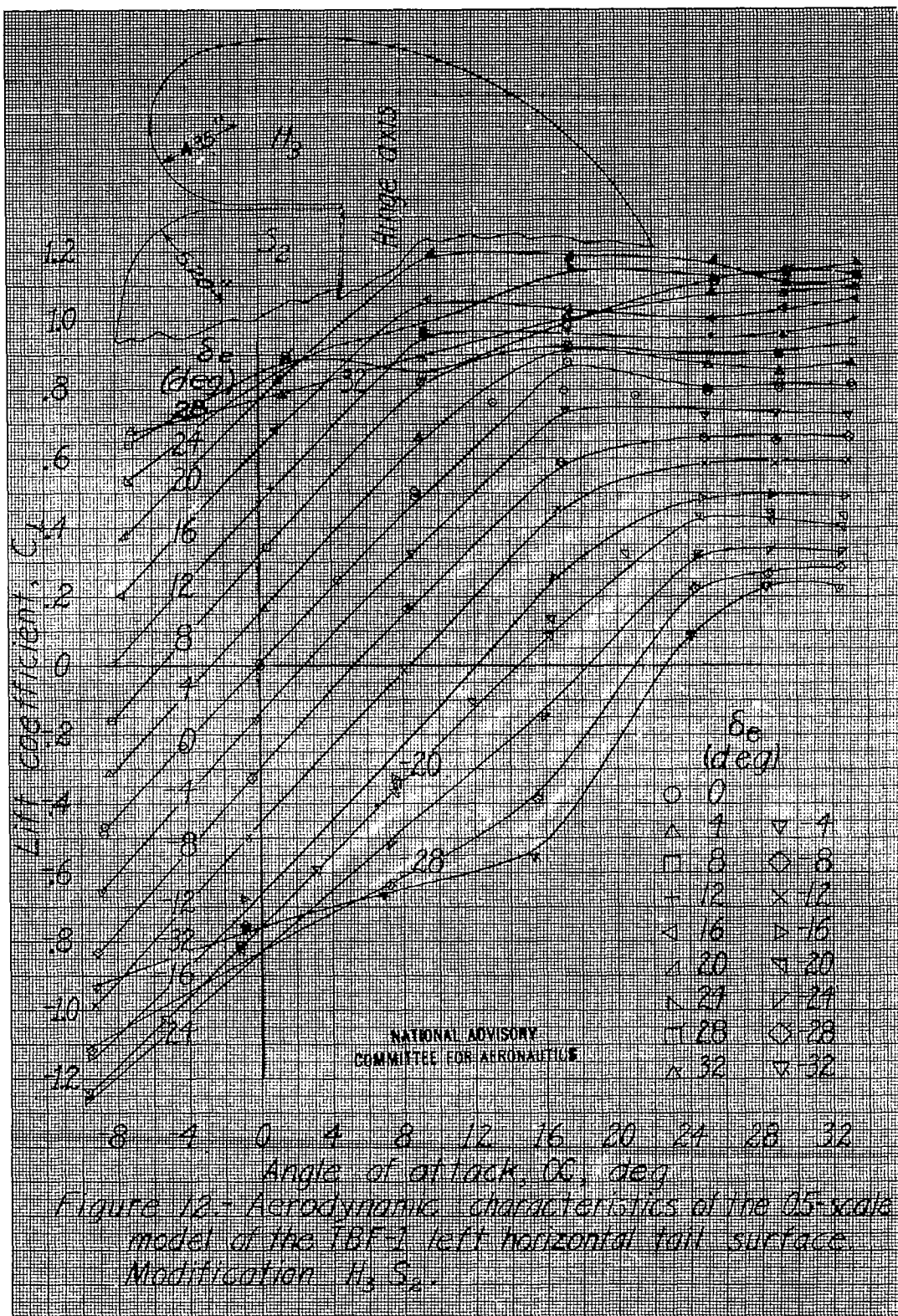
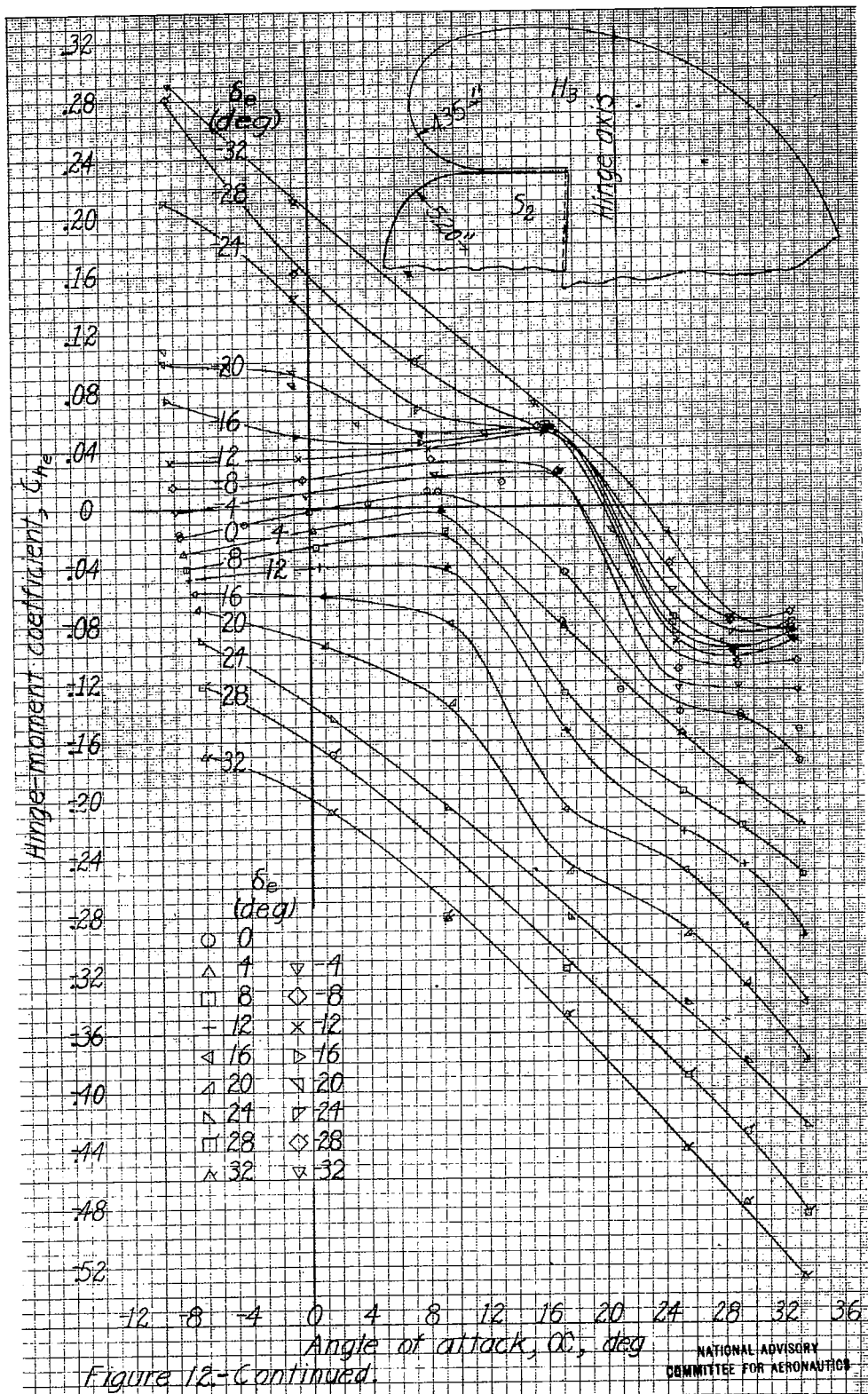


Fig. 12b

NACA ARR No. L4J16



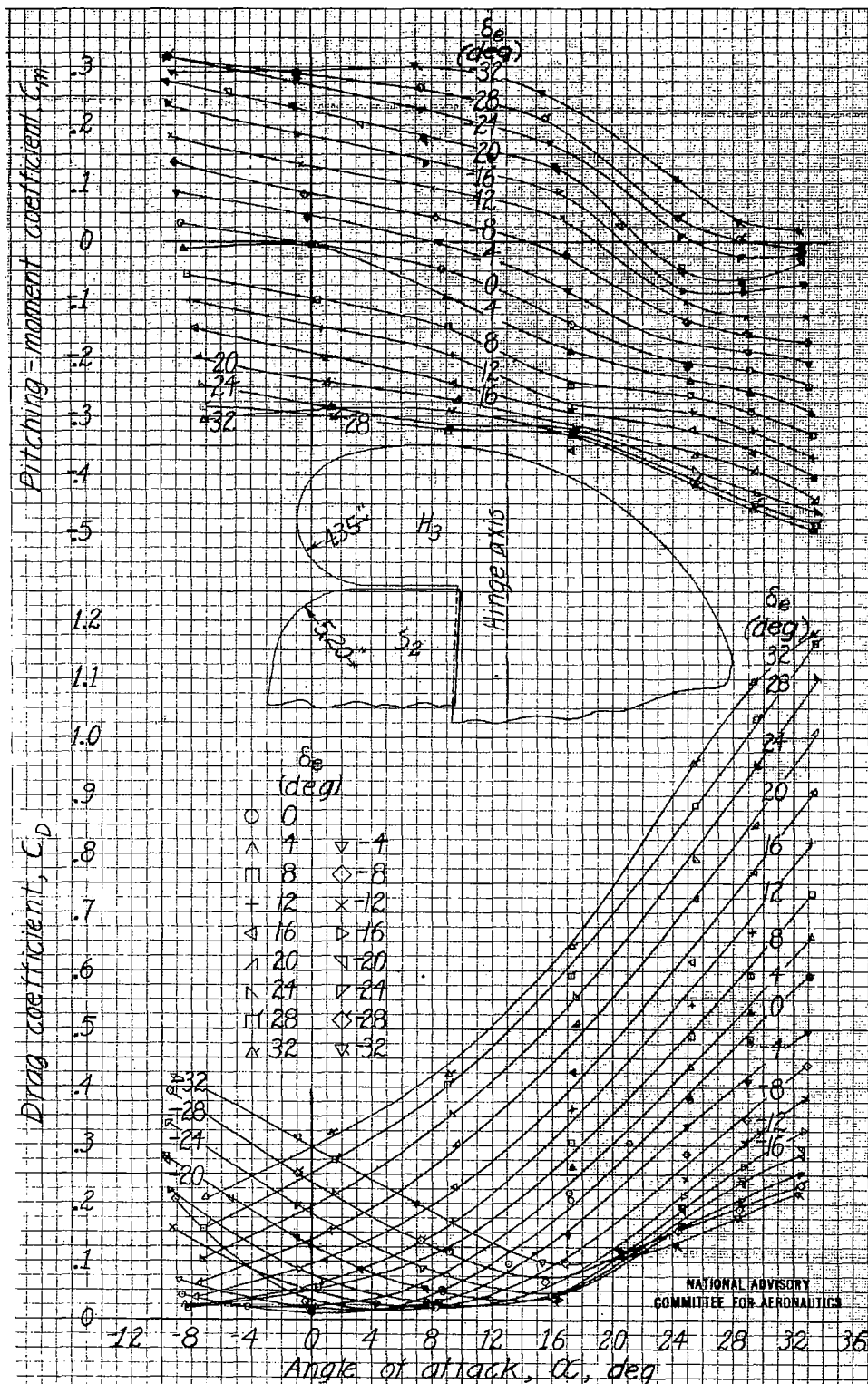


Figure 12.-Concluded.

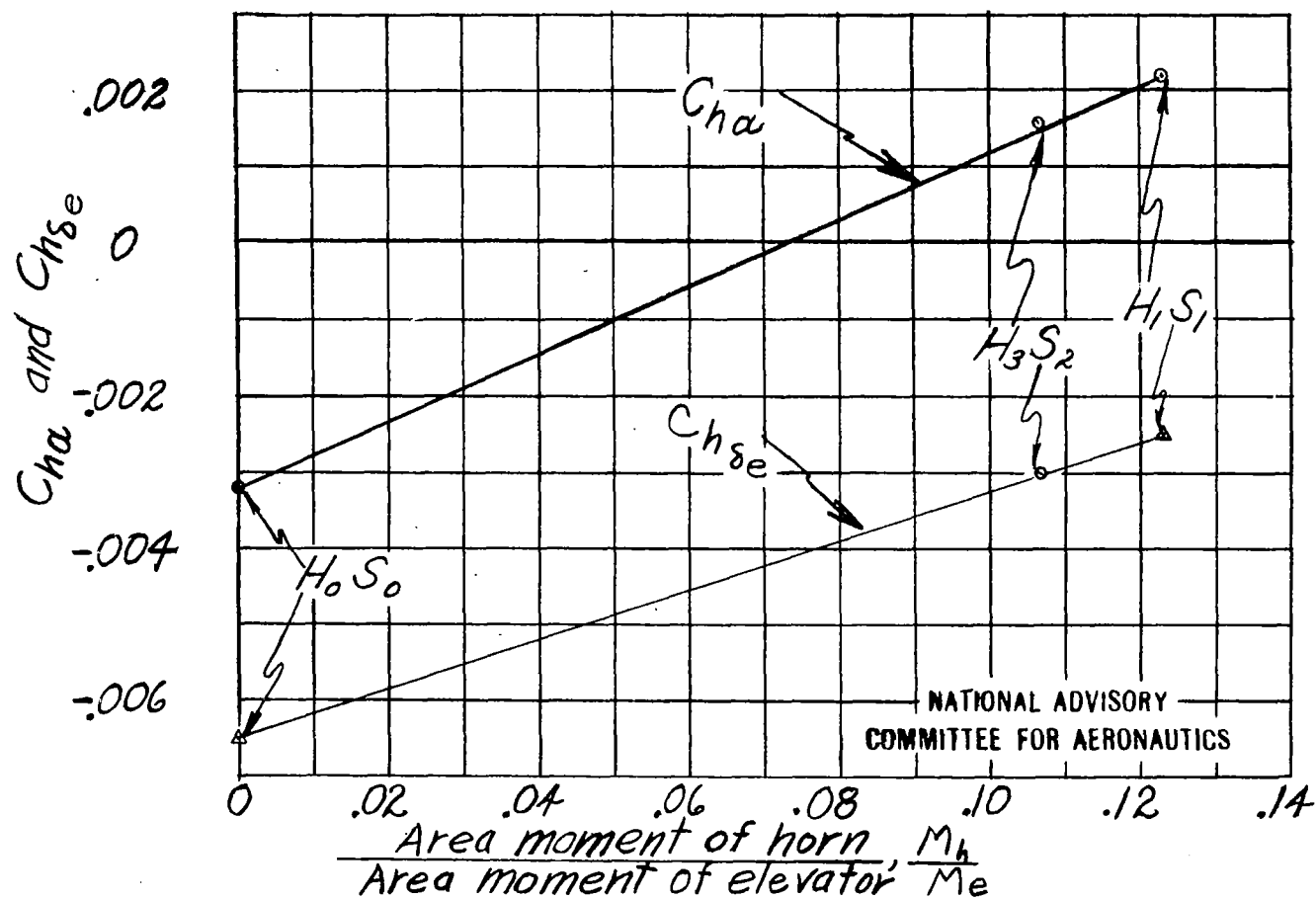
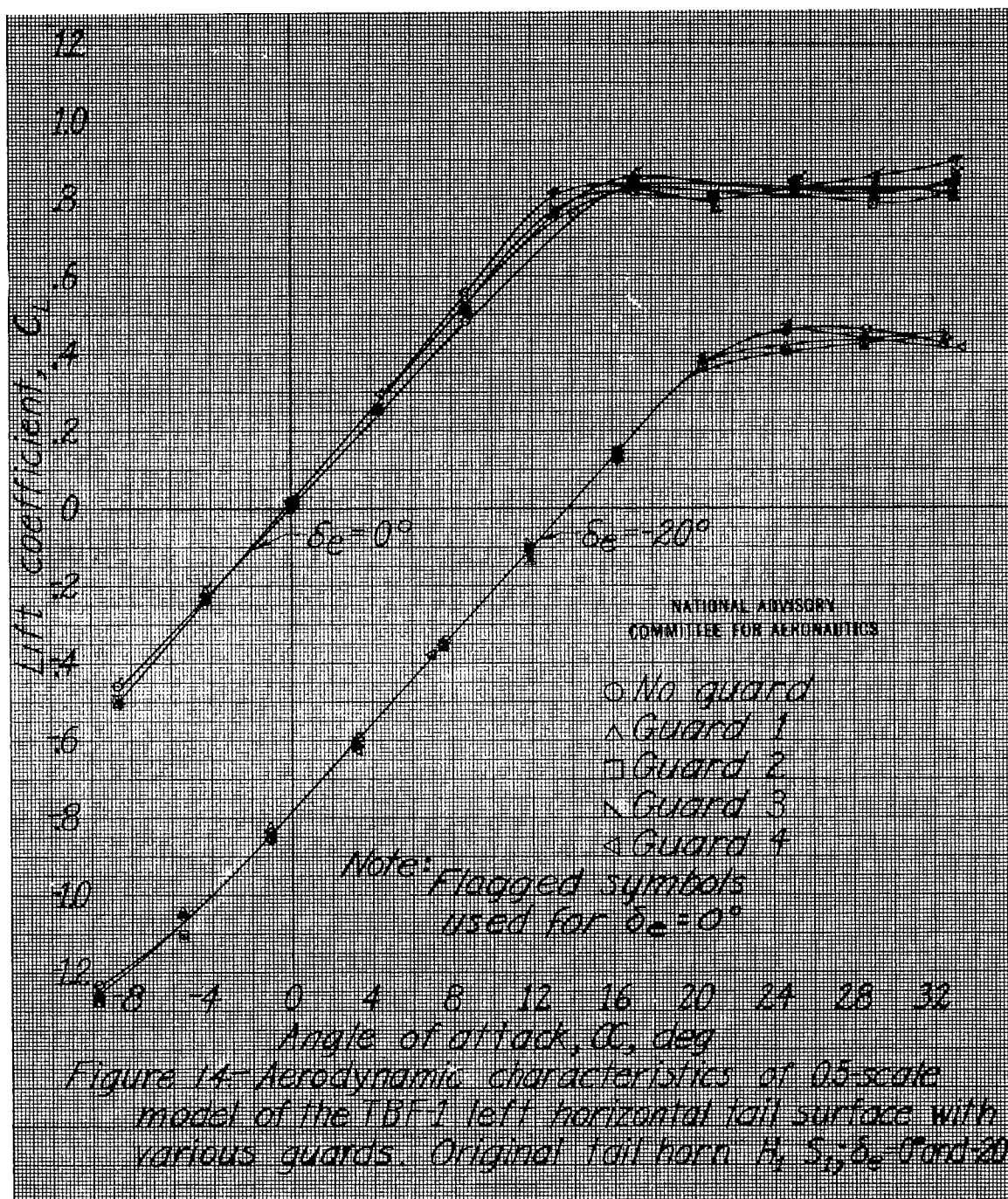


Figure 13.- Variation of hinge-moment parameters,  $C_{h\alpha}$  and  $C_{h\delta e}$ , with ratio of horn area moment to elevator area moment.



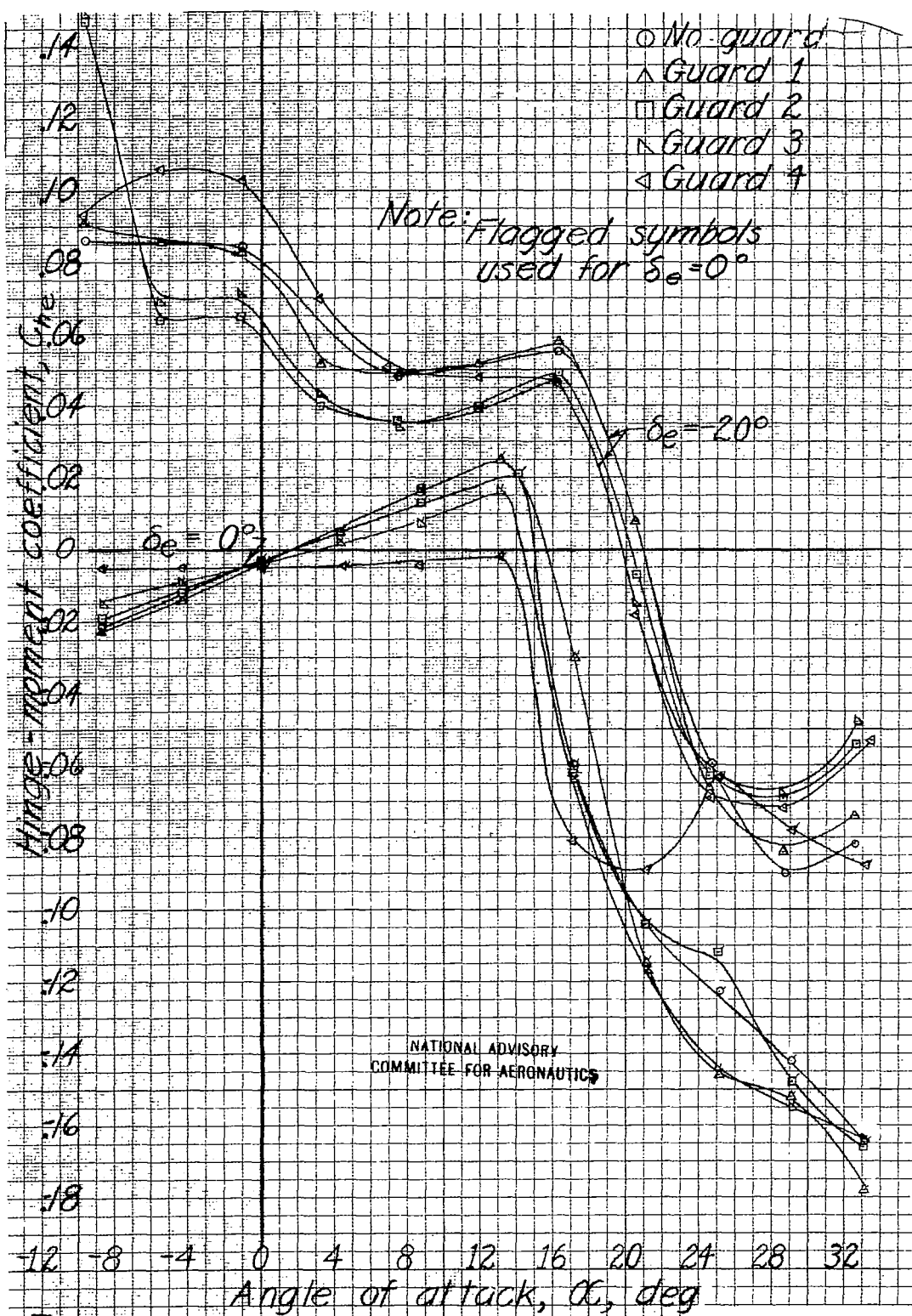
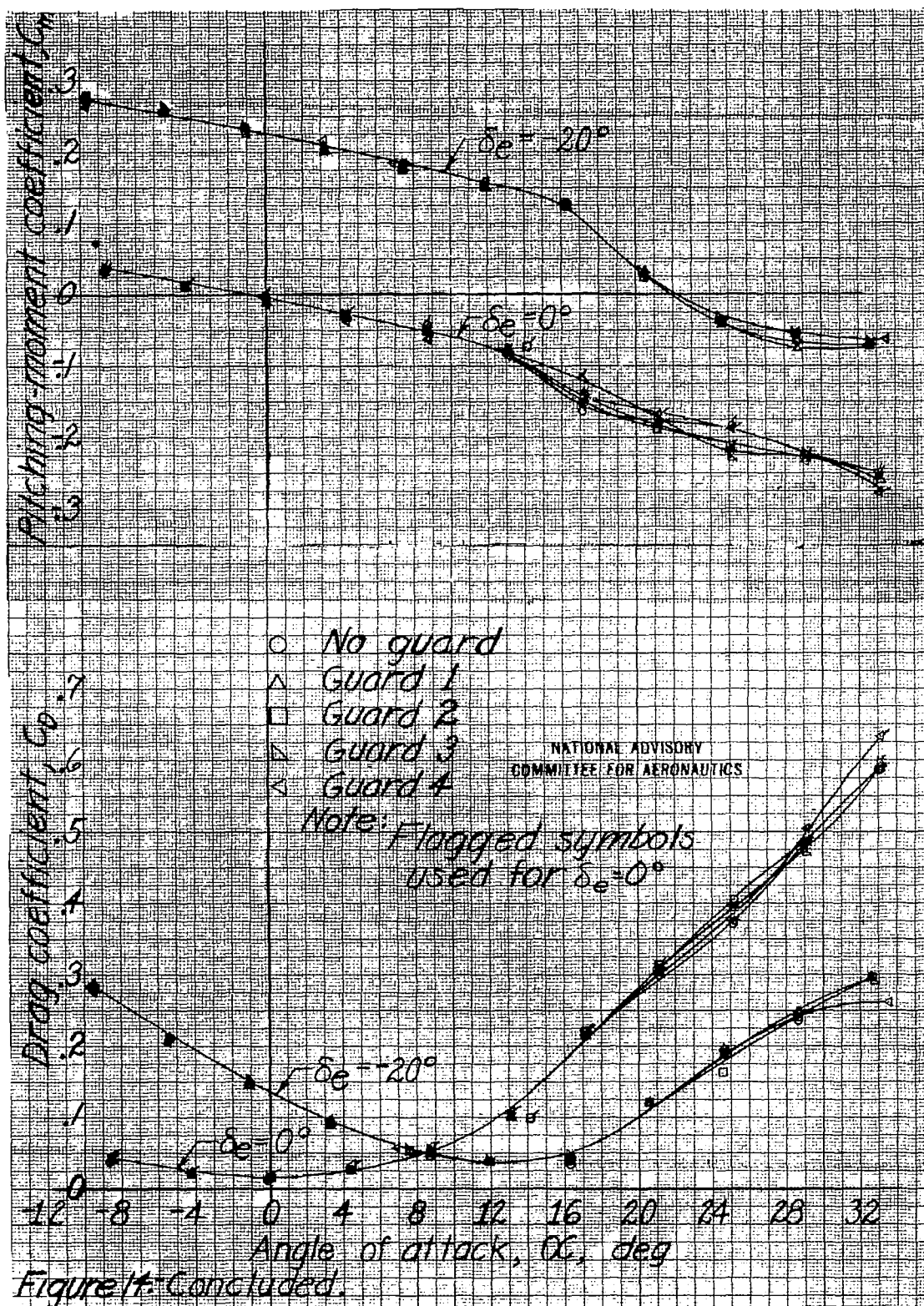
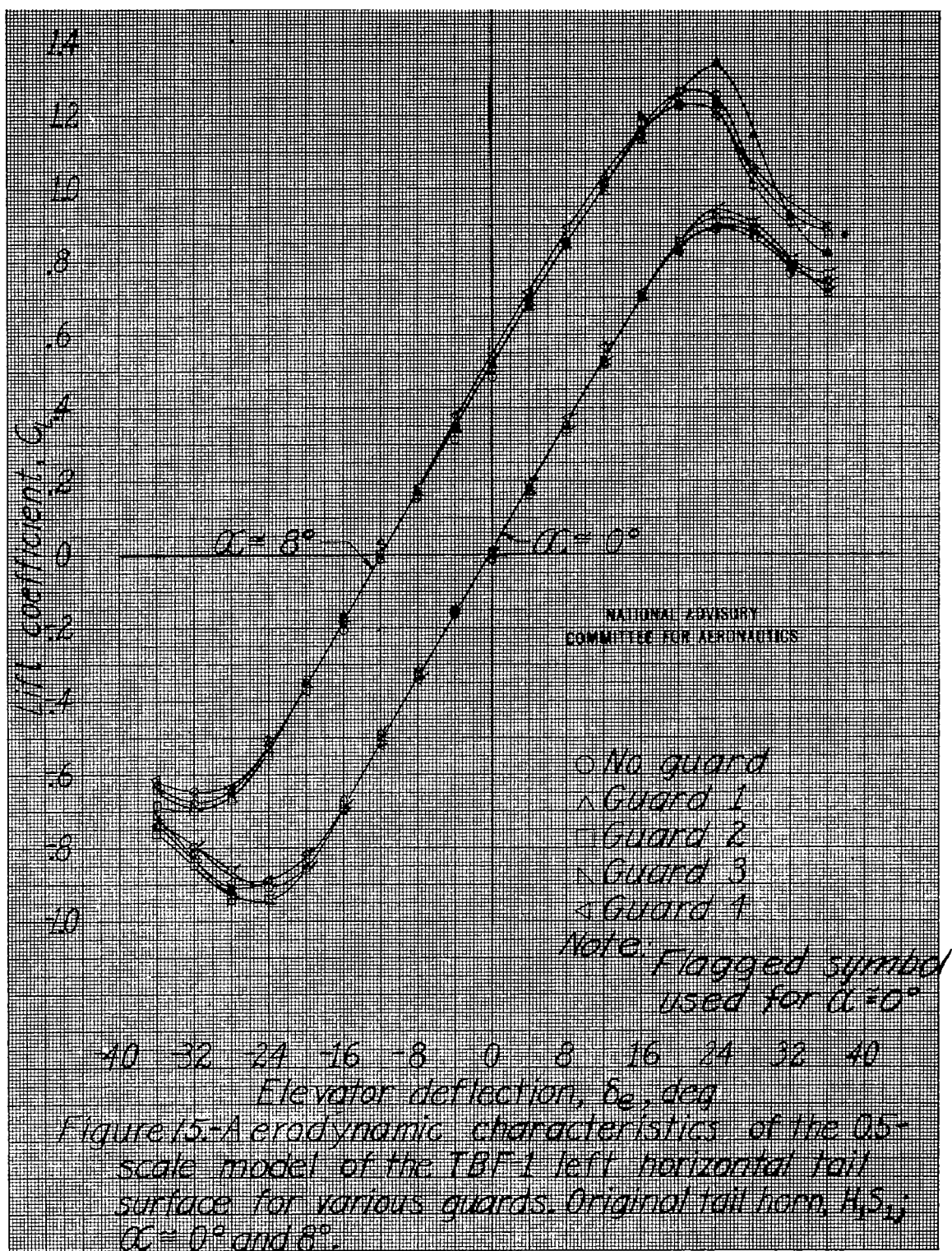
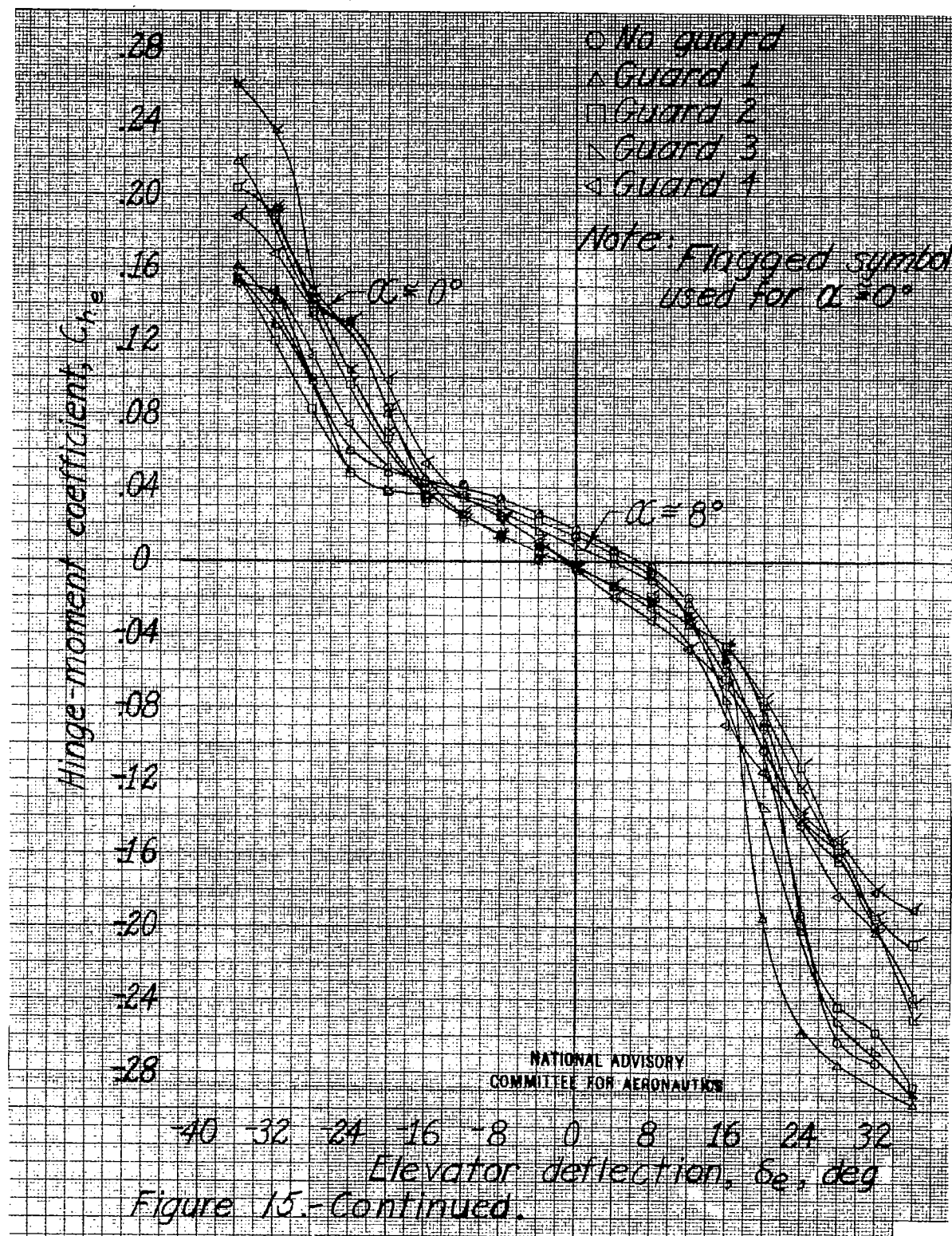
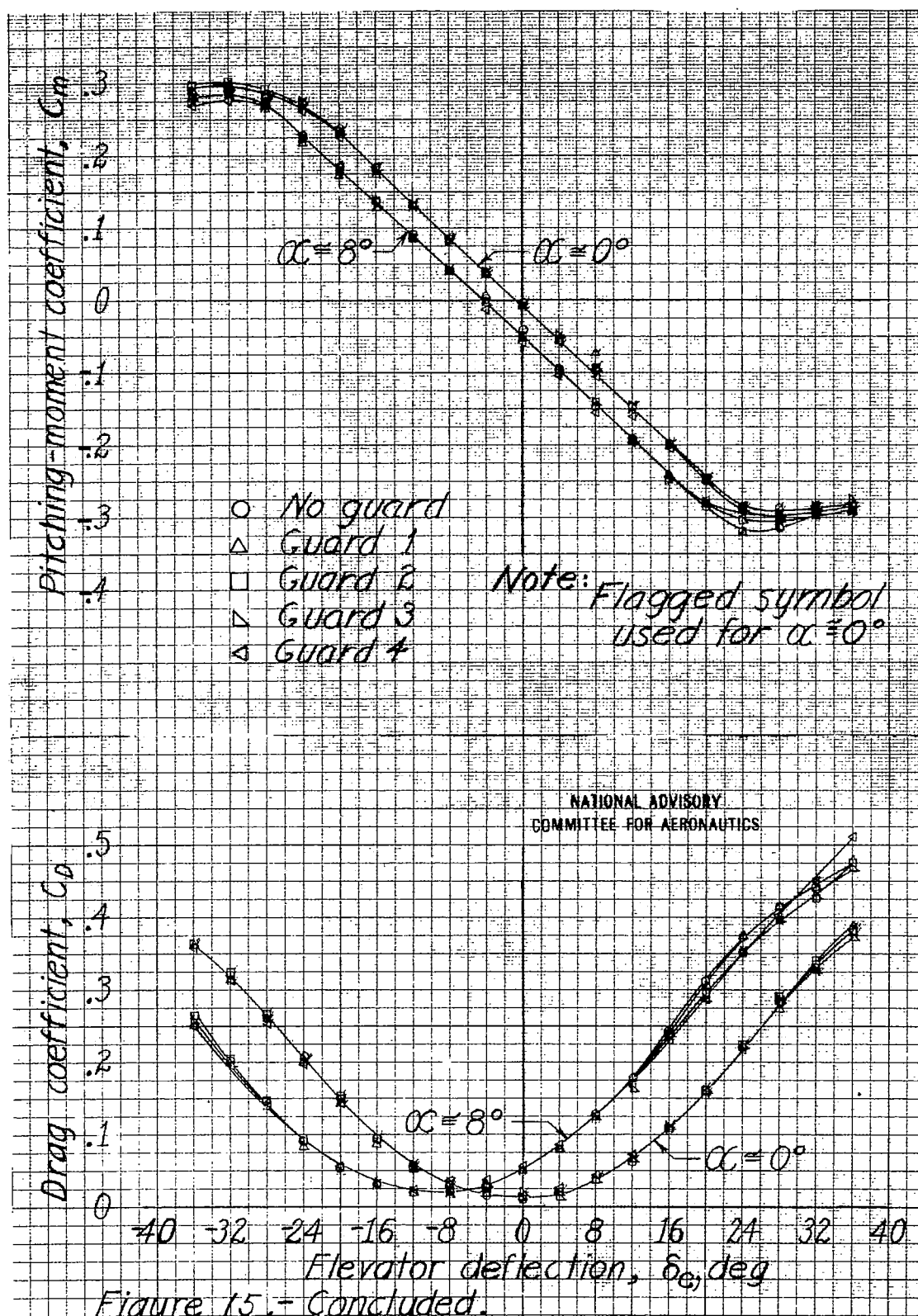


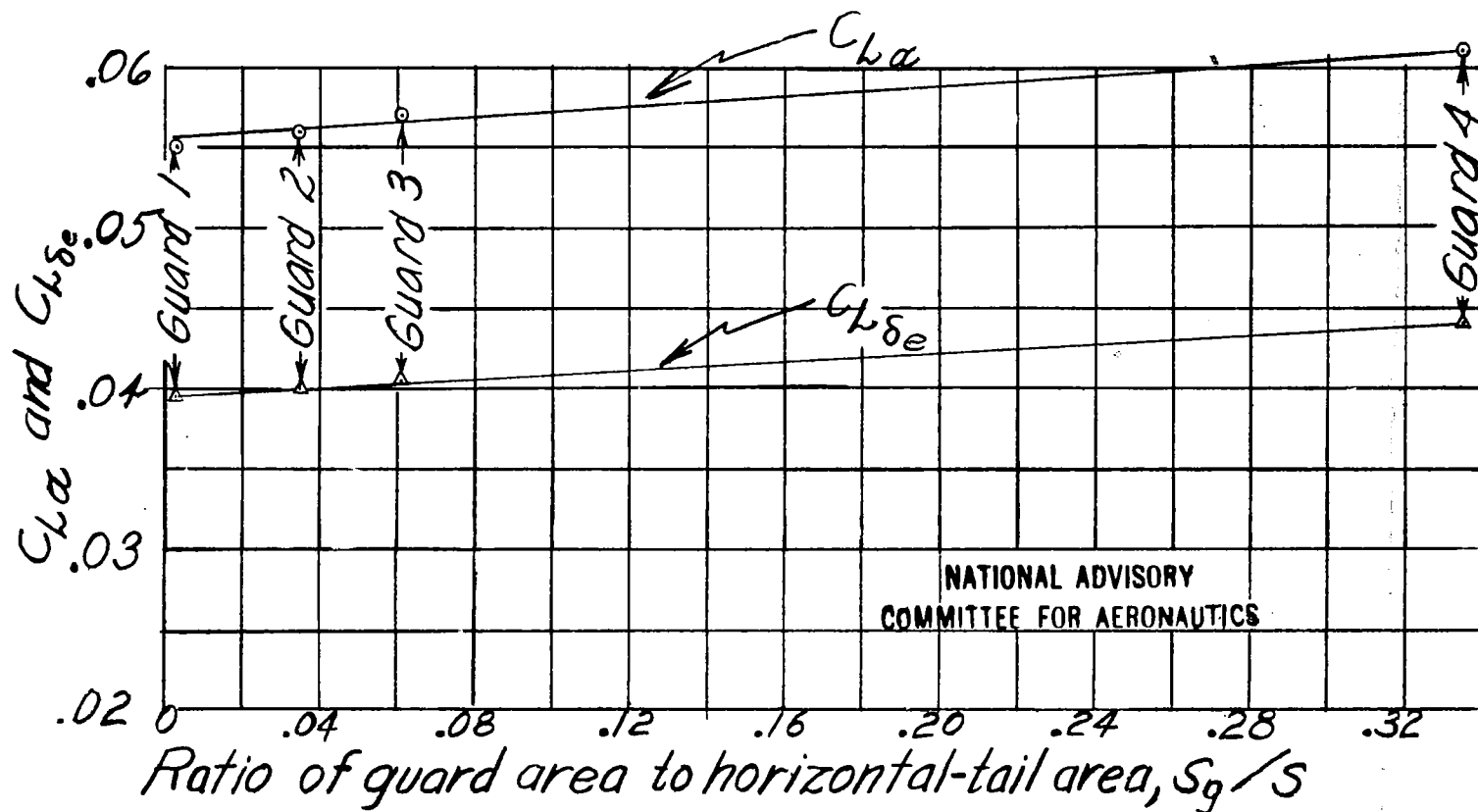
Figure 14-Continued.







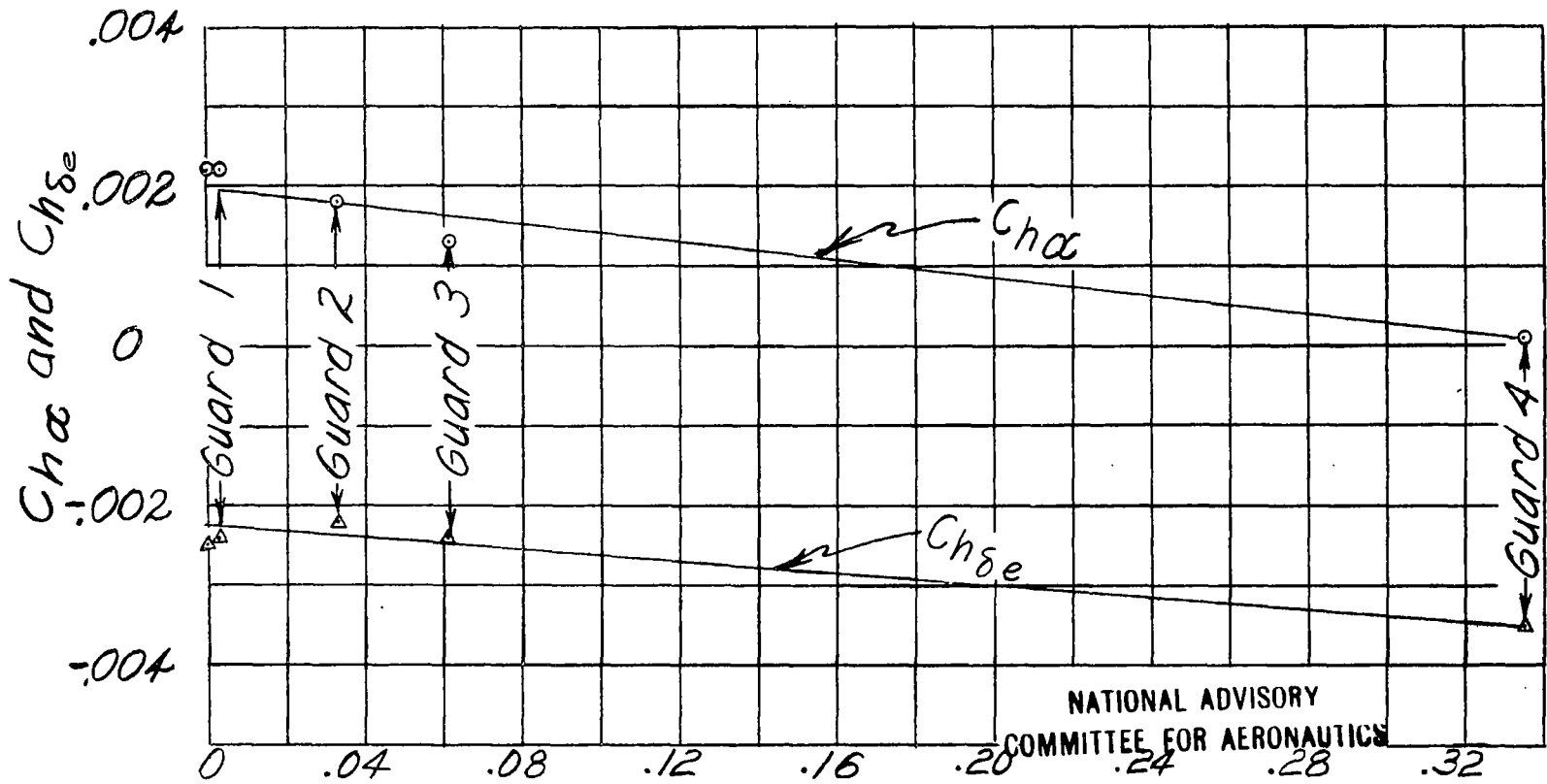




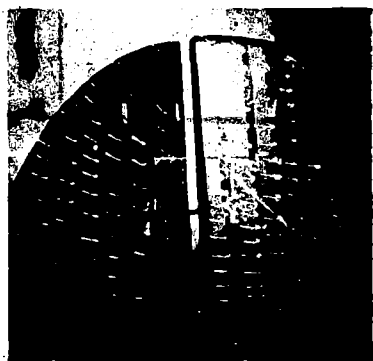
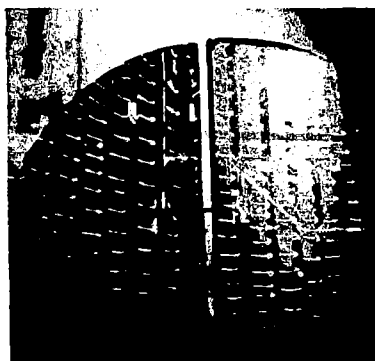
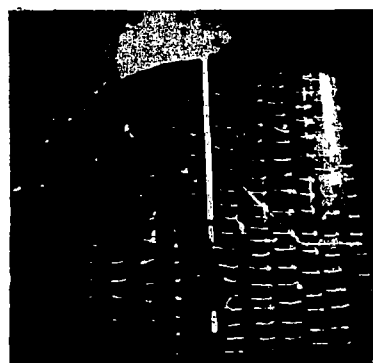
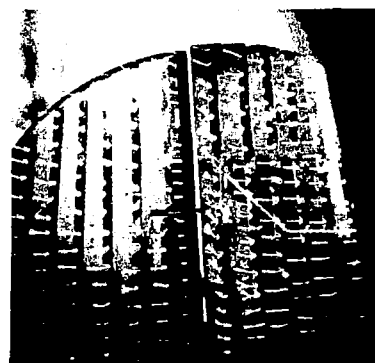
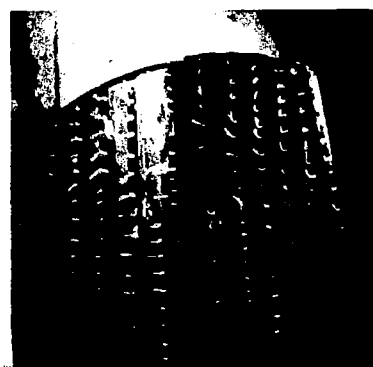
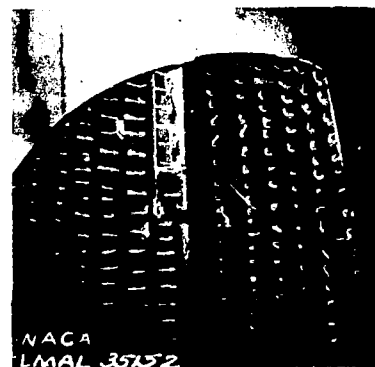
(a) Parameters  $C_{L\alpha}$  and  $C_{L\delta_e}$ .

Figure 16.- Variation of parameters with ratio of guard area to horizontal-tail area.

Fig. 16b

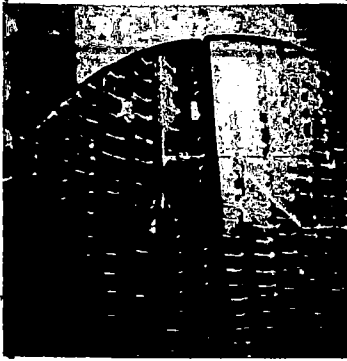


Ratio of guard area to horizontal-tail area,  $S_g/S$   
 (b) Parameters  $Ch_\alpha$  and  $Ch_{\delta_e}$   
 Figure 16.- Concluded.

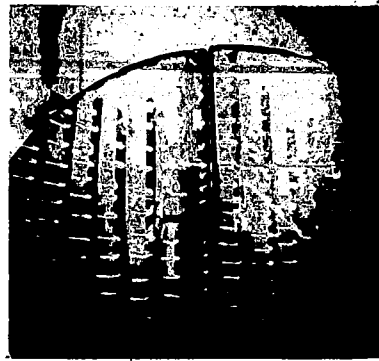

 $\alpha = -8^\circ$ 

 $\alpha = 0^\circ$ 

 $\alpha = 8^\circ$ 

 $\alpha = 16^\circ$ 

 $\alpha = 24^\circ$ 

 $\alpha = 32^\circ$  \*

(a)  $\delta_e = -32^\circ$ .

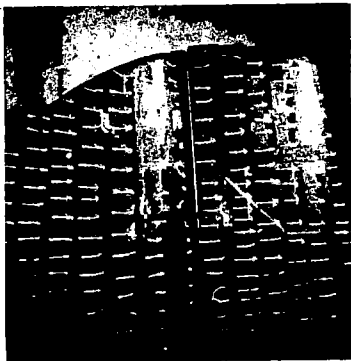
Figure 17.- Tuft study over upper surface of 0.5-scale model of TBF-1 left horizontal tail surface. Modification  $H_0S_0$ ;  $q = 16.37$  pounds per square foot except for tests with asterisk in which  $q = 12.53$  pounds per square foot.



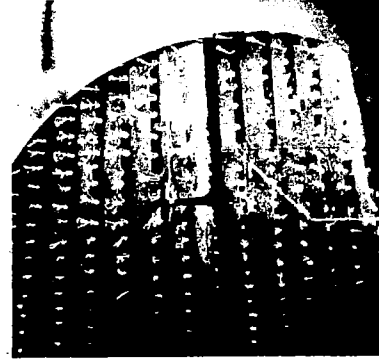
$\alpha = -8^\circ$



$\alpha = 0^\circ$



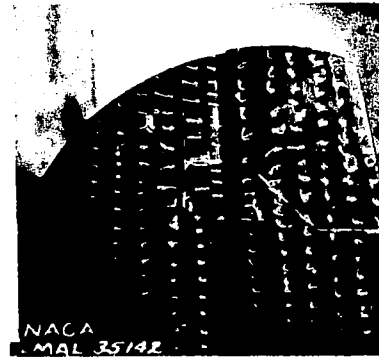
$\alpha = 8^\circ$



$\alpha = 16^\circ$



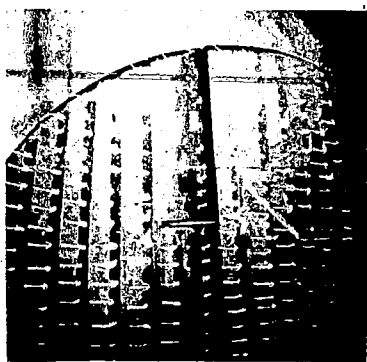
$\alpha = 24^\circ$



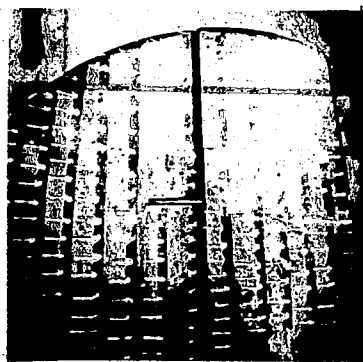
$\alpha = 32^\circ$

(b)  $\delta_e = -16^\circ$ .

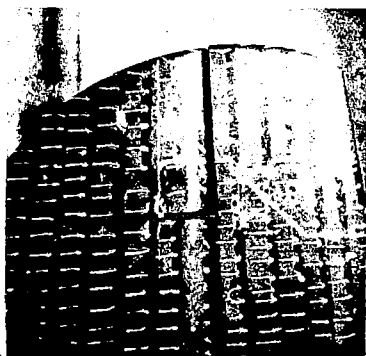
Figure 17.- Continued.



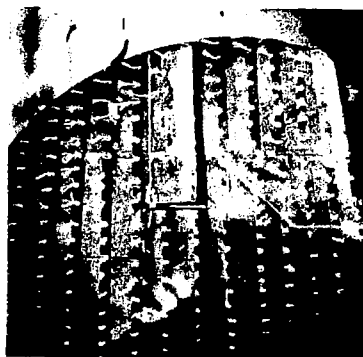
$\alpha = -8^\circ$



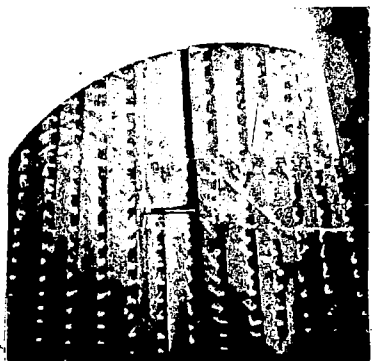
$\alpha = 0^\circ$



$\alpha = 8^\circ$



$\alpha = 16^\circ$



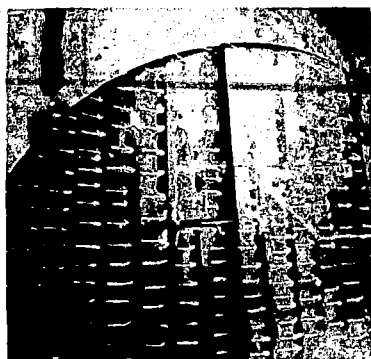
$\alpha = 24^\circ$



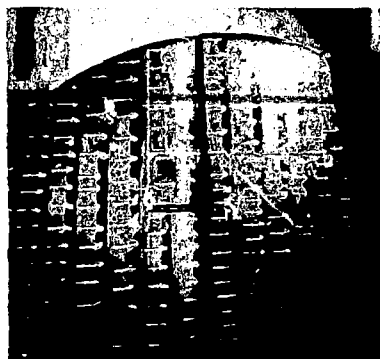
$\alpha = 32^\circ$  \*

(c)  $\delta_e = -8^\circ$ .

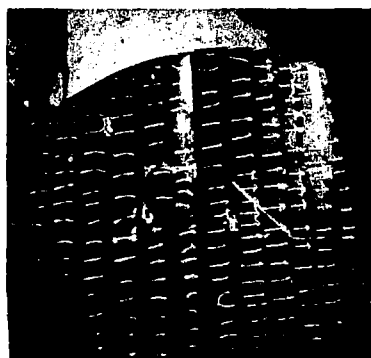
Figure 17.- Continued.



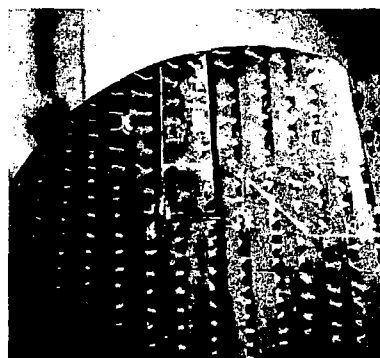
$\alpha = -8^\circ$



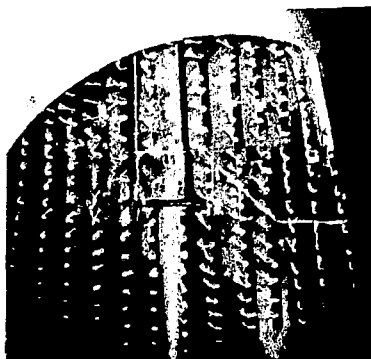
$\alpha = 0^\circ$



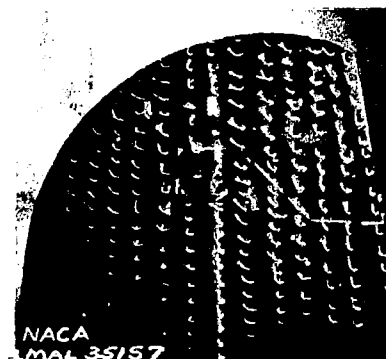
$\alpha = 8^\circ$



$\alpha = 16^\circ$



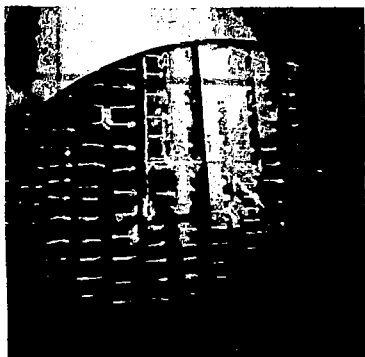
$\alpha = 24^\circ$



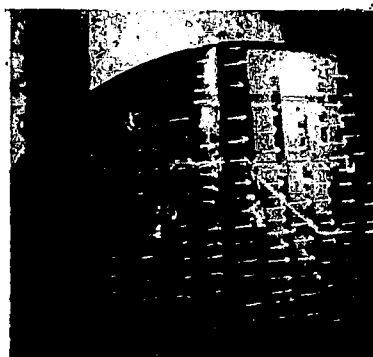
$\alpha = 32^\circ$

(d)  $\delta_e = 0^\circ$ .

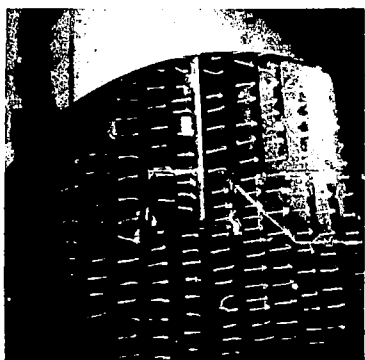
Figure 17.- Continued.



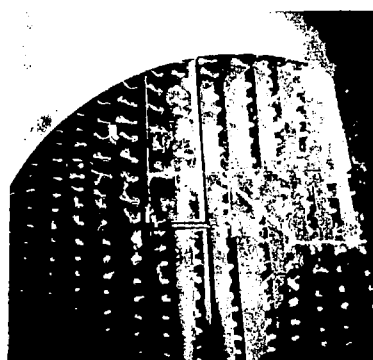
$\alpha = -8^\circ$



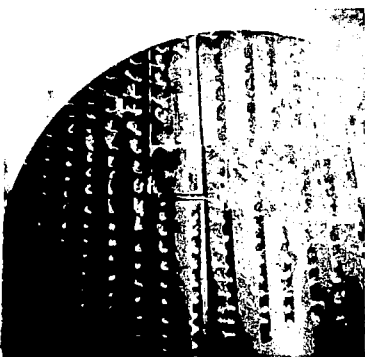
$\alpha = 0^\circ$



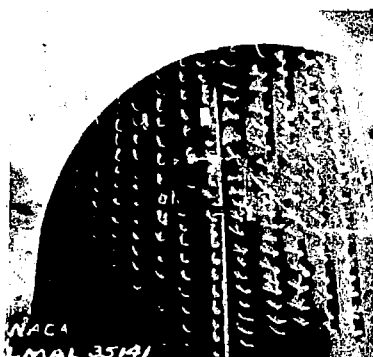
$\alpha = 8^\circ$



$\alpha = 16^\circ$



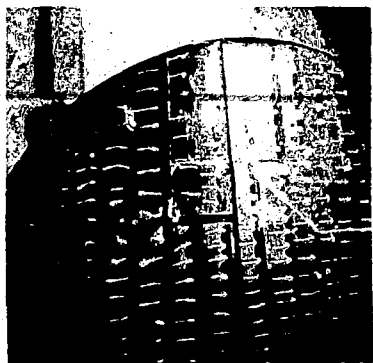
$\alpha = 24^\circ$  \*



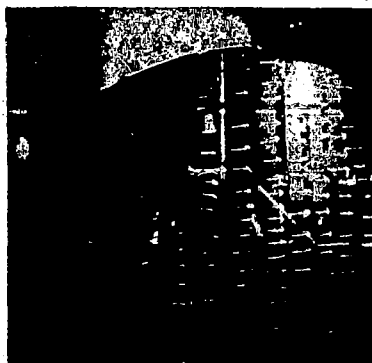
$\alpha = 32^\circ$  \*

(e)  $\delta_e = 8^\circ$

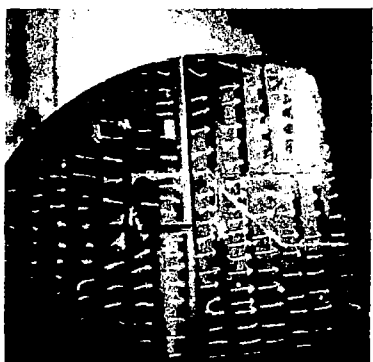
Figure 17.- Continued.



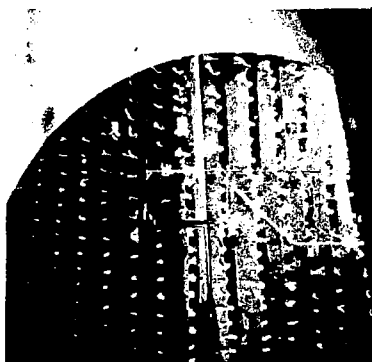
$\alpha = -8^\circ$



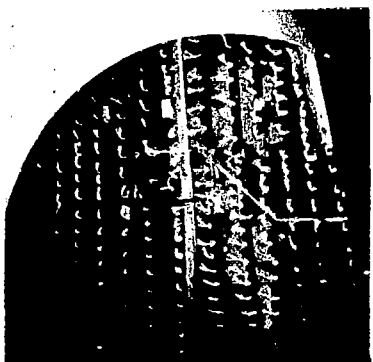
$\alpha = 0^\circ$



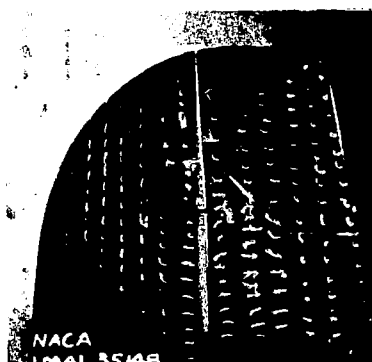
$\alpha = 8^\circ$



$\alpha = 16^\circ$



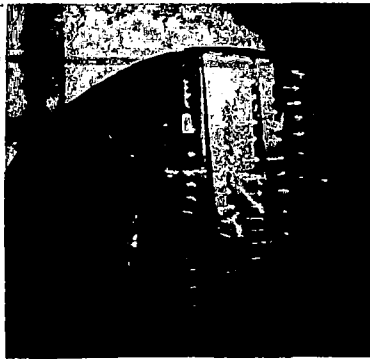
$\alpha = 24^\circ$  \*



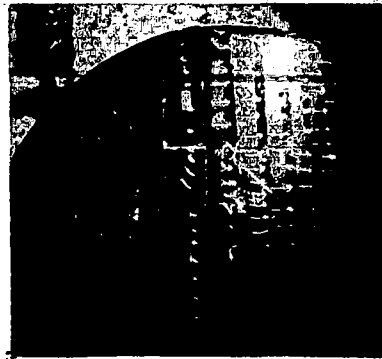
$\alpha = 32^\circ$  \*

(f)  $\delta_e = 16^\circ$ .

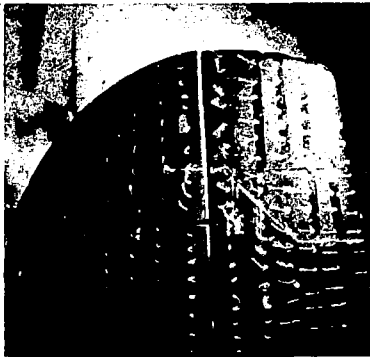
Figure 17.- Continued.



$\alpha = -8^\circ$



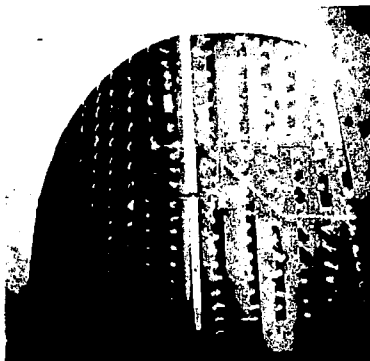
$\alpha = 0^\circ$



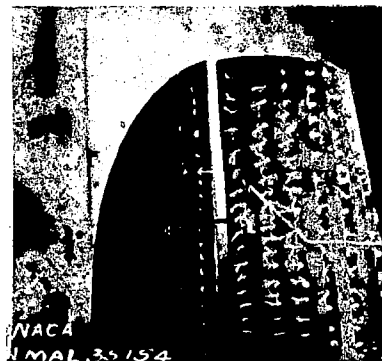
$\alpha = 8^\circ$



$\alpha = 16^\circ$



$\alpha = 24^\circ$  \*



$\alpha = 32^\circ$  \*

(g)  $\delta_e = 32^\circ$ .

Figure 17.- Concluded.

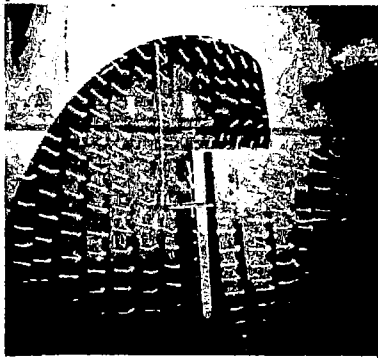
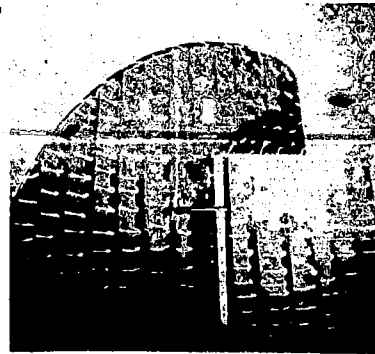
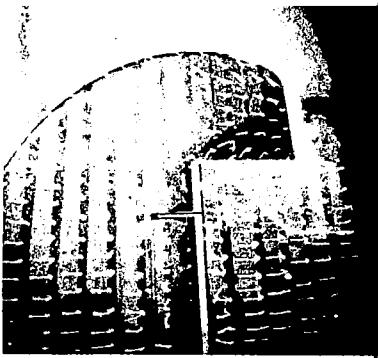
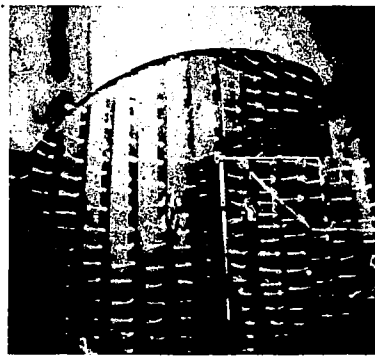
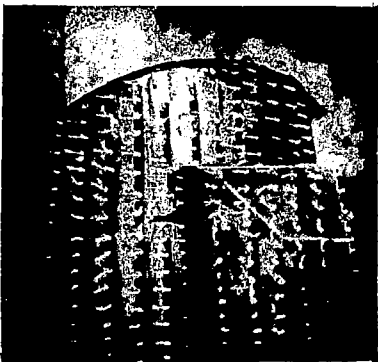
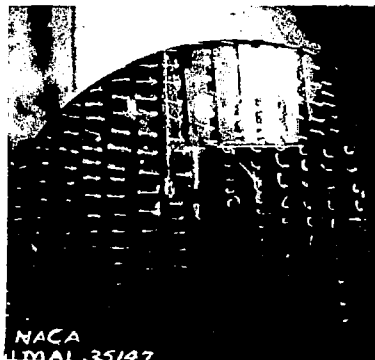
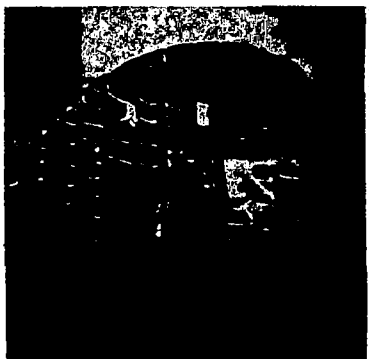
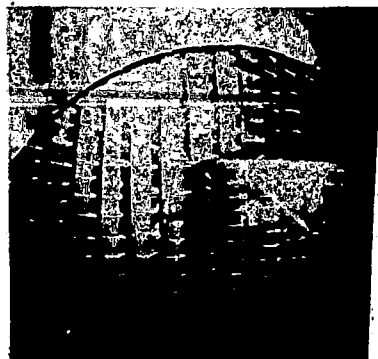
 $\alpha = -8^\circ$  $\alpha = 0^\circ$  $\alpha = 8^\circ$  $\alpha = 16^\circ$  $\alpha = 24^\circ$  \* $\alpha = 32^\circ$  \*(a)  $\delta_e = -32^\circ$ .

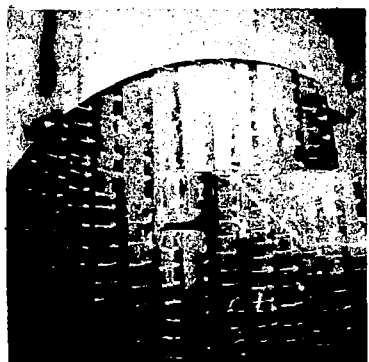
Figure 18.- Tuft study over upper surface of 0.5-scale model of TBF-1 left horizontal tail surface. Original surface  $H_1S_1$ ;  $q = 16.37$  pounds per square foot except for tests with asterisk in which  $q = 12.53$  pounds per square foot.



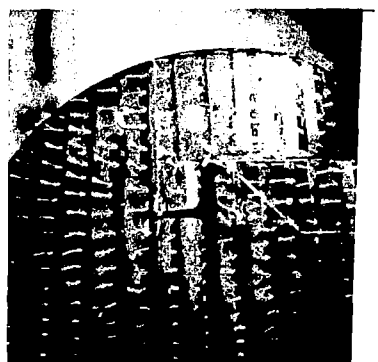
$\alpha = -8^\circ$



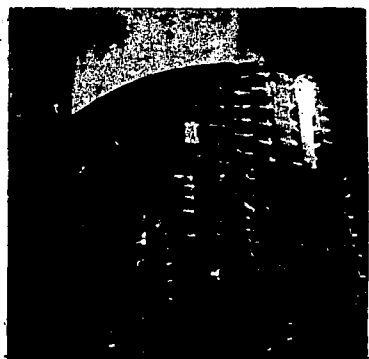
$\alpha = 0^\circ$



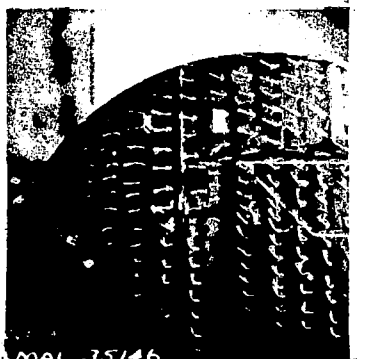
$\alpha = 8^\circ$



$\alpha = 16^\circ$



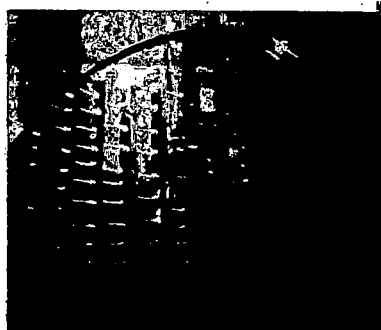
$\alpha = 24^\circ$  \*



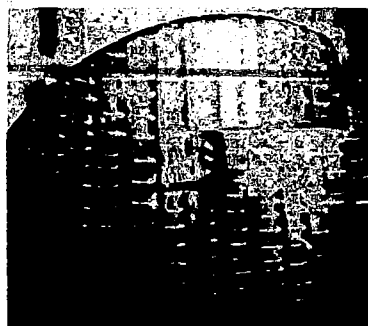
$\alpha = 32^\circ$  \*

(b)  $\delta_e = -16^\circ$ .

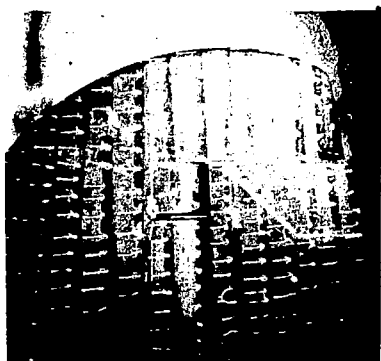
Figure 18.- Continued.



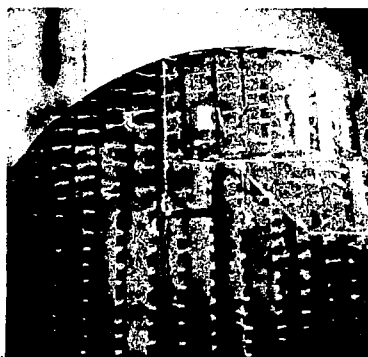
$\alpha = -8^\circ$



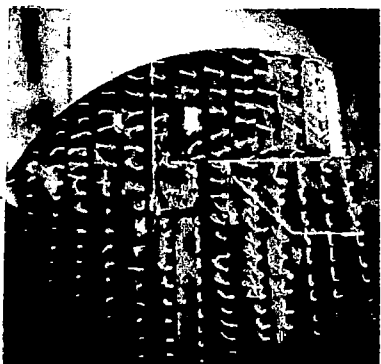
$\alpha = 0^\circ$



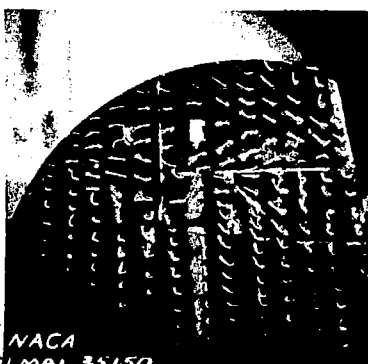
$\alpha = 8^\circ$



$\alpha = 16^\circ$



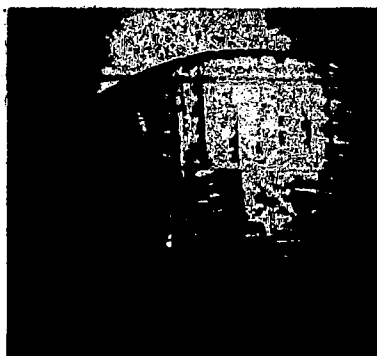
$\alpha = 24^\circ$  \*



$\alpha = 32^\circ$  \*

(c)  $\delta_e = -8^\circ$ .

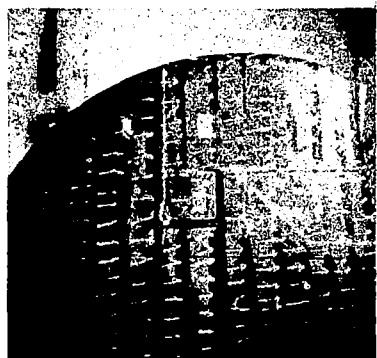
Figure 18.- Continued.



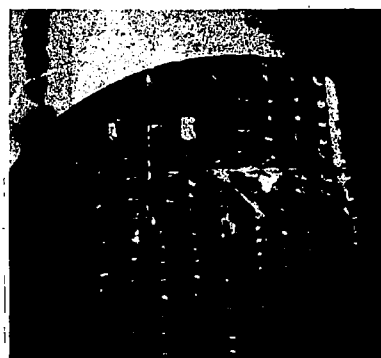
$\alpha = -8^\circ$



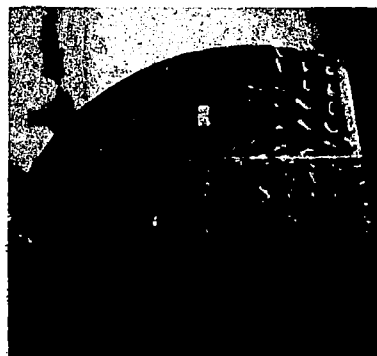
$\alpha = 0^\circ$



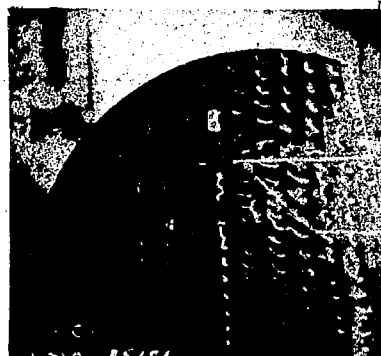
$\alpha = 8^\circ$



$\alpha = 16^\circ$



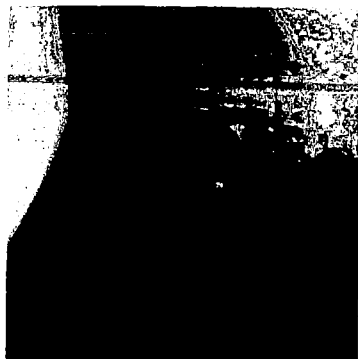
$\alpha = 24^\circ$



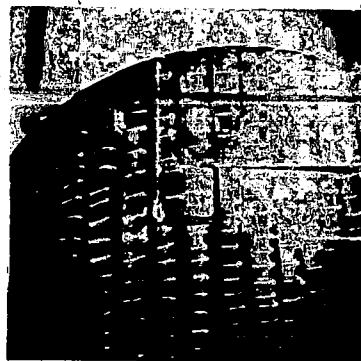
$\alpha = 32^\circ$

(d)  $\delta_e = 0^\circ$ .

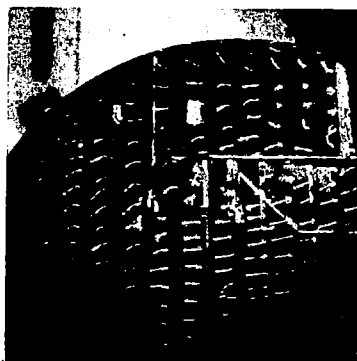
Figure 18.- Continued.



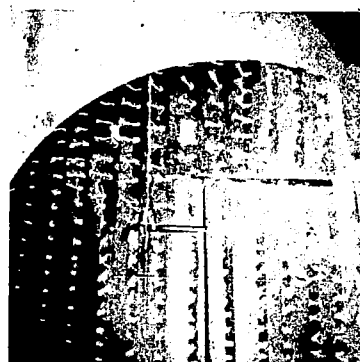
$\alpha = -8^\circ$



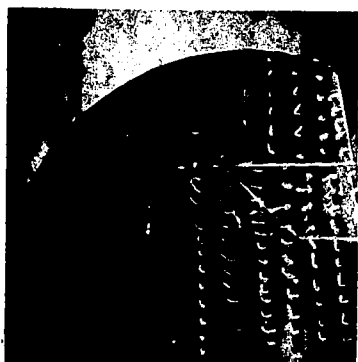
$\alpha = 0^\circ$



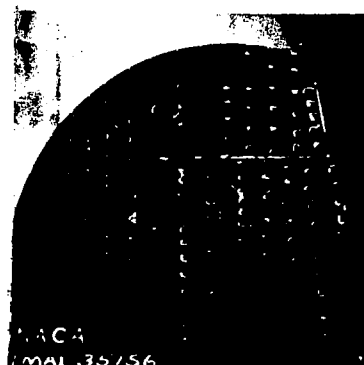
$\alpha = 8^\circ$



$\alpha = 16^\circ$



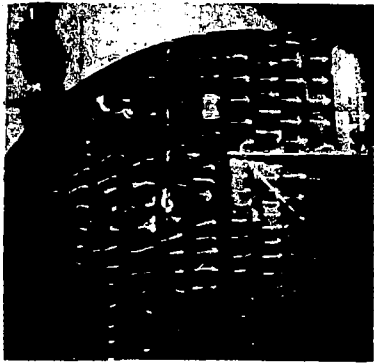
$\alpha = 24^\circ$  \*



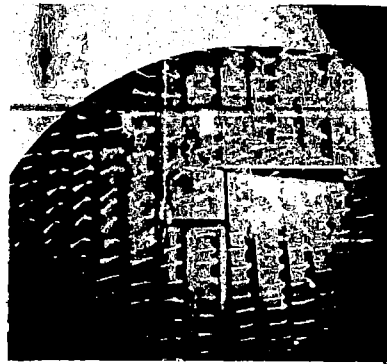
$\alpha = 32^\circ$  \*

(e)  $\delta_e = 8^\circ$ .

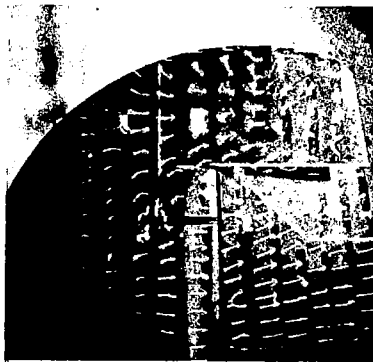
Figure 18.- Continued.



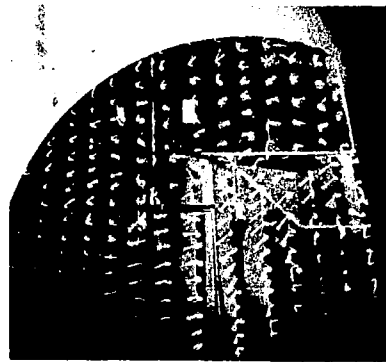
$\alpha = -8^\circ$



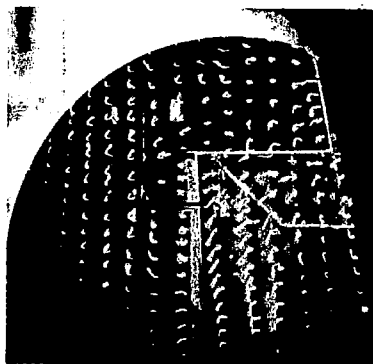
$\alpha = 0^\circ$



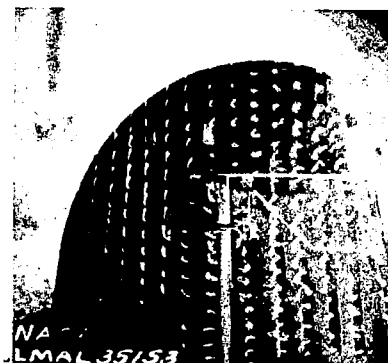
$\alpha = 8^\circ$



$\alpha = 16^\circ$  \*



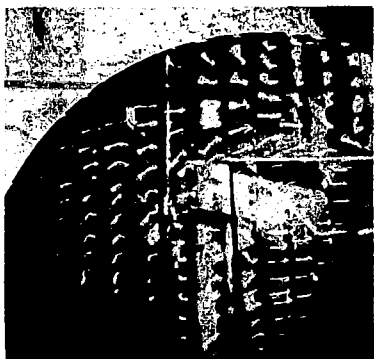
$\alpha = 24^\circ$  \*



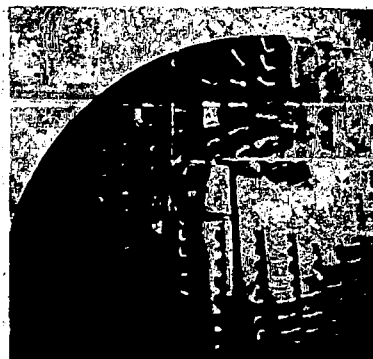
$\alpha = 32^\circ$  \*

(f)  $\delta_e = 16^\circ$ .

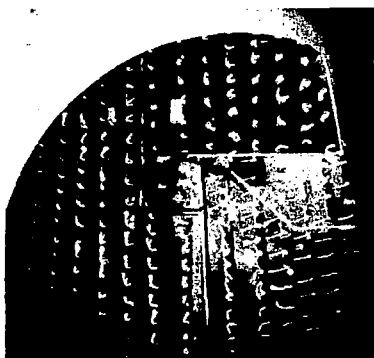
Figure 18.- Continued.



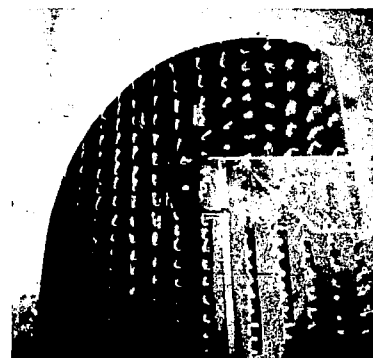
$\alpha = -8^\circ$



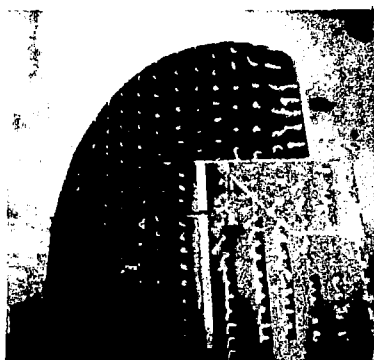
$\alpha = 0^\circ$



$\alpha = 8^\circ$



$\alpha = 16^\circ$  \*



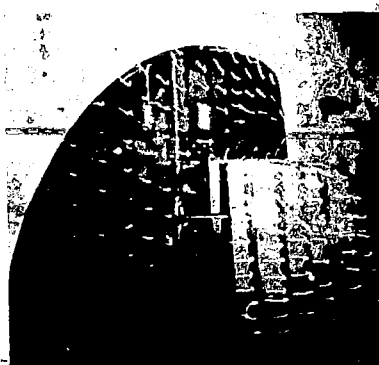
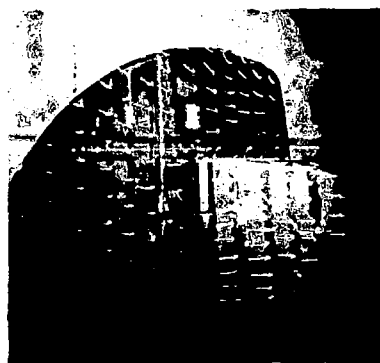
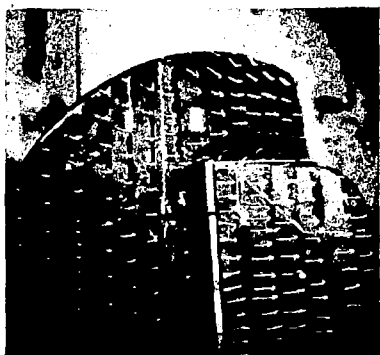
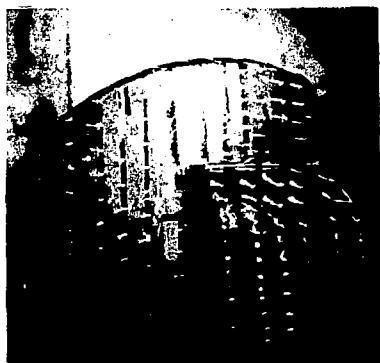
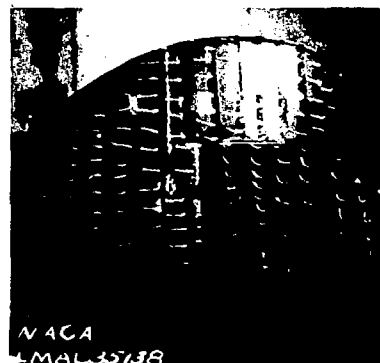
$\alpha = 24^\circ$  \*



$\alpha = 32^\circ$  \*

(g)  $\delta_e = 32^\circ$ .

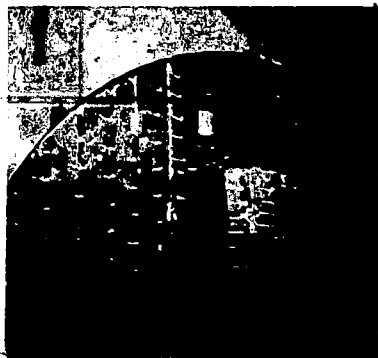
Figure 18.- Concluded.

 $\alpha = -8^\circ$  $\alpha = 0^\circ$  $\alpha = 8^\circ$  $\alpha = 16^\circ$  $\alpha = 24^\circ$  $\alpha = 32^\circ$ 

\*

(a)  $\delta_e = -32^\circ$ .

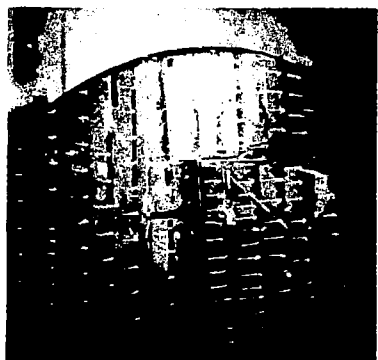
Figure 19.- Tuft study over upper surface of 0.5-scale model of TBF-1 left horizontal tail surface. Modification  $H_1S_2$ ;  $q = 16.37$  pounds per square foot except for tests with asterisk in which  $q = 12.53$  pounds per square foot.



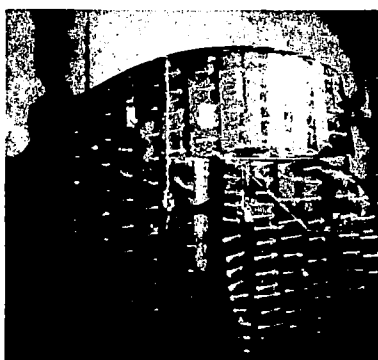
$\alpha = -8^\circ$



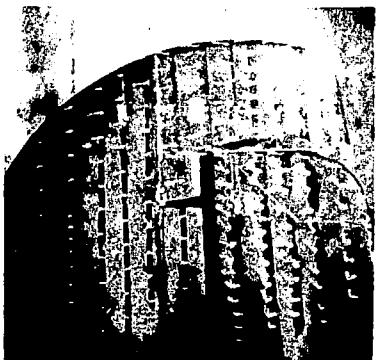
$\alpha = 0^\circ$



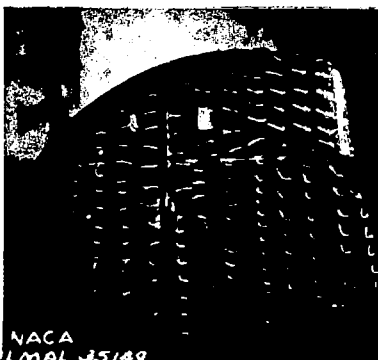
$\alpha = 8^\circ$



$\alpha = 16^\circ$



$\alpha = 24^\circ$



$\alpha = 32^\circ$

\*

(b)  $\delta_e = -16^\circ$ .

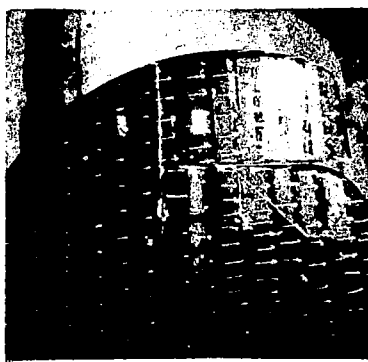
Figure 19.- Continued.



$\alpha = -8^\circ$



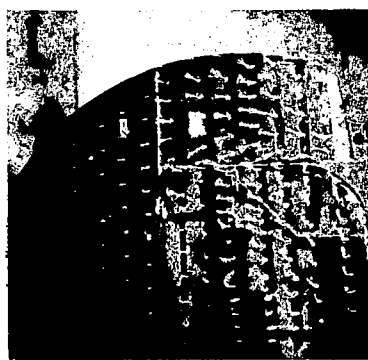
$\alpha = 0^\circ$



$\alpha = 8^\circ$



$\alpha = 16^\circ$



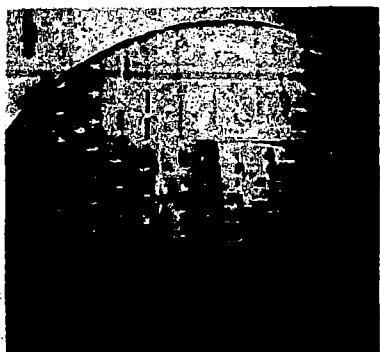
$\alpha = 24^\circ$  \*



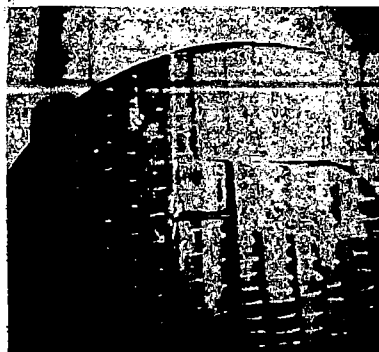
$\alpha = 32^\circ$  \*

(c)  $\delta_e = -8^\circ$ .

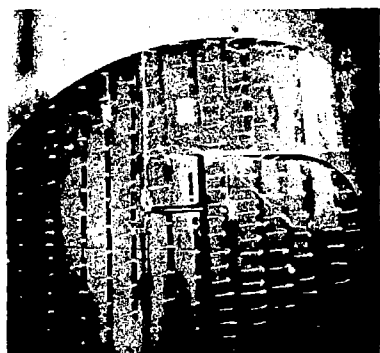
Figure 19.- Continued.



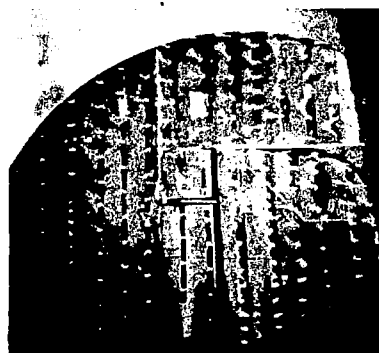
$\alpha = -8^\circ$



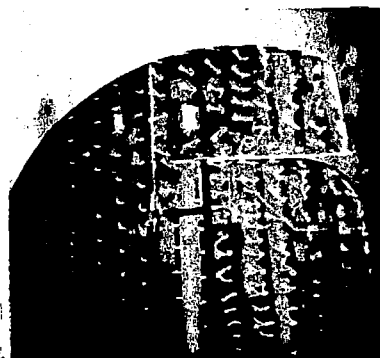
$\alpha = 0^\circ$



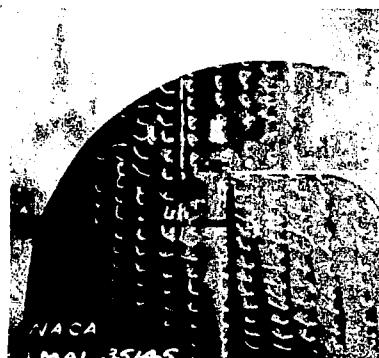
$\alpha = 8^\circ$



$\alpha = 16^\circ$



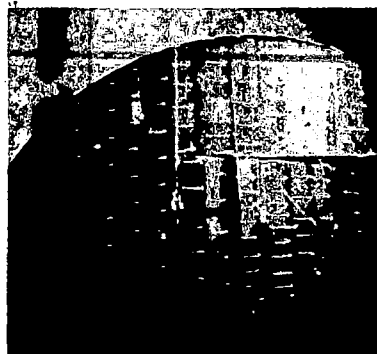
$\alpha = 24^\circ$



$\alpha = 32^\circ$

(d)  $\delta_e = 0^\circ$ .

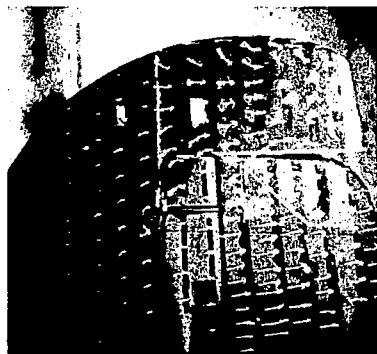
Figure 19.- Continued:



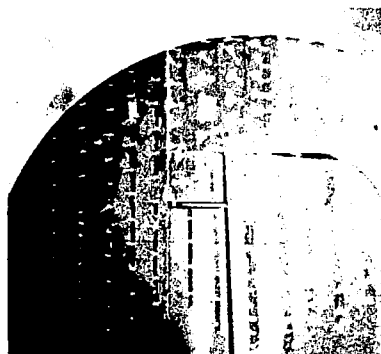
$\alpha = -8^\circ$



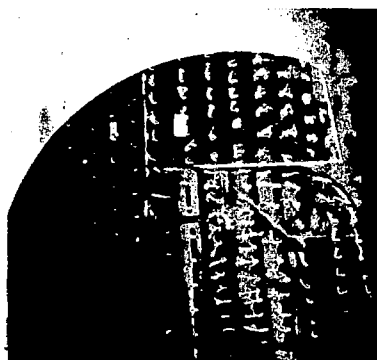
$\alpha = 0^\circ$



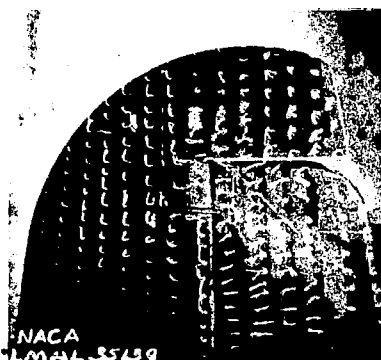
$\alpha = 8^\circ$



$\alpha = 16^\circ$



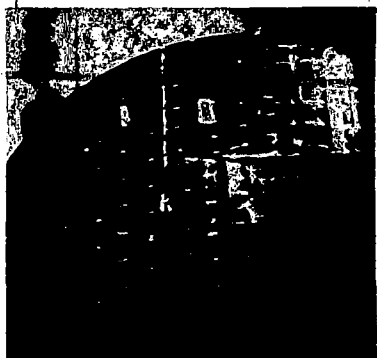
$\alpha = 24^\circ$  \*



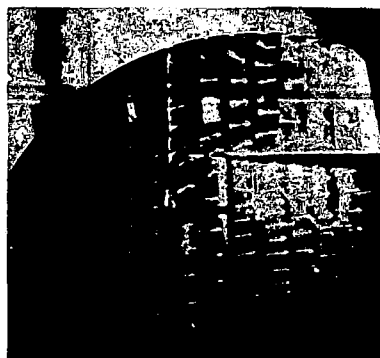
$\alpha = 32^\circ$  \*

(e)  $\delta_e = 8^\circ$ .

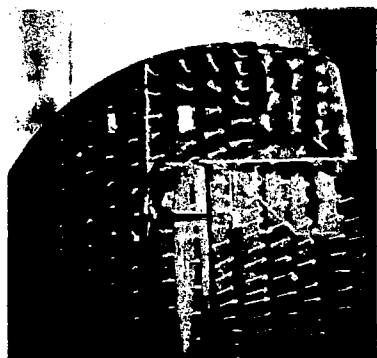
Figure 19.- Continued.



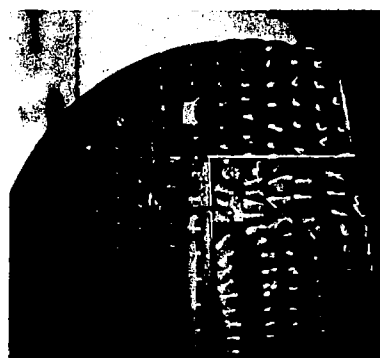
$\alpha = -8^\circ$



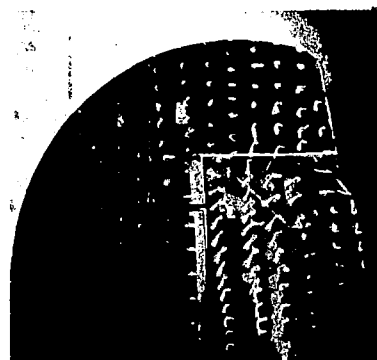
$\alpha = 0^\circ$



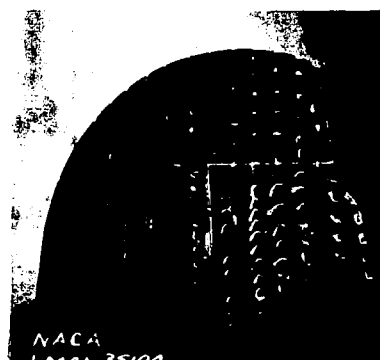
$\alpha = 8^\circ$



$\alpha = 16^\circ$



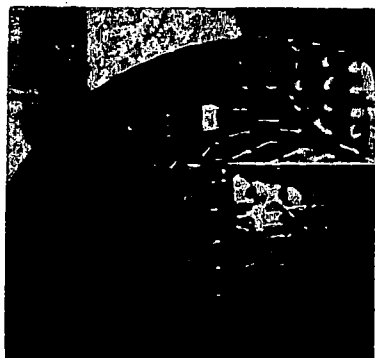
$\alpha = 24^\circ$



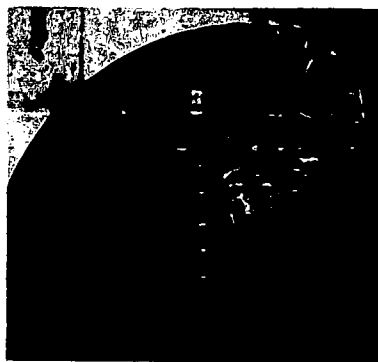
$\alpha = 32^\circ$

(f)  $\delta_e = 16^\circ$ .

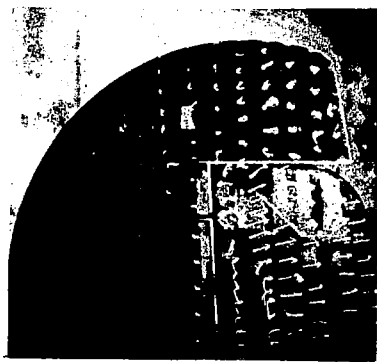
Figure 19.- Continued.



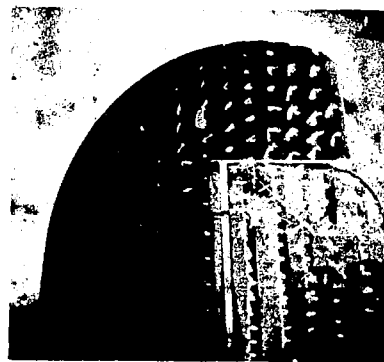
$\alpha = -8^\circ$



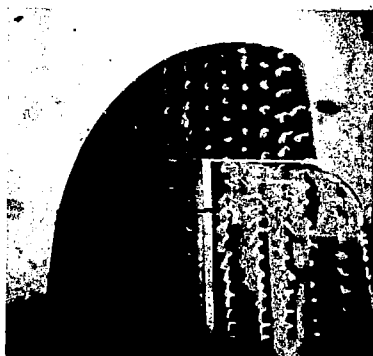
$\alpha = 0^\circ$



$\alpha = 8^\circ$



$\alpha = 16^\circ$  \*



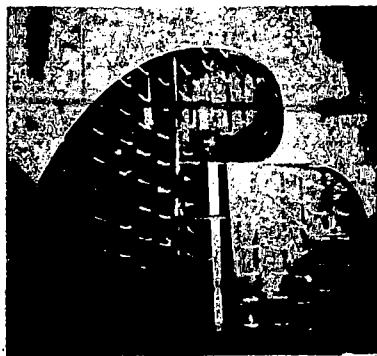
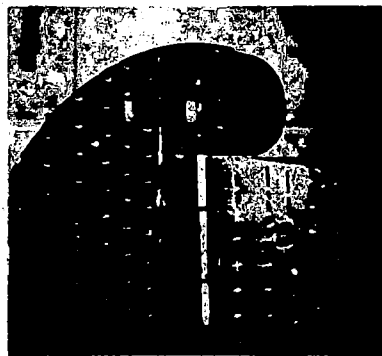
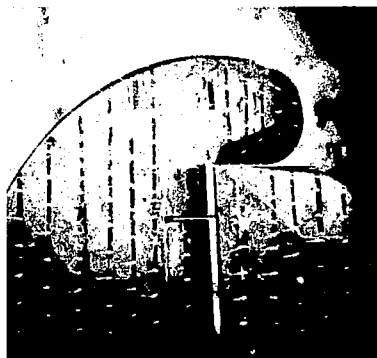
$\alpha = 24^\circ$  \*



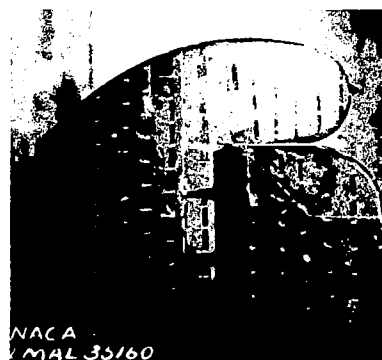
$\alpha = 32^\circ$  \*

(g)  $\delta_e = 32^\circ$ .

Figure 19.- Concluded.


 $\alpha = -8^\circ$  \*

 $\alpha = 0^\circ$ 

 $\alpha = 8^\circ$ 

 $\alpha = 16^\circ$ 

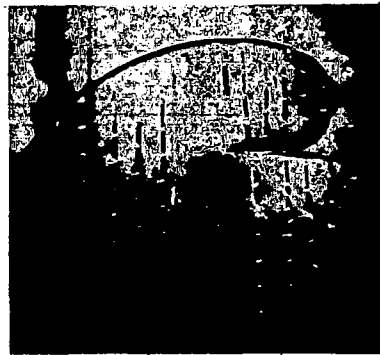
 $\alpha = 24^\circ$  \*

 $\alpha = 32^\circ$  \*

(a)  $\delta_e = -32^\circ$ .

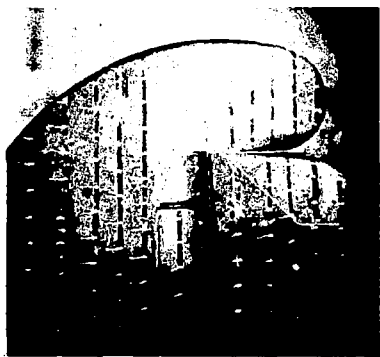
Figure 20.- Tuft study over upper surface of 0.5-scale model of TBF-1 left horizontal tail surface. Modification  $H_3S_2$ ;  $q = 16.37$  pounds per square foot except for tests with asterisk in which  $q = 12.53$  pounds per square foot.



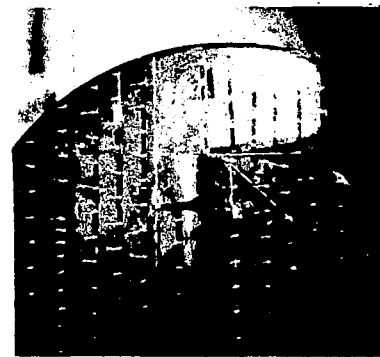
$\alpha = -8^\circ$  \*



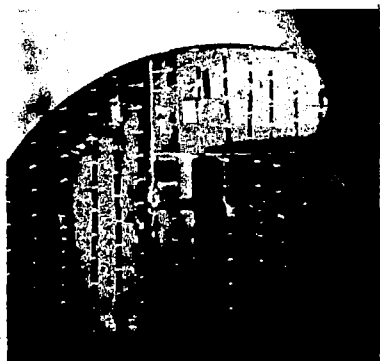
$\alpha = 0^\circ$



$\alpha = 8^\circ$



$\alpha = 16^\circ$



$\alpha = 24^\circ$  \*



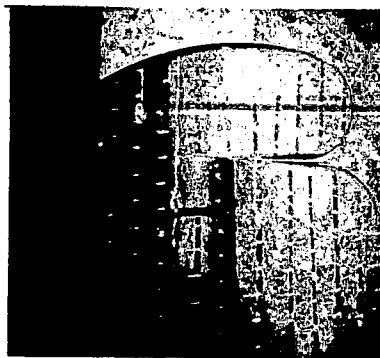
$\alpha = 32^\circ$  \*

(b)  $\delta_e = -16^\circ$ .

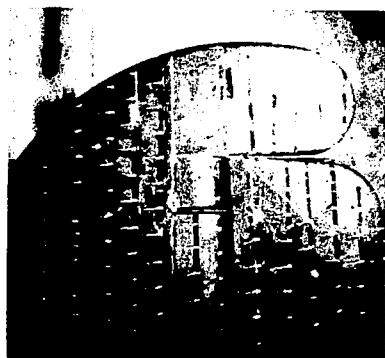
Figure 20.- Continued.



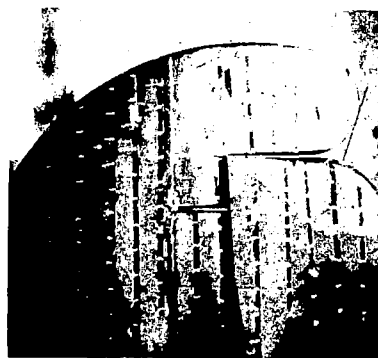
$\alpha = -8^\circ$  \*



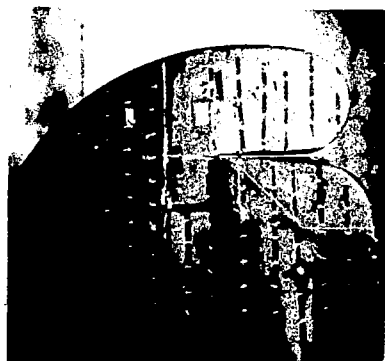
$\alpha = 0^\circ$



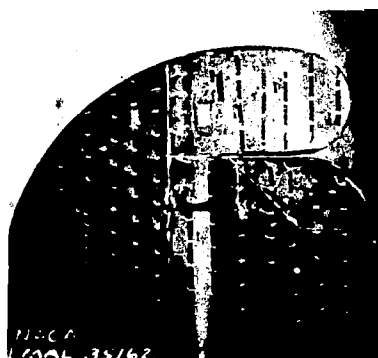
$\alpha = 8^\circ$



$\alpha = 16^\circ$



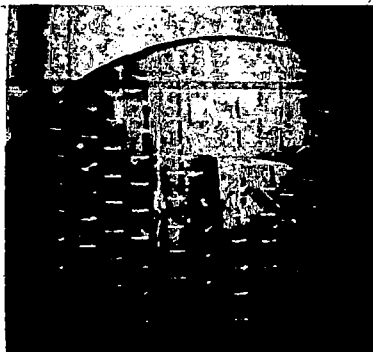
$\alpha = 24^\circ$  \*



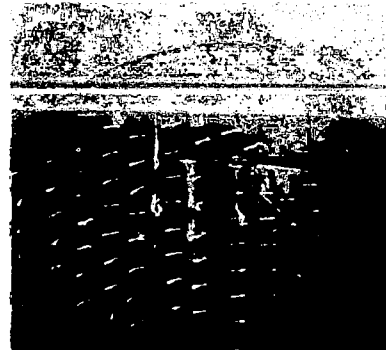
$\alpha = 32^\circ$  \*

(c)  $\delta_e = -8^\circ$ .

Figure 20.- Continued.



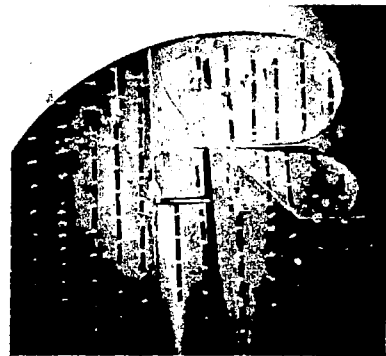
$\alpha = -8^\circ$  \*



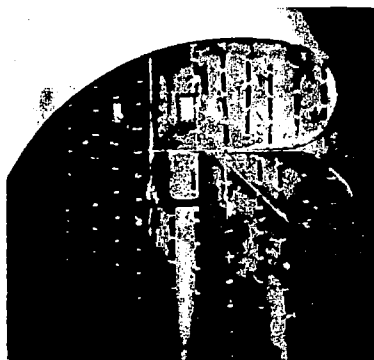
$\alpha = 0^\circ$



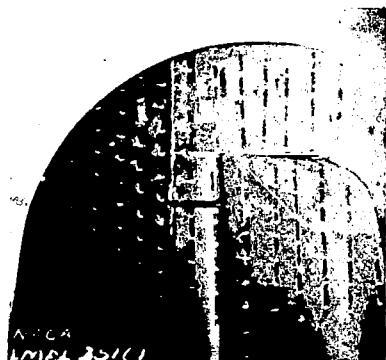
$\alpha = 8^\circ$



$\alpha = 16^\circ$



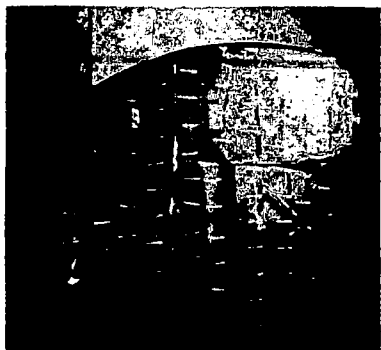
$\alpha = 24^\circ$  \*



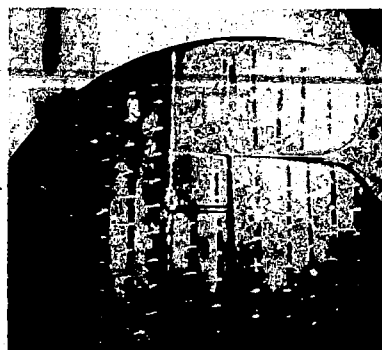
$\alpha = 32^\circ$  \*

(d)  $\delta_e = 0^\circ$ .

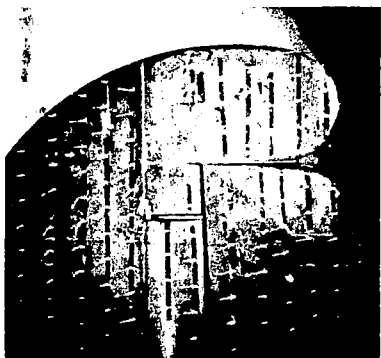
Figure 20.- Continued.



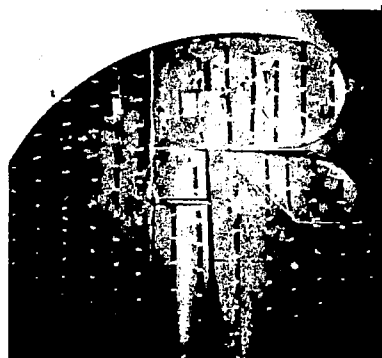
$\alpha = -8^\circ$



$\alpha = 0^\circ$



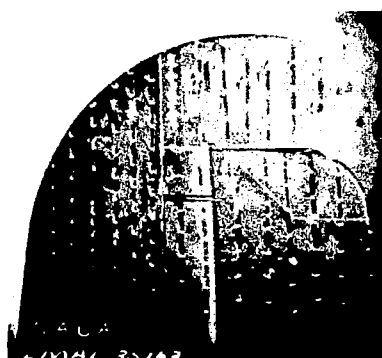
$\alpha = 8^\circ$



$\alpha = 16^\circ$



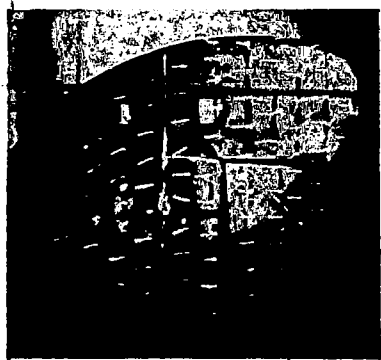
$\alpha = 24^\circ$  \*



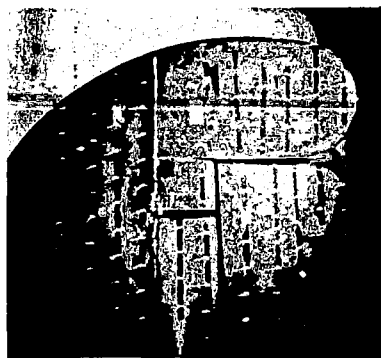
$\alpha = 32^\circ$  \*

(e)  $\delta_e = 8^\circ$ .

Figure 20.- Continued.



$\alpha = -8^\circ$



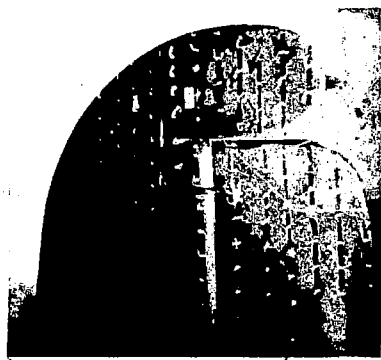
$\alpha = 0^\circ$



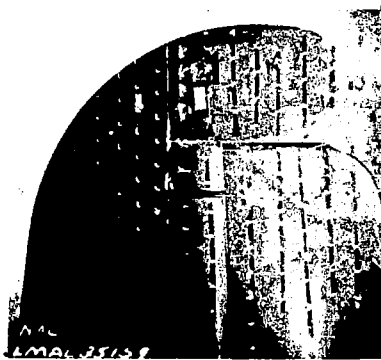
$\alpha = 8^\circ$



$\alpha = 16^\circ$



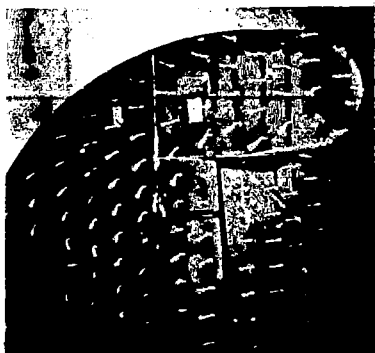
$\alpha = 24^\circ$



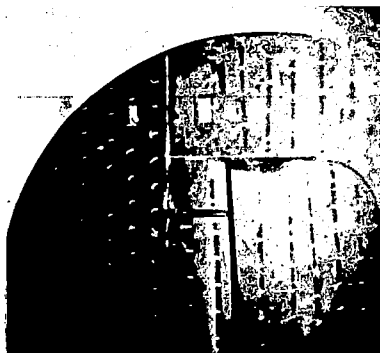
$\alpha = 32^\circ$

(f)  $\delta_e = 16^\circ$ .

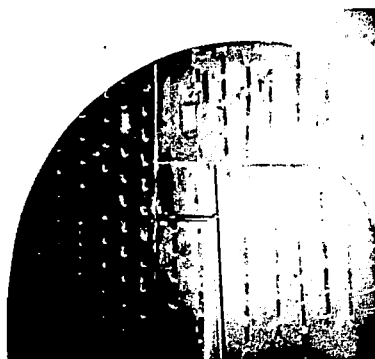
Figure 20.- Continued.



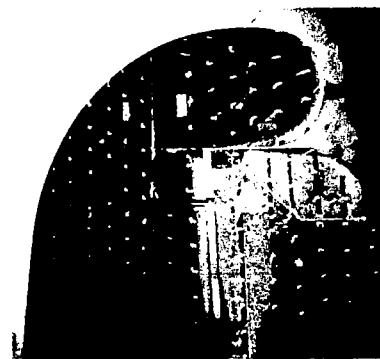
$\alpha = -8^\circ$



$\alpha = 0^\circ$



$\alpha = 8^\circ$  \*



$\alpha = 16^\circ$  \*



$\alpha = 24^\circ$  \*



$\alpha = 32^\circ$  \*

(g)  $\delta_e = 32^\circ$ .

Figure 20.- Concluded.

LANGLEY RESEARCH CENTER



3 1176 01364 8887